[AMERICAN JOURNAL OF SCIENCE, VOL. 294, OCTOBER, 1994, P. 989–1057]

MASS TRANSFER DURING BARROVIAN METAMORPHISM OF PELITES, SOUTH-CENTRAL CONNECTICUT. I: EVIDENCE FOR CHANGES IN COMPOSITION AND VOLUME

JAY J. AGUE
Department of Geology and Geophysics,
Yale University,
P.O. Box 208109,
New Haven, Connecticut 06520-8109

ABSTRACT. Evidence for mass and volume changes attending the Barrovian (chlorite to kyanite zone) metamorphism of aluminous pelites of the Wepawaug Schist, Connecticut, is examined using a petrologic mass balance approach that takes full account of the closure problem and the multivariate nature of compositional data. Quartz veins are not included in the analysis so that mass and volume changes in aluminous pelite can be effectively isolated and quantified. Statistical analysis and regional mapping of chemistry and density variations strongly suggest that the physicochemical properties of the pelites are correlated with geographic position and metamorphic grade. The nature and degree of the variations indicate that they are the result of metamorphism, not sedimentary or diagenetic processes. The concentration systematics of relatively "immobile" low solubility elements (for example, Ti, Zr, and Nb) are consistent with the hypothesis that the garnet, staurolite, and kyanite zone pelites had initial (protolith) compositions that were comparable to those of the presently exposed chlorite and biotite zone rocks.

Mass balance analysis strongly suggests that metamorphism led to significant mass and volume changes over minimum length scales on the order of typical hand sample dimensions. The average degree of physicochemical change increases in a general way with metamorphic grade. Average total mass change estimates, computed relative to the low-grade chlorite and biotite zone rocks using a Ti reference frame, are -10 ± 9 percent, -19 ± 6 percent, and -23 ± 6 percent for the garnet, staurolite, and kyanite zone pelites, respectively ($\pm 2\sigma$; negative values indicate mass loss). A diverse spectrum of elements were apparently mobile during metamorphism. Si was lost from upper greenschist and amphibolite facies pelites; average silica mass change values are -15^{+17}_{-14} percent, -32^{+11}_{-9} percent, and -38^{+9}_{-8} percent for the garnet, staurolite, and kyanite zones, respectively ($\pm 2\sigma$). P was lost from kyanite zone pelites, and Na was lost from the amphibolite facies pelites. On average, Mn and Zn were added to staurolite and kyanite zone pelites, and K and Ba were added to staurolite zone pelites. Amphibolite facies pelites may have lost some Ca and Sr, but the analysis is complicated by protolith heterogeneity. The grain density (rock density on a porosity-free basis) of the pelites increases systematically as metamorphic grade increases. The mass loss and grain density increases are interpreted to have caused significant decreases in volume. Estimates of average volume change for the garnet, staurolite, and kyanite zone pelites are -12 ± 10 percent, -22 ± 6 percent, and -28 ± 6 percent, respectively ($\pm 2\sigma$), relative to the chlorite and biotite zone

rocks. The degree of mass transfer and volume change was variable within individual outcrops.

The results of this study indicate that significant, heretofore unrecognized changes in the composition and volume of aluminous pelite may occur during Barrovian style metamorphism.

INTRODUCTION

Regional metamorphic terranes develop as dynamic hydrothermal systems in which fluid flow plays an active role in driving mineral reactions and transporting heat (Garlick and Epstein, 1966; Rye and others, 1976; Rumble and others, 1982; Tracy and others, 1983; Bickle and McKenzie, 1987; Brady, 1988; Chamberlain and Rumble, 1988; Hoisch, 1991; Symmes and Ferry, 1991; Ferry, 1992). Major fluid movement will also have the potential to produce widespread metasomatic alteration of rocks owing to solute transport by the processes of advection, hydrodynamic dispersion, and diffusion. However, metasomatism during regional metamorphism has received surprisingly little attention in recent years, even though a number of studies provide strong evidence of fluid-driven mass transfer of major and trace elements in a diverse spectrum of crustal processes. Examples include: (1) shear zone development (Beach, 1976; Kerrich and others, 1980; Sinha and others, 1986; O'Hara and Blackburn, 1989; Dipple and Ferry, 1992); (2) subduction (Sorenson, 1988; Bebout and Barton, 1989; Philippot and Selverstone, 1991); (3) seafloor hydrothermal alteration of basalt (Wood, Sibson, and Thompson, 1976); (4) granulite facies metamorphism (Bridgwater and others, 1989); and (5) fluid-rock interactions involving metacarbonates (Orville, 1969; Vidale and Hewitt, 1973; Thompson, 1975; Ferry, 1982; Tracy and others, 1983; Leger and Ferry, 1993).

Although mass transfer processes may operate in a number of regional metamorphic settings, the role of metasomatism during typical "Barrovian" style metamorphism of pelitic rocks remains highly controversial and largely unexplored. The ubiquitous presence of syn-metamorphic quartz veins in pelitic terranes demonstrates unequivocally that mass transfer of rock-forming elements does occur during Barrovian metamorphism (Vidale, 1974; Walther and Orville, 1982). Nonetheless, except for the loss of volatiles and the movement of certain trace elements, the regional metamorphism of pelitic rocks has been traditionally regarded as an isochemical process (Shaw, 1956; Butler, 1965; Ronov Migdisov, and Lobach-Zhuchenko, 1977; Yardley, 1977, 1986; Ferry, 1982; Haack and others, 1986; Wood and Walther, 1986; Moss and others, 1992). In contrast to this view, Ague (1991) has presented geochemical evidence for major mass loss of silica and mobility of alkali and alkaline earth elements as a result of metamorphic processes operative in the greenschist and amphibolite facies. Mass balance relations strongly suggest that the average pelitic rock may lose 20 to 30 percent of its mass and volume during metamorphism to amphibolite facies conditions (Ague, 1991). Furthermore, large mass losses have been inferred to

occur during penetrative cleavage development in pelitic and siliciclastic rocks (Wright and Platt, 1982; Erslev and Mann, 1984; Bell, 1985; Beutner and Charles, 1985; Henderson, Wright, and Henderson, 1988), although considerable disagreement exists over the amounts, scales, and processes of deformation-related mass transfer (Wintsch, Kvale, and Kisch, 1991).

The possible occurrence of widespread mass transfer during regional metamorphism has fundamental implications for the physicochemical evolution of the crust. Chemical alteration of rocks will influence directly the mineral reactions that may take place during burial and uplift. As shown by Hosheck (1967), the index minerals chloritoid and staurolite only grow in a restricted range of bulk compositions, characterized by low molar (Ca + Na + K)/Al. Metasomatic modifications of bulk-rock chemistry involving alkali transport during metamorphism could, therefore, provide potentially powerful constraints on the development of key index minerals in orogenic belts (Phillips, 1988). Changes in volume due either to fluid-driven mass influx or outflow must be known in order to clarify strain partitioning in mountain belts. Furthermore, it is essential to quantify metasomatic volume changes before the reaction progress approach (Brimhall, 1979; Ferry, 1983; Ferry and Dipple, 1991) can be used to calculate fluid fluxes, heat budgets, and directions of fluid motion relative to temperature and pressure gradients. Metamorphic mass transfer may also exert profound controls on the major and trace element composition of magmas derived ultimately from partial melting during orogenesis.

In order to obtain a better understanding of the nature and magnitudes of metasomatic mass and volume change that may occur during the regional metamorphism of pelites, a petrologic mass balance study of the Wepawaug Schist, a classic Barrovian terrane in southern New England, has been carried out. In the first part of this paper, a general overview of the geologic history and mineralogy of the Wepawaug Schist is presented. The mass balance approach to metasomatic problems is then discussed. Because many previous mass balance studies have been compromised by the fact that compositional data are inherently multivariate and subject to closure (Chayes, 1960; Aitchison, 1986), special emphasis is placed on the statistical methods required to analyze quantitatively compositional data sets. Finally, variations in the chemical compositions and bulk grain densities of the schists as functions of metamorphic grade and geographic position are investigated, and metasomatic changes in composition and volume are quantified. Future papers in this series will be devoted to determining the role that metasomatism may play in the mineralogical evolution of pelites and the processes of local and regional scale mass transfer.

GEOLOGIC RELATIONS

Overview.—The Wepawaug Schist lies within the Orange-Milford belt of the Connecticut Valley Synclinorium (Rodgers, 1985) (fig. 1). The

synclinorium is composed primarily of Middle to Early Paleozoic (350-500 Ma) metasedimentary and metaigneous rocks whose protoliths are interpreted to have formed in the Iapetus ocean basin. Fritts (1962a, b, 1963, 1965a, b) carried out the first petrologic studies and detailed mapping in the Wepawaug and surrounding areas. Typical chlorite zone outcrops of the Wepawaug are composed of ~70 volume percent pelite and ~30 volume percent massive metasandstone and massive metasiltstone. The pelitic units can be easily distinguished from the metasandstones and metasiltstones in the field at all metamorphic grades (fig. 2). In addition, the formation contains ~1 percent impure marble (Hewitt, 1973; Palin and Rye, 1992) and dispersed intrusive and extrusive igneous rocks of broadly tonalitic composition (Fritts, 1962a, b, 1963, 1965a). Metamorphism of the Orange-Milford belt sequence is thought to be primarily the result of the Acadian orogeny (Palin and Seidemann, 1990; Lanzirotti and Hanson, 1992). The most striking metamorphic feature of the Wepawaug is the east-to-west progression of Barrovian zone isograds across the Formation (Fritts, 1963, 1965a, b) (fig. 3). Metamorphic grade increases from chlorite zone in the east to kyanite zone in the west. "Peak" metamorphic temperatures ranged from ~400°C in the chlorite zone to ~650° in the kyanite zone, and "peak" pressures were 0.7 to 0.9 GPa throughout the field area (Ague, 1994). The marbles of the Wepawaug Schist have been the focus of several comprehensive petrologic and stable isotopic studies (Hewitt, 1973; Tracy and others, 1983; Palin, ms; Palin and Rye, 1992), but the pelites have received considerably less attention.

Prograde mineralogy.—The mineral assemblages that grew during metamorphism correspond to those in the classical Barrovian sequence (Barrow, 1893, 1912; Harte and Hudson, 1979; McLellan, 1985). Chlorite zone pelites (phyllites) are characterized by the following assemblage:

Quartz + muscovite + chlorite + albite
± ankerite ± calcite ± Mn-rich garnet.

The minerals have been listed in the approximate order of decreasing abundance. The garnets occur sporadically, are small (~0.5-2.0 mm), and have spessartine mole fractions in the range of 0.16 to 0.20 (mineral chemistry is presented in detail in Ague II, this journal, November, 1994). Both rutile and ilmenite may be present. Biotite zone assemblages are similar; biotite occurs intimately intergrown with muscovite and chlorite.

The garnet isograd is mapped here on the basis of the first field occurrence of garnets that are large enough to be easily discerned by the naked eye (2-10 mm). The rims of the garnets contain significantly more almandine component and less spessartine than the garnets in the lower-grade rocks. The typical garnet zone assemblage is:

Quartz + muscovite + biotite + oligoclase + garnet ± chlorite.

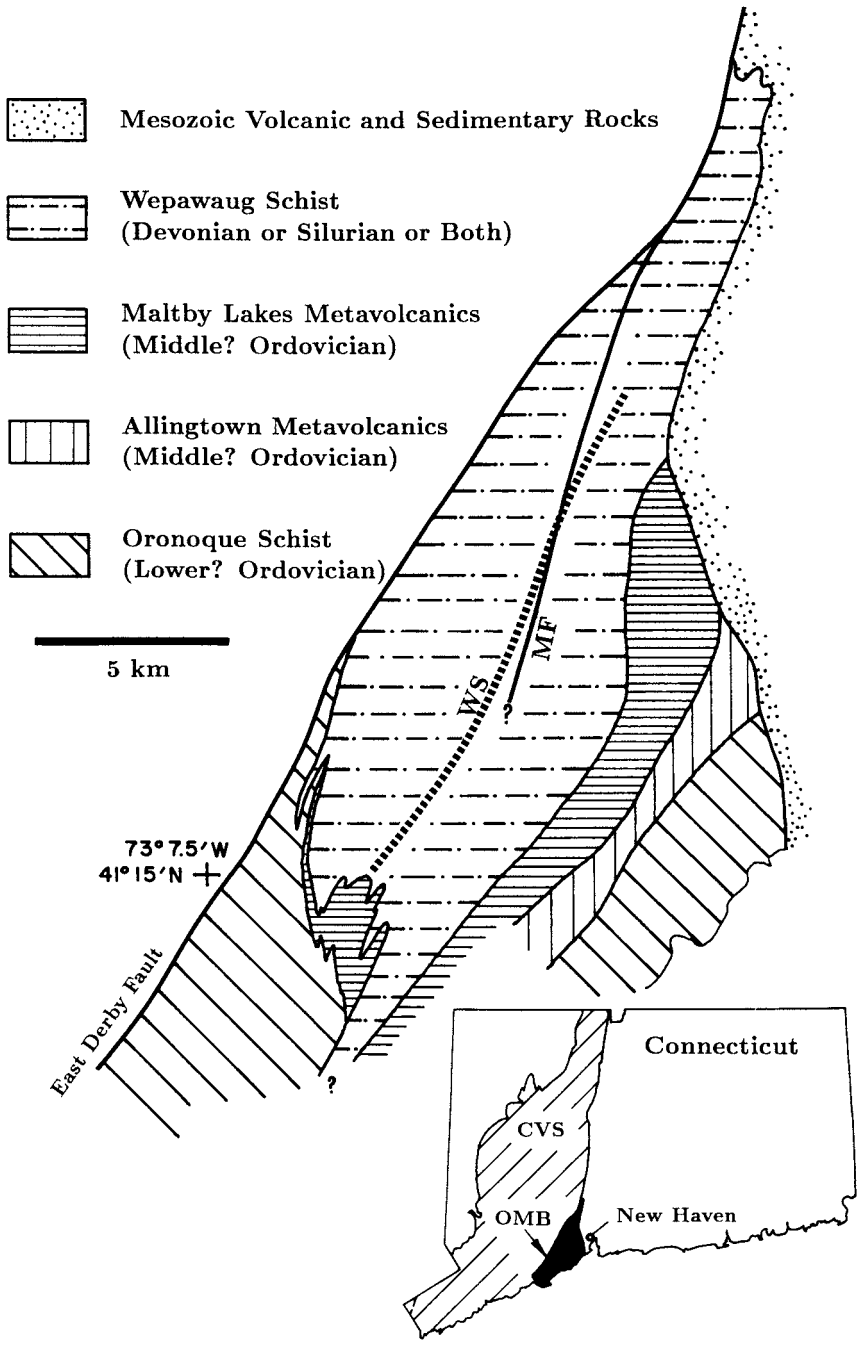

Fig. 1. Generalized geologic map of the Orange-Milford belt of south-central Connecticut, modified from Fritts (1962b, 1963, 1965a,b), Dieterich (ms), and Rodgers (1985). WS: axis of the Wepawaug syncline based on the work of Fritts (1965a), Dieterich (ms), and Ague (unpublished mapping). MF: Mixville fault. Dip-slip displacements on this fault, quantified from observations of Mesozoic rocks to the north of the Wepawaug Schist, are small (~ 100 m; Fritts, 1965a). The position of the Orange-Milford belt (OMB) in the Connecticut Valley Synclinorium (CVS) is shown on the inset location map.

Fig. 2. Field appearance of the Wepawaug Schist. The bulk of the outcrop is composed of aluminous pelite cut by quartz veins. At the right are two massive psammitic layers (arrows) separated by a thin band of pelite containing a quartz vein. Outcrop is ~0.5 km west (upgrade) of the garnet isograd in the garnet zone.

Rutile and ilmenite are generally present near the biotite isograd, but as the staurolite isograd is approached, rutile becomes the sole prograde oxide phase. Chloritoid is absent from the greenschist facies pelites.

The most common staurolite zone assemblage is:

Muscovite + quartz + biotite + garnet + oligoclase ± staurolite.

Rutile is the prograde oxide, but it is sometimes altered to ilmenite along its margins, especially at contacts with what are inferred on textural grounds to be small patches of retrograde chlorite. In addition, rare kyanite may be found in some staurolite zone pelites at contacts with quartz veins.

The typical kyanite zone assemblage is:

muscovite + biotite + quartz + garnet
+ oligoclase ± staurolite ± kyanite.

Kyanite and staurolite porphyroblasts range from several millimeters to several centimeters in length; the average length is ~3 mm. Rutile (sometimes altered to ilmenite along cracks and grain boundaries) is the primary oxide, but some rocks in the western portion of the kyanite zone contain intergrowths of euhedral rutile and ilmenite. In amphibolite

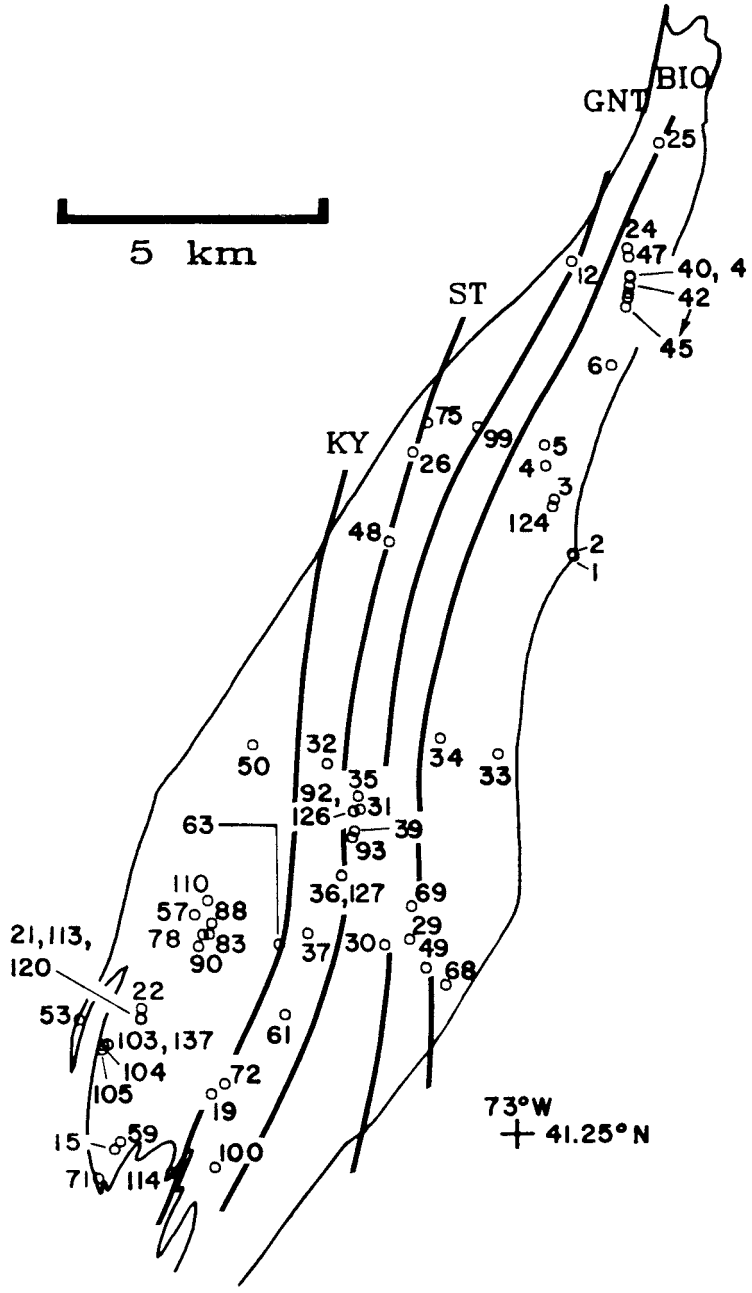

Fig. 3. Sample locations. Isograd positions modified from Fritts (1963, 1965a, b) based on field mapping by Ague (5/90-1/93). All samples belong to sample set JAW.

facies pelites, staurolite, and, at appropriate metamorphic grade, kyanite porphyroblasts tend to be concentrated in ~1–10 cm wide zones adjacent to quartz veins.

With respect to accessory phases, sulfides, zircon, apatite, monazite, and metamorphosed organic matter are widespread in the pelites at all metamorphic grades. Chlorite zone rocks contain pyrite, whereas higher grade rocks contain pyrrhotite (sometimes altered to pyrite along cracks). Traces of chalcopyrite have been found in some staurolite and kyanite zone samples.

MASS BALANCE APPROACH

In this section, the mass balance equations and statistical methods required to assess quantitatively metasomatic phenomena are presented in order to provide a rigorous foundation for interpreting the compositional systematics of the metapelites as a function of metamorphic grade.

A metasomatic process can be defined in a general sense as ". . . any process involving a change in the bulk composition of the mineral assemblage" (Thompson, 1959). With respect to the metasomatic alteration of rocks, study of mass transfer associated with veins has been central to the discipline of economic geology for many decades. In metamorphic systems, the classical articles of Korzhinski (1950) and Thompson (1959) laid a firm thermodynamic foundation for the interpretation of metasomatic processes.

For our purposes, two types of chemical element behavior can be distinguished. "Immobile" or, alternatively, reference or residual species are those that are not transported into or out of the chemical system of interest. On the other hand, mobile elements have their chemical potentials fixed outside the system of interest, and, therefore, they can be transported into or out of this system during alteration.

The mass balance approach is one of the most powerful methods available for assessing metasomatic changes in rocks. The basic premise of a mass balance study is to compare the chemical compositions and physical properties of unaltered rocks, or "protoliths," with their altered equivalents in order to obtain information relating to volume changes and chemical mass transfer. The two fundamental requirements of any quantitative mass balance study are: (1) the protolith material must be characterized, and (2) a frame of reference for assessing mass and volume changes between the protolith and altered states must be established (Thompson, 1959). Determining gains and losses of mobile elements in altered rocks relative to the protolith state can be done in terms of: (1) constant mass of a residual species, (2) a constant volume system, or (3) a constant mass system. Because cases (2) and (3) would appear to be the exception rather than the norm during alteration, attention is focused only on the first case in the following discussion.

Mass balance approaches describing various aspects of metasomatic mass and volume change have been advanced by a number of workers over the years, including Emmons (1918), Ridge (1949, 1961), Ramberg

(1952), Poldervaart (1953), Turner and Verhoogen (1960), Gresens (1967), Meyer and others (1968), and Grant (1986). The work presented here is based on the recent formulations of Brimhall and Dietrich (1987) and Brimhall and others (1988), because they provide simple and direct constitutive relations between rock physical, chemical, volumetric, and mechanical properties in metasomatic systems.

The appropriate mass balance equations for determining rock mass changes, mobile element mass changes, and volume strain are summarized briefly here. Detailed derivations are given in app. A. A primary goal of the derivations was to arrive at final mass balance expressions that were amenable to statistical analysis.

Total rock mass change determined using a reference species i, defined here as T_i (Ague, 1991), is given by:

$$T_i \equiv \left[\frac{\textit{Final Mass} - \textit{Initial Mass}}{\textit{Initial Mass}}\right] = \left[\frac{C_i^o}{C_i'} - 1\right], \tag{1}$$

where C_i^o and C_i' are the initial (protolith) and final (altered state) concentrations (for example, wt percents) of i. Negative and positive T_i values denote mass loss and mass gain, respectively. For example, a T_i value of -0.5 means that 50 percent of the rock mass was lost during alteration. Residual enrichment or dilution of i results from the net removal or addition of mobile species, respectively. The *concentration* of i changes as a result of metasomatism because of closure (all components in the composition must sum to 100 percent), but the *mass* of i remains unchanged.

Changes in the masses of individual mobile species j can be determined using the transport function τ of Brimhall and others (1988). As discussed by Ague (1991), the mass change of j computed using the reference species i, denoted as τ_i^j, can be written as:

$$\tau_i^j \equiv \left[\frac{\textit{Final Mass } j - \textit{Initial Mass } j}{\textit{Initial Mass } j}\right] = \left[\left(\frac{C_i^o}{C_i'}\right)\left(\frac{C_j'}{C_j^o}\right) - 1\right]. \tag{2}$$

The advantage of characterizing metasomatic behavior using the transport function is that there are no assumptions about local fluid-rock equilibrium, fluid-rock ratios, time-integrated fluid-fluxes, or elemental fluid-rock distribution coefficients inherent in the calculations.

Volume strain computed on the basis of a reference species i, denoted as ϵ_i, is given by (Brimhall and Dietrich, 1987; Brimhall and others, 1988):

$$\epsilon_i \equiv \left[\frac{\textit{Final Volume} - \textit{Initial Volume}}{\textit{Initial Volume}}\right] = \left[\left(\frac{C_i^o}{C_i'}\right)\left(\frac{\rho_g^o}{\rho_g'}\right)\left(\frac{(1 - n^o)}{1 - n'}\right) - 1\right], \tag{3}$$

where ρ_g^o and ρ_g' are the initial and final grain densities (rock density on a porosity-free basis), and n^o and n' are the initial and final rock porosities,

respectively. As discussed in app. A, $(1 - n^o)/(1 - n')$ will be ~ 1 for regionally metamorphosed pelites and can safely be neglected.

Statistical treatment of compositional data.—Because protoliths are heterogeneous, and altered rocks may undergo different degrees of metasomatism, uncertainties in calculated mass balance results should be given. However, the application of statistical techniques is complicated by the fact that compositional data are inherently multivariate and subject to closure such that the sum of all components in the composition must be one. Until the recent work of Aitchison (1986), no clear-cut methods of dealing with these complications were available. Fortunately, rigorous statistical treatments of compositional data sets are now possible, largely because Aitchison (1986) made the important realization that multivariate statistical methods can be applied to compositional data, if the data are cast in terms of appropriate logratios. In this section, we will examine how Aitchison's (1986) novel statistical approach can be used to analyze mass balance problems.

Many standard statistical concepts (for example, the average) cannot be used directly with compositional data if the unit-sum constraint (closure) and the multivariate nature of the data are not taken into account. The key to the closure problem is that the statistical analysis of compositions must focus on the ratios of components in a composition, not the absolute values of each component (Chayes 1960; Aitchison, 1986; Nicholls, 1988). A composition provides information only about the relative magnitudes of its components.

A number of difficulties are encountered, however, when dealing with the statistics of ratio data (Spiegel, 1961, p. 60; Aitchison, 1986; Woronow and Love, 1990). For example, ratios of the concentrations of two species, such as C_i/C_j, are generally not normally distributed, and the variance of C_i/C_j is not precisely related to the variance of C_j/C_i. Aitchison (1986) has shown that these and other difficulties are largely overcome by considering the means and variances of the logarithms of the ratios, rather than the means and variances of the ratios themselves. For a compositional data set of N compositions, each comprising D individual constituents, the logratio mean, $\hat{\Xi}_{i,j}$, and variance, $\hat{s}^2_{i,j}$, for the constituents i and j can be expressed as:

$$\hat{\Xi}_{i,j} = N^{-1} \sum_{l=1}^{N} \ln (C_{i,l}/C_{j,l}) \tag{4}$$

and,

$$\hat{s}^2_{i,j} = (N - 1)^{-1} \sum_{l=1}^{N} [\ln (C_{i,l}/C_{j,l}) - \hat{\Xi}_{i,j}]^2. \tag{5}$$

Aitchison (1986, 1990) showed how the $\hat{\Xi}_{i,j}$ and $\hat{s}^2_{i,j}$ values for a given problem may be cast into a "compositional variation array" which summa-

rizes compositional variability in terms of the mean logratios and their covariance structure. Woronow and Love (1990) discussed why the ratios of concentrations will tend to have lognormal distributions.

Turning first to the problem of computing a mean composition, Aitchison (1989) showed that the $\hat{\Xi}_{i,j}$ values for a given data set can be transformed into a measure of location free from the pathologies of the closure problem. This mean composition vector, herein referred to as the Aitchison measure of location, $\hat{\eta}$, is given by:

$$\hat{\eta} = \frac{(g_1, g_2, \ldots, g_D)}{\sum_{m=1}^{D} g_m}, \tag{6}$$

where g_m denotes the geometric mean concentration of constituent m:

$$g_m = \exp\left[N^{-1} \sum_{l=1}^{N} \ln (C_{m,l})\right]. \tag{7}$$

Thus, the Aitchison measure of location (or AML) is an average composition formed from the geometric means of all components in the composition by the process of closure. It should be pointed out that even if the underlying distribution of a given variable is normal (gaussian), calculation of the "average" and dispersion using the geometric mean and its associated standard deviation is generally acceptable (Gaddum, 1945). For example, a normal distribution with an arithmetic mean of 10 and a sample standard deviation of 1 has a geometric mean of 9.95 and corresponding standard deviation limits of +1.06 and −0.96. Therefore, geometric means are suitable for a broad spectrum of statistical analyses.

In cases where there is substantial curvature to the compositional data set (Aitchison, 1989), or when the amount of variability in the compositional data set is large, the AML will be clearly superior to the conventional arithmetic mean. In situations where the amount of compositional variability is small, however, the AML and the conventional arithmetic mean may be quite similar. Although it is possible to use the conventional arithmetic mean under some circumstances, the reader should bear in mind that, in the strict sense, the means and variances of raw compositional proportions have no direct interpretive value (Aitchison, 1989).

Evaluation of the mean and dispersion of τ_i^j, T_i, and ϵ_i values must also be carried out using ratios in a multivariate way. With respect to the transport function, the first step is to recast eq (2) as:

$$\tau_i^j = \left[\left(\frac{C_i^o}{C_j^o}\right)\left(\frac{C_j^t}{C_i^t}\right) - 1\right], \tag{8}$$

so that statistical analysis based on logratio-means (Woronow and Love, 1990) can be done. The logratio-means are given by:

$$\hat{\Xi}^{o}_{i,j} = N^{o-1} \sum_{l=1}^{N^o} \ln (C^{o}_{i,l}/C^{o}_{j,l}) \tag{9}$$

and,

$$\hat{\Xi}'_{j,i} = N'^{-1} \sum_{l=1}^{N'} \ln (C'_{j,l}/C'_{i,l}), \tag{10}$$

where N^o and N' are the numbers of samples representing the protolith and altered states, respectively. The standard deviation on $\hat{\Xi}^{o}_{i,j}$ (standard error) is then:

$$\hat{\sigma}^{o}_{i,j} = N^{o-1/2}\left((N^o - 1)^{-1} \sum_{l=1}^{N^o} [\ln (C^{o}_{i,l}/C^{o}_{j,l}) - \hat{\Xi}^{o}_{i,j}]^2 \right)^{1/2} \tag{11}$$

The standard error associated with $\hat{\Xi}'_{j,i}$, $\hat{\sigma}'_{j,i}$, is computed in the same fashion. By analogy with eq (8), the average, or "most probable," $\hat{\tau}^{j}_{i}$ value computed using logratio-means is:

$$\hat{\tau}^{j}_{i} = \exp (\hat{\Xi}^{o}_{i,j} + \hat{\Xi}'_{j,i} \pm \sigma_{Tot}) - 1, \tag{12}$$

where σ_{Tot} is the total standard error associated with the sum of $\hat{\Xi}^{o}_{i,j}$ and $\hat{\Xi}'_{j,i}$, estimated by adding the individual $\hat{\sigma}^{o}_{i,j}$ and $\hat{\sigma}'_{j,i}$ terms in quadrature:

$$\sigma_{Tot} = [(\hat{\sigma}^{o}_{i,j})^2 + (\hat{\sigma}'_{j,i})^2]^{1/2}. \tag{13}$$

The calculation of σ_{Tot} is based on the reasonable assumption that $\hat{\sigma}^{o}_{i,j}$ and $\hat{\sigma}'_{j,i}$ are independent random variables.

A new bootstrap statistical technique has been devised to evaluate the standard deviation on the average T_i and ϵ_i for a group of samples. The average T_i value, $\hat{T}_i$, can be computed easily by:

$$\hat{T}_i = \left(\frac{\hat{C}^{o}_{i}}{\hat{C}'_{i}} - 1 \right), \tag{14}$$

where the $\hat{C}_i$ terms denote mean values calculated using the AML. Because uncertainties in the numerator and denominator in the concentration ratio term are not readily computable, it is best to assess uncertainties in $\hat{T}_i$ using non-parametric bootstrap techniques. Non-parametric techniques are powerful in that they do not require specific statistical model assumptions (Efron, 1982). Bootstrap methods are based on repeated resampling of the original data sets so as to form a large number of hypothetical data sets, or "bootstrap samples." The resampling is done with replacement such that each observation may occur more than once in a given bootstrap sample. The statistic of interest, $\hat{\theta}$, is then calculated

using each bootstrap sample in order to produce a large number of "replicates," $\hat{\theta}^*$. In the case of estimating standard deviations on $\hat{T}_i$ values, the calculations are carried out according to the following Monte Carlo algorithm. First, bootstrap sample composition vectors are constructed from the set of protolith and altered rock compositions. Second, the $\hat{C}_i^{o*}$ and $\hat{C}_i'^*$ values for the bootstrap samples are computed using the AML. Third, $\hat{\theta}^*$ is calculated as:

$$\hat{\theta}^* = \left(\frac{\hat{C}_i^{o*}}{\hat{C}_i'^*}\right) - 1. \tag{15}$$

The above steps are independently repeated a large number (typically ~ 5000) B of times so as to construct the replicates $\hat{\theta}^{*1}$, $\hat{\theta}^{*2}$, . . . $\hat{\theta}^{*B}$. The standard deviation on $\hat{\theta}$, $\hat{\sigma}_{boot}$, can then be evaluated by:

$$\hat{\sigma}_{boot} = \left[(B-1)^{-1} \sum_{b=1}^{B} (\hat{\theta}^{*b} - \hat{\theta}^{*\cdot})^2\right]^{1/2}, \tag{16}$$

where $\hat{\theta}^{*\cdot}$ denotes the average:

$$\hat{\theta}^{*\cdot} = B^{-1} \sum_{b=1}^{B} \hat{\theta}^{*b}. \tag{17}$$

Thus, the $\hat{T}_i$ value and its associated standard error can be given as:

$$\hat{T}_i = \left[\left(\frac{\hat{C}_i^o}{\hat{C}_i'}\right) - 1\right] \pm \hat{\sigma}_{boot}. \tag{18}$$

The frequency distributions of the $\hat{\theta}^{*b}$ values for the rock suites studied herein are normal, or very nearly so, which justifies the use of the arithmetic mean in eqs (16) and (17). The small downward bias in bootstrap standard deviation estimates was eliminated by using bootstrap samples containing $N-1$ observations, where N is the original number of observations in the data set (see Efron, 1982, p. 62).

A fully analogous procedure can be used to estimate uncertainties on the mean volume strain. The appropriate $\hat{\theta}^*$ statistic is (compare eq 3):

$$\hat{\theta}^* = \left(\frac{\hat{C}_i^{o*}}{\hat{C}_i'^*}\right)\left(\frac{\hat{\rho}_g^{o*}}{\hat{\rho}_g'^*}\right) - 1, \tag{19}$$

where the $\hat{}$ symbol over the density terms denotes averaging. In practice, it has been found that the arithmetic mean is adequate for computation of mean densities. Because ρ_g is closely related to bulk-rock composition, the rock samples used in computing $\hat{\rho}_g^{o*}$ for a given replicate must be the same as those used to calculate the corresponding $\hat{C}_i^{o*}$. The computation of $\hat{\rho}_g'^*$ and $\hat{C}_i'^*$ values must be handled in the same fashion.

One further consideration involves the problem of testing the statistical significance of differences among means of compositional data suites. Aitchison (1986) discussed techniques appropriate for deciding whether or not two composition vectors are different from one another. Woronow and Love (1990) provided a method for isolating the differences between compositional data suites which has wide applicability in studies of metasomatism. Briefly, Woronow and Love (1990) pointed out that the significance tests should focus on the geometric mean ratios of components, not on the mean values of the components themselves. The discussion here will assume that a reference species has been identified, and that it is the final component in an $l = 1 \ldots D$-part composition. The key step of the analysis is to construct logratio-mean vectors for the protolith and altered states with the following general form:

$$(\hat{\Xi}_{1,D}, \hat{\Xi}_{2,D}, \ldots, \hat{\Xi}_{D-1,D}). \tag{20}$$

For example, for compositions in a ternary system composed of the components SiO_2, MgO, and TiO_2 in which TiO_2 is the reference species, the logratio-mean vector can be written as: $(\hat{\Xi}_{SiO_2,TiO_2}, \hat{\Xi}_{MgO,TiO_2})$. Standard methods, such as the parametric t-test (Press and others, 1992), can then be applied in order to detect statistically significant differences between the $\hat{\Xi}'_{l,D} \pm \hat{s}'_{l,D}$ for an altered suite of rocks and the correspond ing $\hat{\Xi}^o_{l,D} \pm \hat{s}^o_{l,D}$ for the protolith (Woronow and Love, 1990). Similarly, the F-test can be used to determine if the two distributions have significantly different variances.

Graphical evaluation of element mobility.—Although the mass balance equations can be applied easily in an attempt to evaluate mass transfer, the results are worthless if a reference species has not been properly identified, or if the protolith material is poorly characterized. In this section, a simple graphical technique for assessing protolith heterogeneity and immobile and mobile element behavior is discussed.

As a starting point, we seek to develop a relationship between any two reference species i and k in a metasomatic system. Gresens (1967), Grant (1986), MacLean and Kranidiotis (1987), and Woronow and Love (1990), among others, have pointed out that during metasomatism, the ratio C'_k/C'_i must remain constant. From eq (A-4) in app. A it follows that:

$$C'_k = \frac{C^o_k}{C^o_i} C'_i. \tag{21}$$

Differentiation with respect to C'_i yields:

$$\frac{\partial C'_k}{\partial C'_i} = \frac{C^o_k}{C^o_i}. \tag{22}$$

Therefore, on a plot of C_k versus C_i, the slope of lines describing residual enrichment or dilution are given by C^o_k/C^o_i. Although similar equations have been derived and used elsewhere (Gresens, 1967; Grant, 1986;

Dipple, Wintsch, and Andrews, 1990), they have not been applied to the problem of establishing the geochemical reference frame in cases where significant protolith heterogeneity exists.

As a practical example, a plot of the possible concentrations of two ideal reference species i and k is illustrated in figure 4A. The field of protolith compositions is indicated by the ruled circle. The concentrations of i and k in altered rocks derived from this protolith must lie in a *wedge-shaped region* which has its apex at the origin (fig. 4A). Thus, residual enrichment or dilution will not be characterized by simple linear trends in composition space if the protolith material had some initial variability. Residual enrichment is indicated by compositional arrays extending to the right of the protolith field, whereas residual dilution compositional arrays extend to the left of it (fig. 4A). If the protolith has been incorrectly identified, then it is likely that data arrays formed by the altered rock compositions will not emanate from the assumed protolith compositional field (fig. 4A). Eq (22) will hold true for any two *mobile* species only under the highly fortuitous circumstances that both have undergone precisely the same amounts of relative enrichment or dilution. It is important to point out in this regard that if two species have undergone different degrees of metasomatic mass change, then the concentration systematics shown in figure 4A will not hold, thereby facilitating the identification of metasomatic behavior (fig. 4B).

It should be noted that additional statistical tests, including tests for subcompositional invariance and subcompositional independence, may be employed to help establish the geochemical reference frame (Aitchison, 1986; Woronow and Love, 1990). For the particular mass balance problem at hand, however, the simple graphical techniques discussed above (fig. 4) have proven to be highly effective.

GEOCHEMISTRY AND DENSITY OF ALUMINOUS PELITE

We now turn to the central question of this study: is the Barrovian metamorphism of pelitic schist necessarily an isochemical process? Our first step in addressing this question will be to test the null hypothesis that the composition of aluminous pelite in the Wepawaug is independent of metamorphic grade.

Length scales of mass transfer.—The length scales of material transport must be constrained in any mass balance analysis. In this study, the chemistry and density of ~0.5 to 1.0 kg bulk pelite samples were determined. Quartz veins were not analyzed; all samples were taken at least 0.25 cm away from the nearest quartz vein contact. Consequently, the results presented here provide no direct information about the maximum length scales of transport and volume change. However, the minimum length scales must be on the order of typical hand sample dimensions. This length scale is critical to investigate because virtually the entire body of modern field-based knowledge regarding metapelite petrology, including mineral chemistry, P-T-t evolution, and mineral reactions, is based on the study of hand samples and thin sections. Attention is focused on the vein-free system in order to isolate and

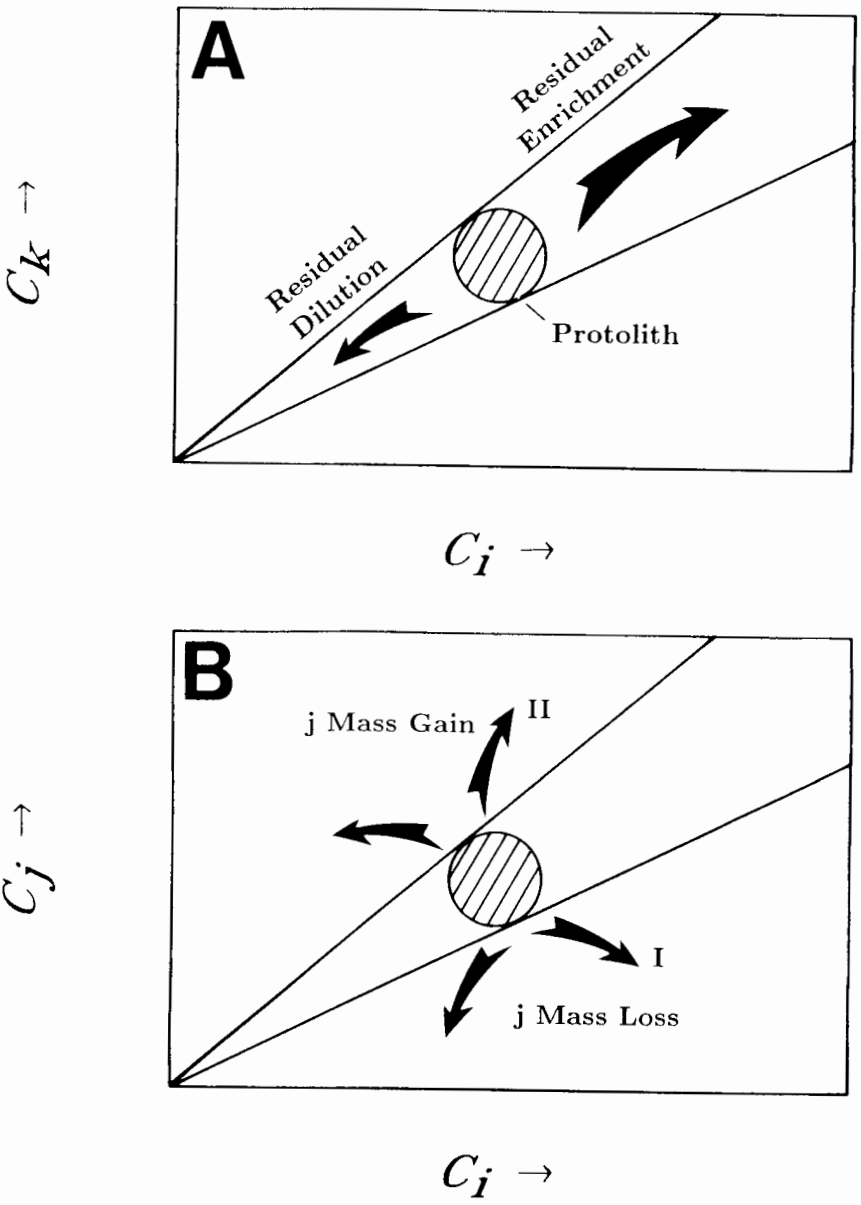

Fig. 4(A) Residual enrichment or dilution trends for two ideal reference species i and k. The field of protolith C_i and C_k values is indicated by the ruled circle. The concentrations of i and k in metasomatic rocks derived from this protolith must lie in the wedge-shaped region. Residual enrichment results in increases in the concentrations of i and k, due to the net loss of mobile constituents. Note, however, that the *masses* of i and k do not change during alteration. In the residual dilution case, the concentrations of i and k decrease due to the net addition of mobile species. (B) Metasomatic chemical trajectories. Species i is a reference species, whereas j is mobile. For example, trajectory I is indicative of mass loss of j. The concentration of i increases due to net mass loss from the rock. Along trajectory II, j is gained by the rock. However, because the concentration of i increases, the metasomatism resulted in a net mass loss (of species other than j) from the rock.

quantify effectively chemical and volumetric changes in aluminous pelite independently of any assumptions regarding vein formation processes. Forthcoming papers (including Ague, this journal, November, 1994) will address more fully the problems of channelized fluid flow and regional scale physicochemical change in the Wepawaug.

Methods of investigation.—Sampling and limited mapping were undertaken at 143 field localities. Petrographic observations were made on 125 thin sections cut from 89 rock samples. In addition, macroscopic observations were made in the field and on over 300 cut rock slabs. Seventy bulk samples of pelitic rock (fig. 2) from 58 localities were chosen for grain density and chemical composition determinations on the basis of freshness and the absence of retrograde metamorphic effects (fig. 3; app. B, C, and D). The prograde mineralogy of the samples is listed in app. B. In order to assess chemical variability within outcrops, multiple samples from several localities were studied. Rock grain densities (ρ_g) were measured on pulverized samples using a Micromeritics 1305 manual gas pycnometer at Yale University. The ρ_g measurements are accurate to within ± 0.005 g cm^{-1}, based on replicate analyses of a pulverized quartz standard. Whole-rock major, minor, and trace element chemical analyses were done using X-ray fluorescence methods by X-ray Assay Laboratories, Ltd., Don Mills, Ontario. The accuracy of the analyses made by this laboratory has been verified previously (Ferry, 1988), and the long-term reproducibility of results is documented in app. D.

Chemical behavior consistent with residual enrichment or residual dilution.—The geochemical reference frame must be rigorously identified if mass balance analysis is to be successful. Good reference species have: (1) low total concentrations in metamorphic fluids, and (2) small changes in concentration with respect to temperature (T) and pressure (P) gradients along fluid flow paths. Both experimental results and field observations provide critical constraints on the reference frame. For example, the experimental results of Ayers and Watson (1991, 1993) indicate that rutile and zircon solubilities and solubility gradients in the P-T fields characteristic of greenschist–amphibolite facies metamorphism will be extremely low for typical water-rich fluid compositions. Significant mobility of Ti and Zr appears to take place only under the extreme P-T conditions realized in the deep parts of subduction zones or in halogen-rich fluids (Philippot and Selverstone, 1991; Ayers and Watson, 1991, 1993). Furthermore, if significant mobility of Ti and Zr took place during metamorphism, then it is likely that rutile and zircon would have grown in metasomatic vein structures (Schandl and others, 1990; Zeitler and others, 1990). However, no primary Ti- or Zr-bearing phases have been identified in the veins that cut the Wepawaug pelites. In view of the above evidence, Ti and Zr provide a logical starting point in the search for the best geochemical reference frame.

Two important observations can be made from the concentration systematics of Ti and Zr (fig. 5A). First, the Ti and Zr contents of the chlorite and biotite zone pelites form a tight cluster on figure 5A at

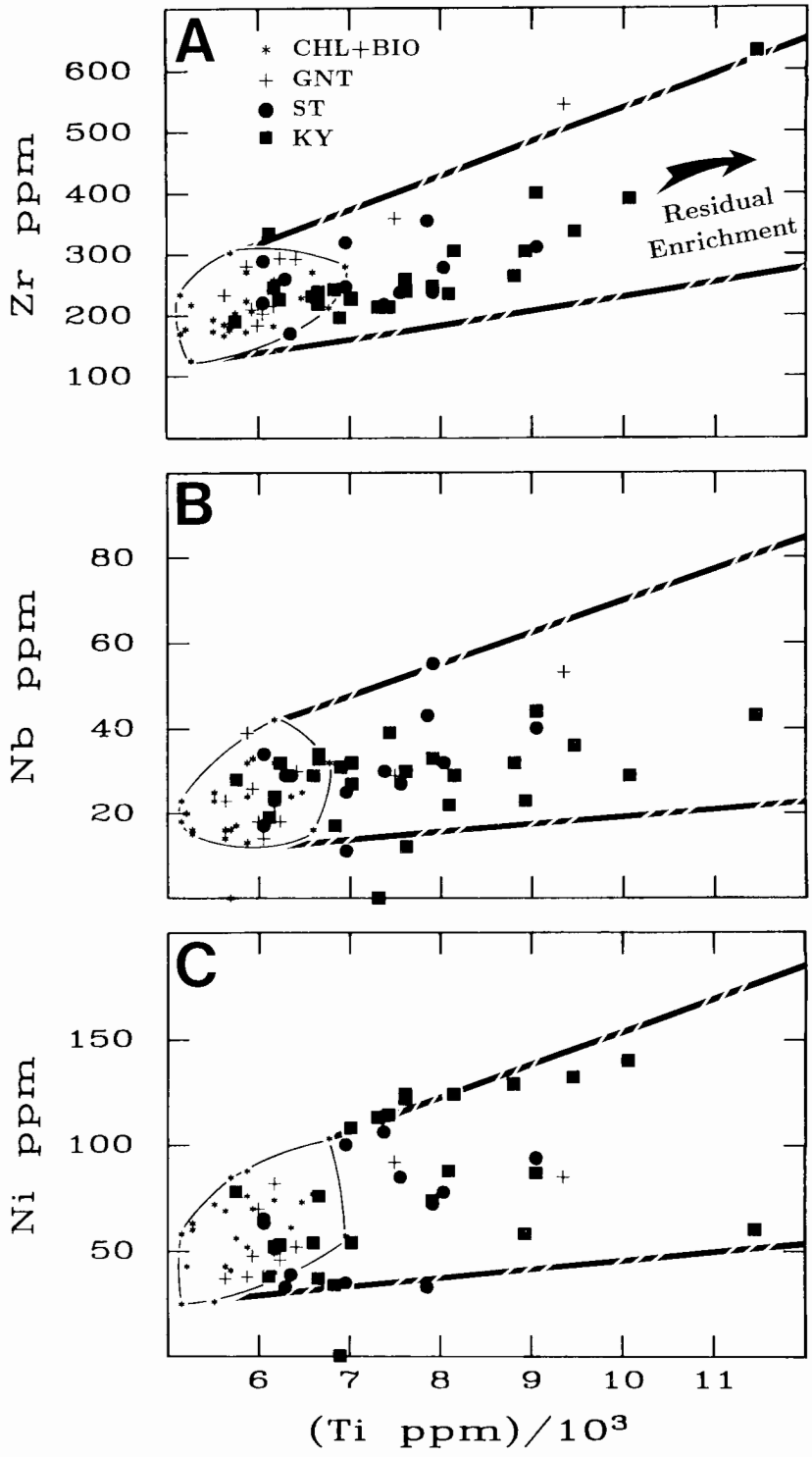

Fig. 5. Reference species. Metamorphic zones: CHL + BIO = chlorite + biotite; GNT = garnet; ST = staurolite; KY = kyanite. (A) Zr versus Ti. The simultaneous increases in Zr and Ti contents in the higher-grade rocks are interpreted to reflect residual enrichment due to mass loss of mobile constituents (compare fig. 4A). (B) Nb versus Ti. Two samples (JAW-2 and 113B) have Nb contents below the limit of detection (10 ppm); they are plotted using Nb = 0 ppm. (C) Ni versus Ti. One sample (JAW-110) has a Ni content below the limit of detection (10 ppm); it is plotted at Ni = 0 ppm.

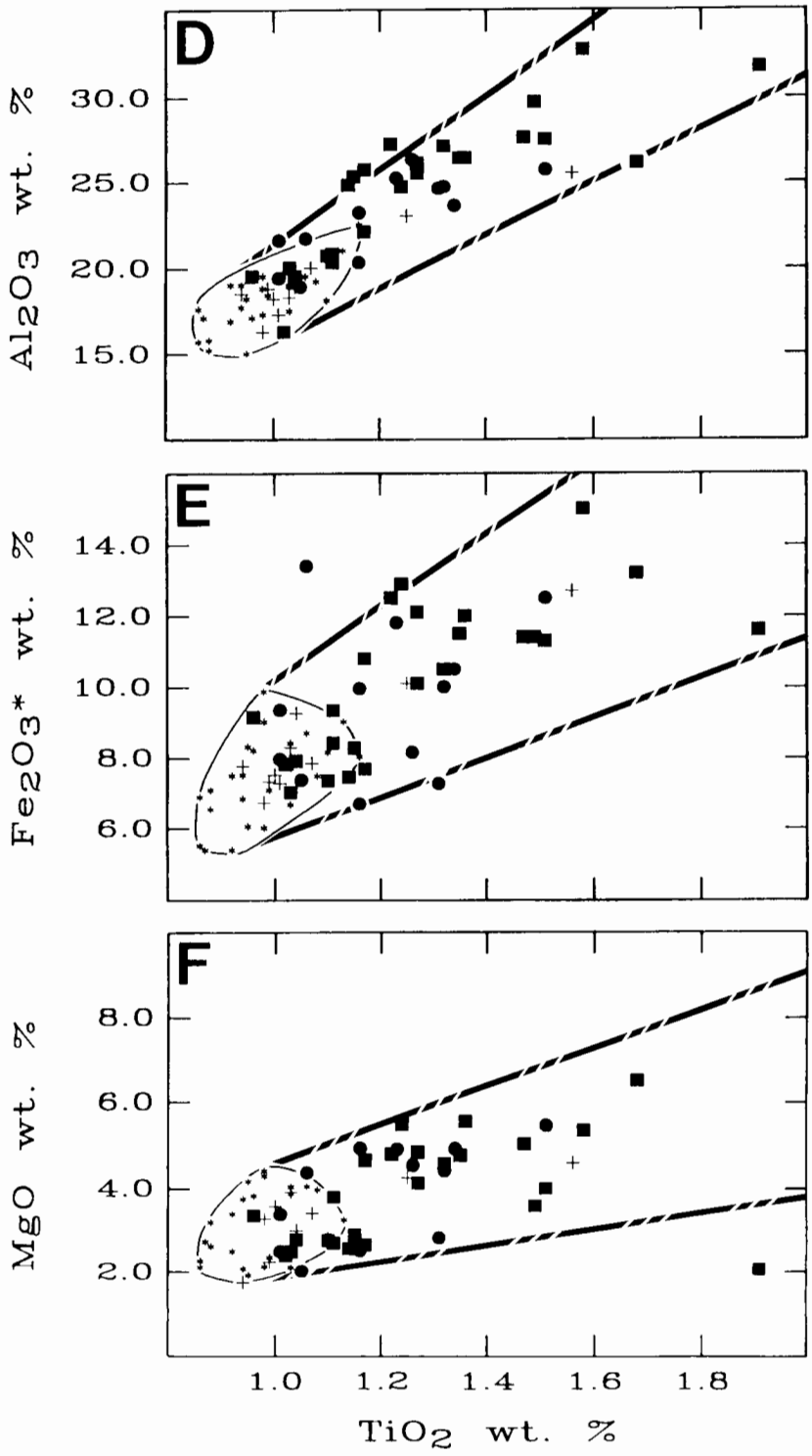

Fig. 5(D) Al_2O_2 versus TiO_2. (E) $Fe_2O_3^*$ versus TiO_2. All Fe as Fe^{3+}. (F) MgO versus TiO_2.

average concentration levels that are markedly lower than those found in the higher-grade rocks. Second, the Ti and Zr contents of garnet, staurolite, and kyanite zone samples form a data array extending to the right of the chlorite + biotite zone field to Ti and Zr concentrations that may be as much as ~100 percent greater than those of the average low-grade pelite. Furthermore, the kyanite zone rocks have the highest average Ti and Zr contents. Similar chemical relations are evident for Nb, Ni, Al, Fe, and Mg (fig. 5B-F). The relations shown in figure 5 strongly suggest that compositional variations in the Wepawaug are correlated with metamorphic intensity.

The concentration systematics of reference species must be consistent with the residual enrichment/dilution model (abbreviated as "residual model") shown in figure 4. This requirement is satisfied for the arrays of Ti, Zr, Nb, Ni, Al, Fe, and Mg abundances defined by nearly all of the garnet, staurolite, and kyanite zone samples, under the constraint that the low-grade chlorite and biotite zone rocks are representative of the "protolith" (fig. 5). This result holds true regardless of which element is used as the x-axis variable (the full set of graphs is not shown for brevity). Consequently, Ti, Zr, Nb, Ni, Al, Fe, and Mg are viable candidates for the geochemical reference frame.

It should be noted that in the following discussion, the chlorite and biotite zone rocks are grouped together because no significant differences in composition were found between them, other than minor differences in volatile content.

Evidence of element mobility.—The residual model (fig. 4) and $\hat{\Xi}_{j,i}$ values (eq 4) serve as powerful tools for determining if evidence for element mobility exists in the Wepawaug Schist. For convenience, the standard of comparison in this effort should be an element whose chemical behavior is consistent with the requirements for a reference species. Although any of the elements shown in figure 5 could serve as the reference, Ti is used here for reasons discussed in detail below.

The geochemical systematics of SiO_2, P_2O_5, and Na_2O relative to TiO_2 are shown in figure 6. The behaviors of Si, P, and Na are grossly inconsistent with the residual model. In general, SiO_2, P_2O_5, and Na_2O concentrations *decrease* with increasing TiO_2 content (fig. 6A, B, and C).

The behavior of Ca is probably inconsistent with the residual model because there is no discernible positive correlation between TiO_2 and CaO for the garnet, staurolite, and kyanite zone pelites (fig. 6D). However, interpretation is made difficult by the fact that there is a large variation in CaO/TiO_2 in the low-grade rocks (CaO/TiO_2 varies over an order of magnitude range). The heterogeneity could be due to a number of factors. For example, because the Ca content of the low-grade pelites is strongly dependent on modal Ca-carbonate content, small variations in carbonate mineral abundance can lead to relatively large variations in whole-rock CaO. Moreover, there is field evidence of very late remobilization of calcite into small (millimeter to centimeter scale) vein structures

associated with kink folding in some of the chlorite zone rocks (Ague, 1994).

MnO-TiO_2 relations are shown in figure 6E. A sizeable proportion ($\sim$25 percent) of the amphibolite facies rocks have MnO/TiO_2 ratios significantly higher than those observed in the chlorite, biotite, and garnet zones. This fact can be highlighted by constructing a theoretical residual enrichment/dilution field using the chlorite + biotite zone rocks as the "protolith" (fig. 6E).

K_2O-TiO_2 relations are illustrated in figure 6F. Many of the samples are consistent with the residual model, but the K_2O/TiO_2 ratios of the staurolite zone rocks are, on average, noticeably higher than those of the other zones.

The geochemical behaviors of the trace elements Rb, Sr, Ba, and Zn are shown relative to Ti in figure 7. Rb-Ti systematics are generally consistent with the residual model (fig. 7A). Sr-Ti and Ba-Ti relations (fig. 7B and C) are similar to those described above for CaO-TiO_2 and K_2O-TiO_2, respectively (compare fig. 6D and F). With respect to Zn, about $\sim$30 percent of the amphibolite facies rocks have Zn/Ti ratios significantly higher than those observed in the chlorite, biotite, and garnet zones (fig. 7D).

While the residual model can be used to ascertain general relations between elements, it is also instructive to examine the geochemistry of the "average" chlorite + biotite, garnet, staurolite, and kyanite zone pelite. Average chemical trends were investigated by examining $\hat{\Xi}_{j,TiO_2}$ values as functions of metamorphic grade.

Significant major and minor element compositional differences exist between the various metamorphic zones. For example, $\hat{\Xi}_{SiO_2,TiO_2}$ values decrease progressively with increasing grade (fig 8A). Kyanite zone rocks have very low $\hat{\Xi}_{P_2O_5,TiO_2}$ (fig. 8B), and staurolite and kyanite zone rocks have $\hat{\Xi}_{Na_2O,TiO_2}$ values markedly lower than the greenschist facies pelites (fig. 8C). The large amount of variability in chlorite + biotite zone pelite CaO/TiO_2 makes interpretation of overall trends in $\hat{\Xi}_{CaO,TiO_2}$ difficult to assess. However, although uncertainties are large, $\hat{\Xi}_{CaO,TiO_2}$ values may decrease slightly from the garnet to the kyanite zone (fig. 8D). Staurolite and kyanite zone rocks have the highest $\hat{\Xi}_{MnO,TiO_2}$ (fig. 8E). The highest values of $\hat{\Xi}_{K_2O,TiO_2}$ are found in the staurolite zone suite (fig. 8F).

A diverse spectrum of chemical behavior is apparent for the trace elements Sr, Ba, Zn, and Rb. The systematics of $\hat{\Xi}_{Sr,Ti}$ and $\hat{\Xi}_{Ba,Ti}$ (fig. 9A and B) are similar to those of $\hat{\Xi}_{CaO,TiO_2}$ and $\hat{\Xi}_{K_2O,TiO_2}$, respectively (compare fig. 8D and F). Although $\hat{\Xi}_{Zn,Ti}$ and $\hat{\Xi}_{MnO,TiO_2}$ relations are also broadly similar (compare figs. 9C and 8E), the correlation between ln (Zn/Ti) and ln (MnO/TiO_2) is poor (fig. 10). Rocks with elevated Zn/Ti need not have elevated MnO/TiO_2 and *vice versa*. Thus, the chemical behaviors of Zn and Mn appear to have been decoupled largely from one another. Finally, $\hat{\Xi}_{Rb,Ti}$ values (not illustrated) do not vary significantly as a function of metamorphic grade.

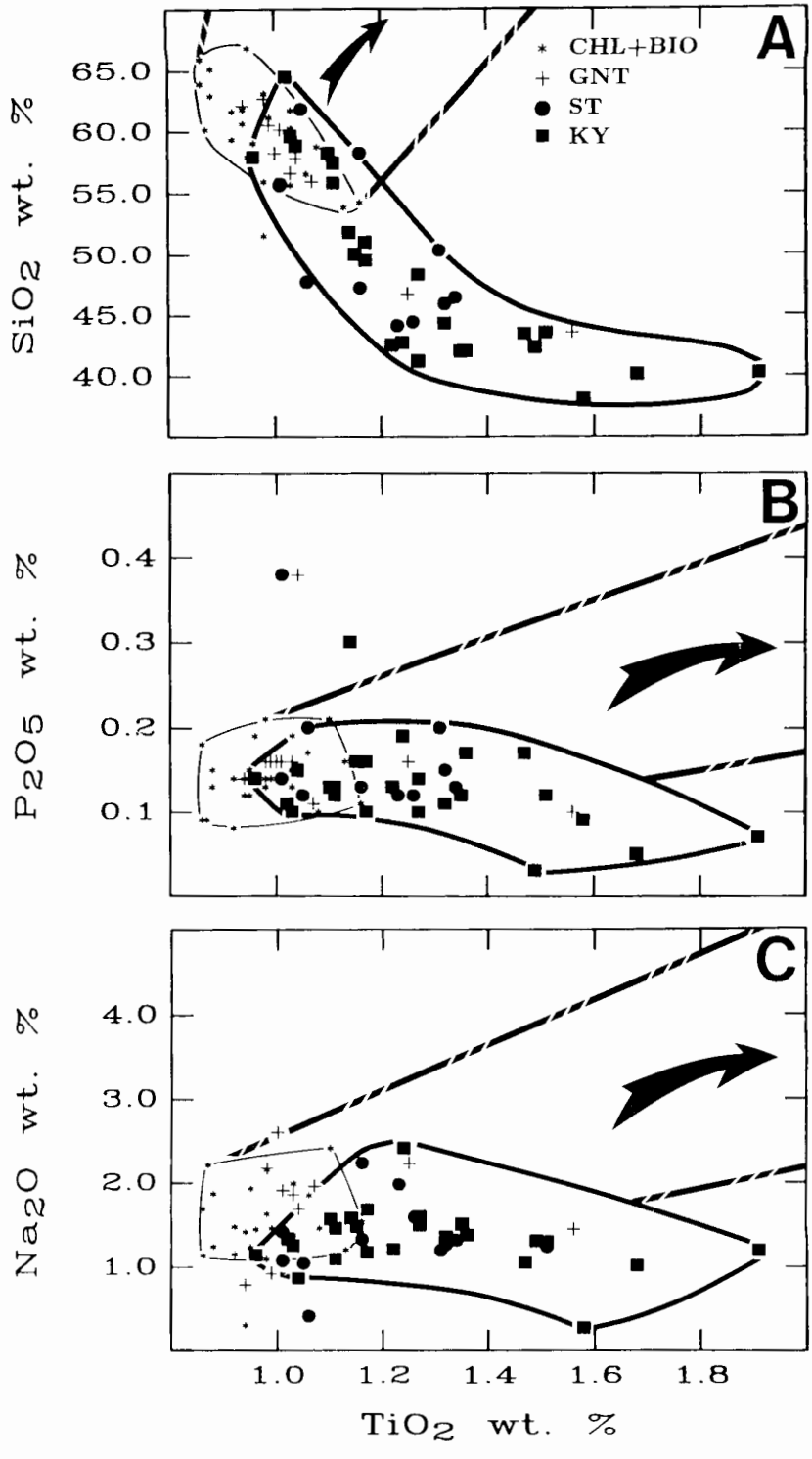

Fig. 6. Evidence of major and minor element mobility. Ti is the reference species. The arrows highlight the ideal residual model trajectory, assuming that the chlorite + biotite zone rocks represent the protolith (compare fig. 4). (A) SiO_2 versus TiO_2. In general, SiO_2 content decreases with increasing TiO_2. (B) P_2O_5 versus TiO_2. (C) Na_2O versus TiO_2.

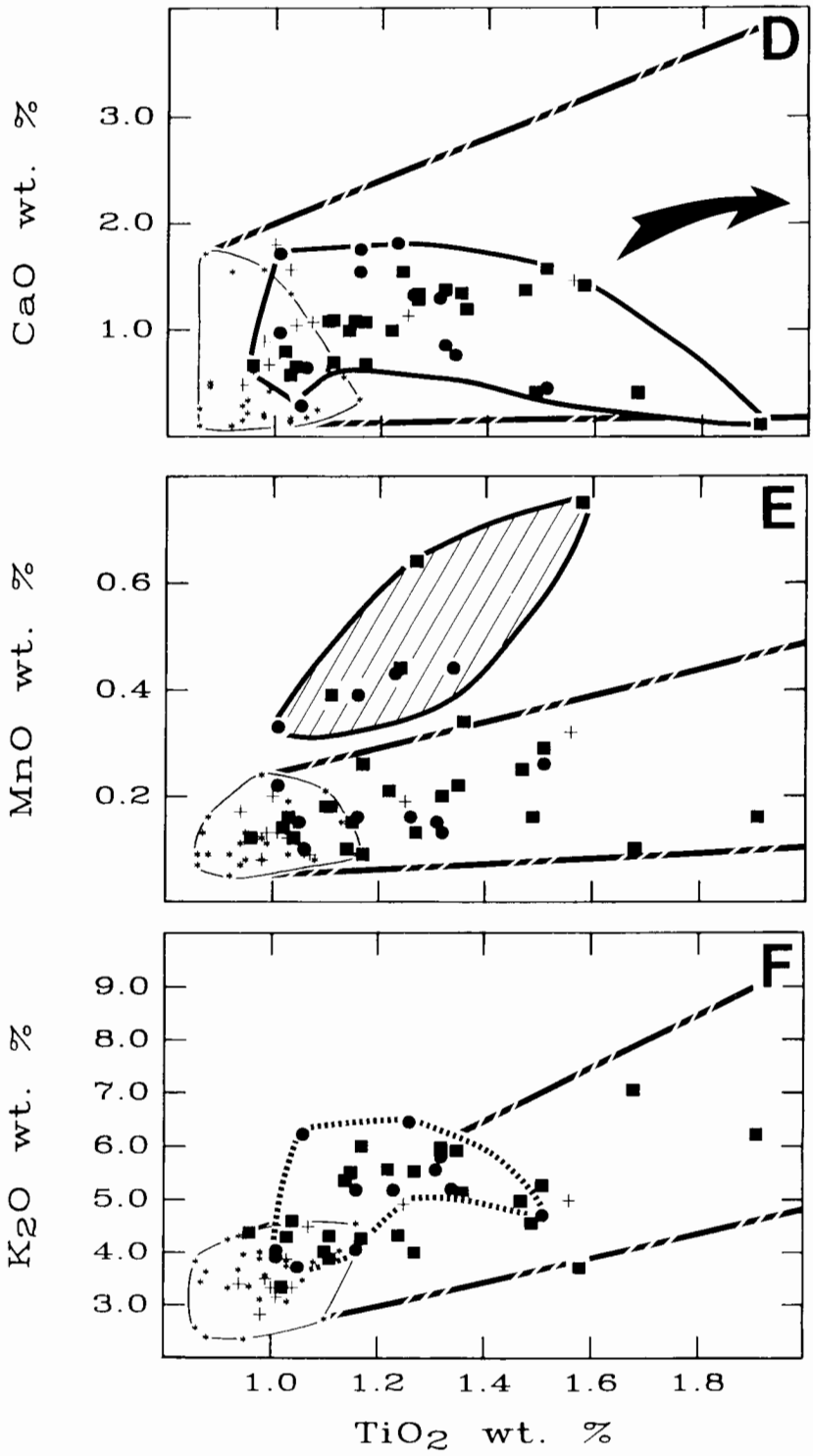

Fig. 6(D) CaO versus TiO_2. (E) MnO versus TiO_2. About 25 percent of the amphibolite facies samples have MnO/TiO_2 ratios in excess of those observed in the chlorite, biotite, and garnet zones. Elevated MnO/TiO_2 samples are highlighted by the diagonal ruled field. (F) K_2O versus TiO_2. Staurolite zone samples are enclosed by the dashed line. Note high average K_2O/TiO_2 ratios of the staurolite zone pelites.

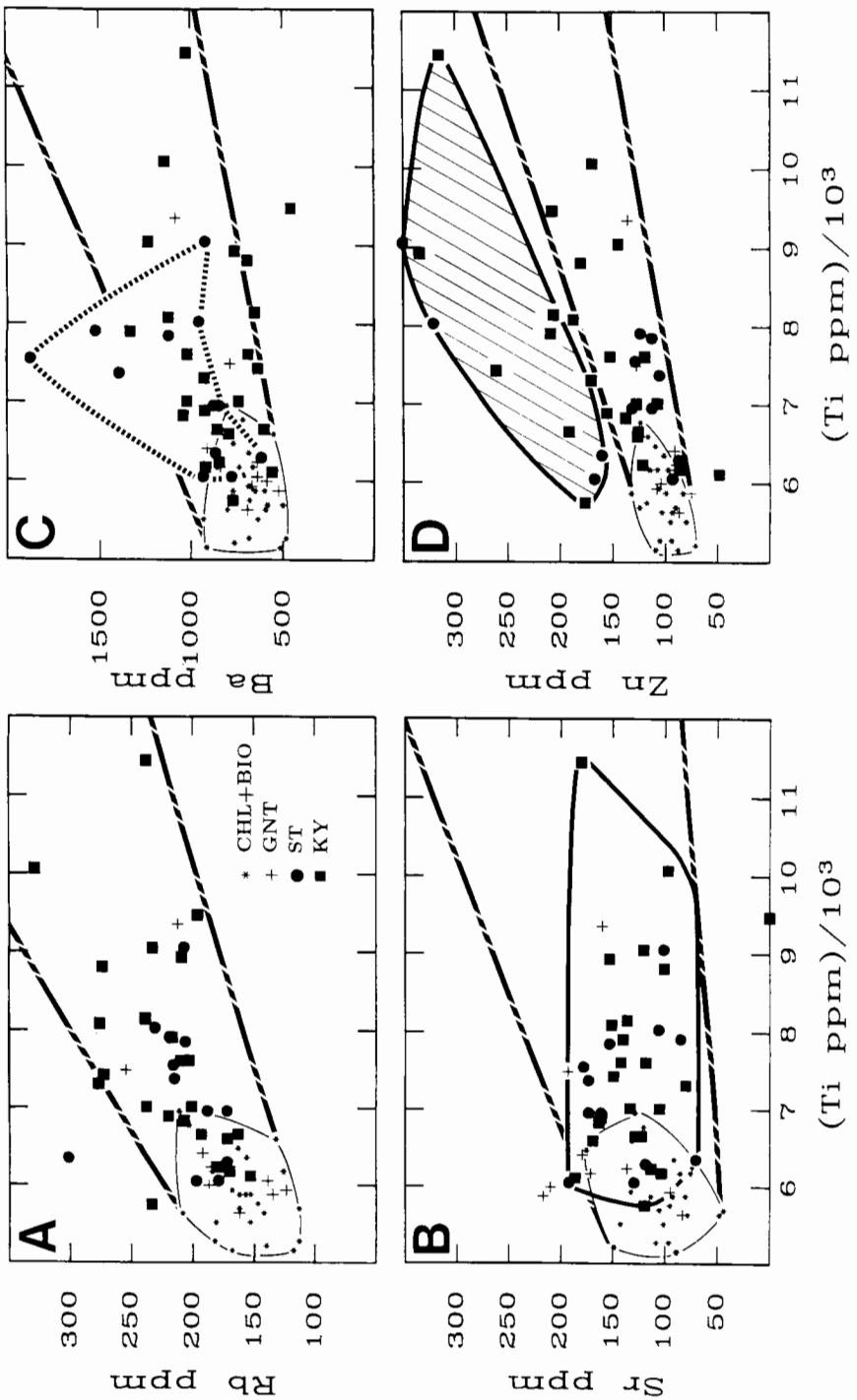

Fig. 7. Selected trace element systematics: (A) Rb versus Ti; (B) Sr versus Ti; (C) Ba versus Ti. Staurolite zone samples are enclosed by the dashed line. Compare with figure 6F; (D) Zn versus Ti. About 30 percent of the amphibolite facies rocks have Zn/Ti ratios in excess of those observed in the chlorite, biotite, and garnet zones. Elevated Zn/Ti samples are highlighted by the diagonal ruled field.

In summary, the relations presented above are inconsistent with the null hypothesis that the chemistry of aluminous Wepawaug pelite is invariant as a function of metamorphic grade. However, it remains to be shown that the chemical variations are the result of metamorphic processes.

Rock density.—Knowledge of rock density variations is essential for computing volume strain. In the Wepawaug pelites, ρ_g increases with increasing metamorphic grade (fig. 11). Average ρ_g values for the chlorite + biotite, garnet, staurolite, and kyanite zones are 2.78 ± 0.008, 2.85 ± 0.038, 2.89 ± 0.026, and 2.95 ± 0.042 g cm^{-3}, respectively ($\pm 2\sigma$).

REGIONAL VARIATIONS IN ALUMINOUS PELITE COMPOSITION AND DENSITY

Mapping of chemical alteration phenomena caused by crustal fluid transport processes provides perhaps the most critical constraints for understanding regional flow patterns in hydrothermal systems (Meyer and others, 1968; Rye and Rye, 1974; Taylor, 1974; Lowell and Guilbert, 1970; Wickham and Taylor, 1985; Chamberlain and Rumble, 1988; Ferry, 1992). Therefore, surface contour maps of key physicochemical variations in the Wepawaug Schist were prepared. The maps were constructed using Precision Visuals Inc. computer subroutines, as discussed previously by Ague and Brimhall (1988). No smoothing of the input data sets was performed, and the contour surfaces pass through all the input data points. In cases where multiple samples from a particular outcrop were analyzed, results were averaged so that the outcrop could be represented by a single value for the purposes of contouring. The contour maps are intended to illustrate *general* changes in bulk-rock chemistry and ρ_g as functions of geographic position; they are not meant to be interpreted as highly precise representations of the full spectrum of composition and density variations that may occur from one outcrop to the next in the field. The physicochemical variations illustrated are independent of any assumptions regarding the protolith or the geochemical reference frame.

The concentrations of species whose chemical behavior is consistent with the residual model (Ti and Zr) increase progressively from east-to-west across the Wepawaug. As an example, contours of TiO_2 content are shown in figure 12A. The regional gradients in TiO_2 content are clearly related to the pattern of metamorphic isograds such that increases in TiO_2 and metamorphic grade are spatially coupled.

The regional variations in grain density (ρ_g) are equally impressive (fig. 12B). The systematic east-to-west increases in ρ_g in the formation mirror the east-to-west increases in both the metamorphic grade of the rocks and the concentrations of residual species such as Ti. These relationships strongly suggest that there are important links between metamorphic grade, chemical composition, and physical properties in the Wepawaug pelites.

Values of ln (SiO_2/TiO_2), ln (P_2O_5/TiO_2), ln (Na_2O/TiO_2), and ln (Na/Al) also vary strongly with geographic position. In general, ln (SiO_2/

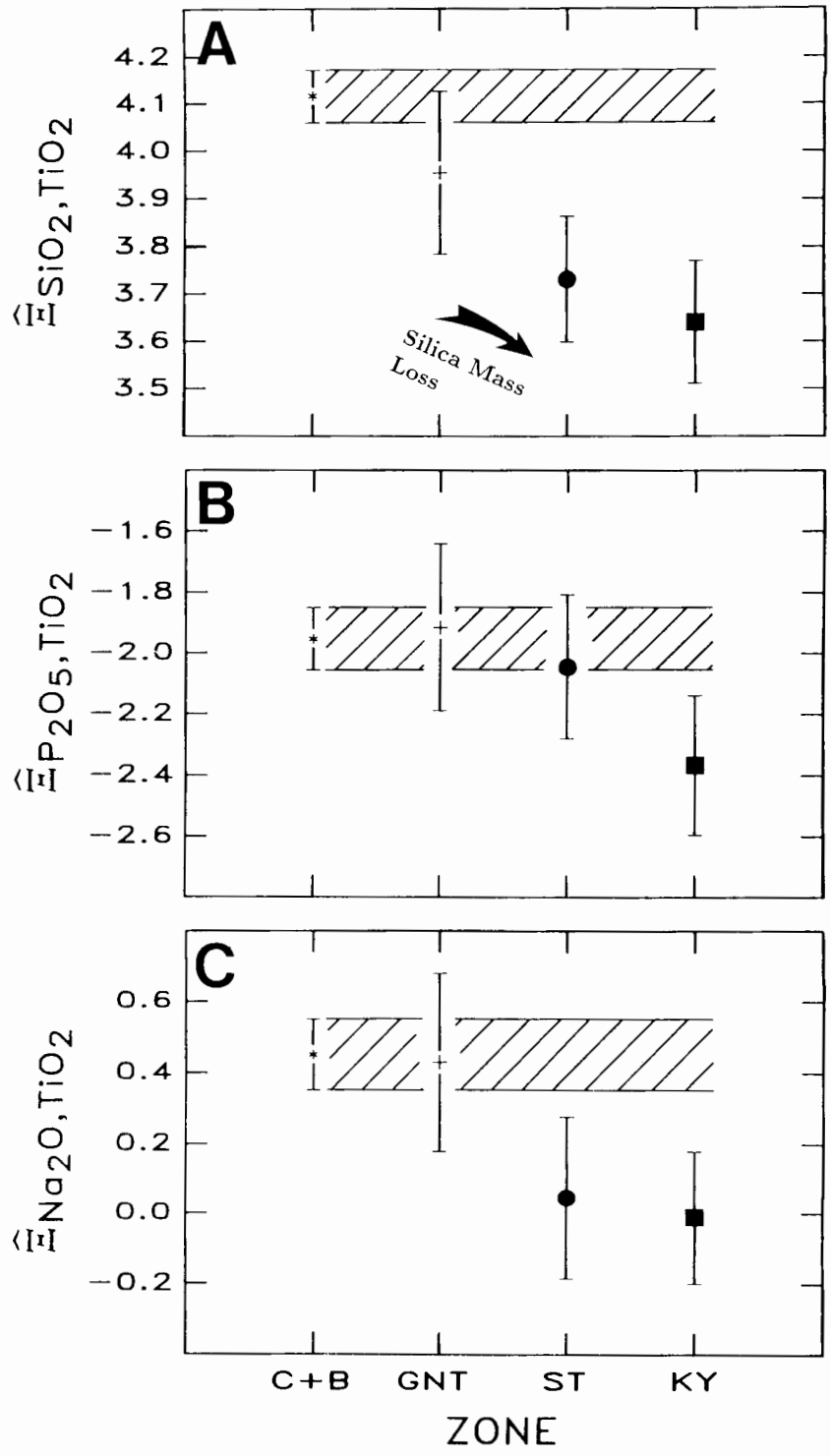

Fig. 8. $\hat{\Xi}_{j,TiO_2}$ (= avg ln (j/TiO_2) values for major and minor elements. Uncertainties are ±2σ. Metamorphic zones: C + B = chlorite + biotite; GNT = garnet; ST = staurolite; KY = kyanite. (A) $\hat{\Xi}_{SiO_2,TiO_2}$. Note the progressive decrease in the proportion of SiO_2, relative to a reference species such as TiO_2, as metamorphic grade increases. (B) $\hat{\Xi}_{P_2O_5,TiO_2}$. A major decrease in $\hat{\Xi}_{P_2O_5,TiO_2}$ is evident in the kyanite zone. (C) $\hat{\Xi}_{Na_2O,TiO_2}$. Note low $\hat{\Xi}_{Na_2O,TiO_2}$ values for the amphibolite facies pelites.

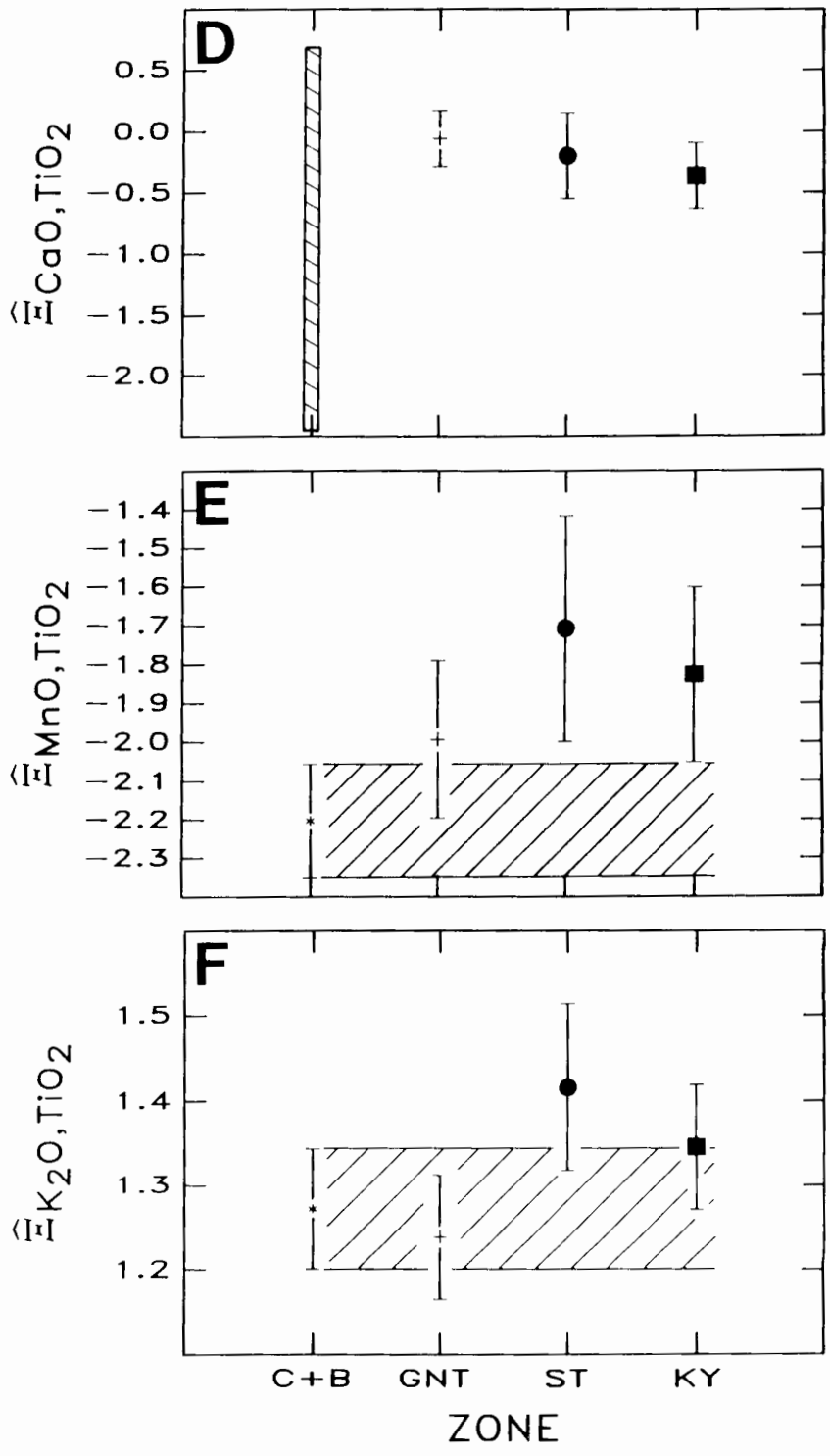

Fig. 8(D) $\hat{\Xi}_{CaO,TiO_2}$. Chlorite + biotite zone CaO contents vary widely; the range of observed ln (CaO/TiO_2) for these zones is shown with the ruled bar (see text). (E) $\hat{\Xi}_{MnO,TiO_2}$. Note elevated $\hat{\Xi}_{MnO,TiO_2}$ in the amphibolite facies. (F) $\hat{\Xi}_{K_2O,TiO_2}$. The staurolite zone samples have the highest average ln (K_2O/TiO_2). $\hat{\Xi}_{K_2O,TiO_2}$ for the chlorite + biotite and staurolite zones are significantly different at the 97.5 percent confidence level (see table 2).

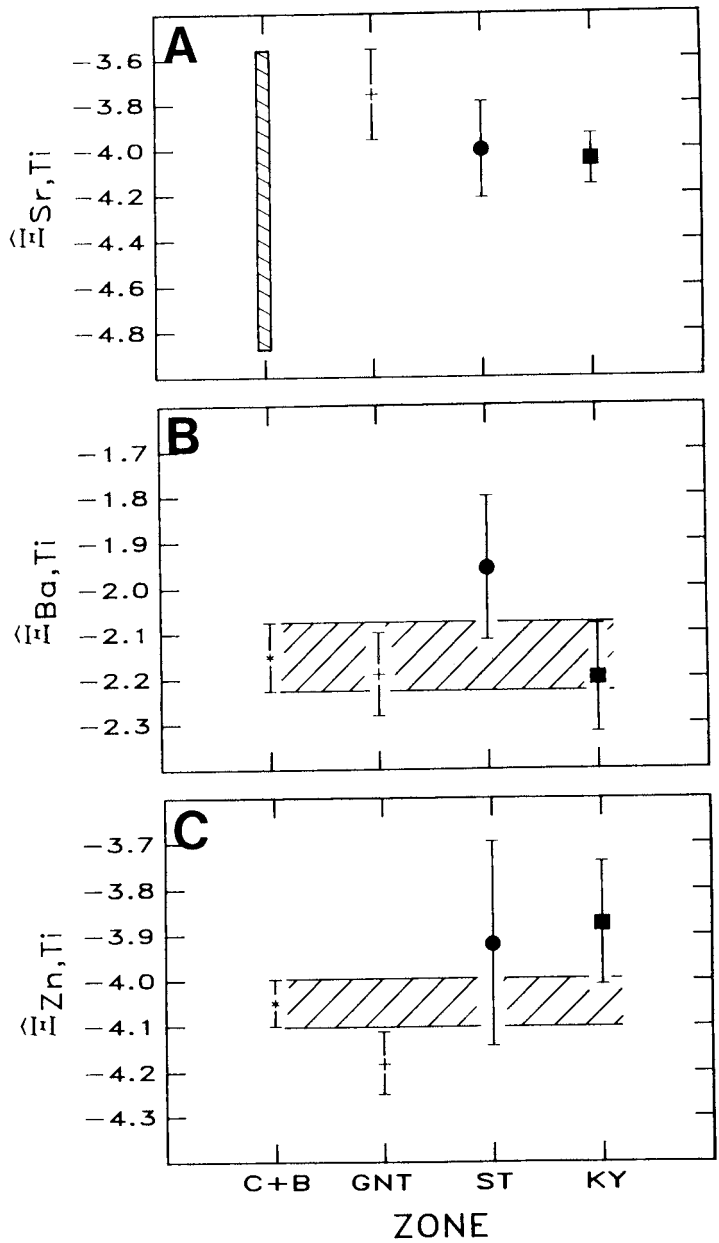

Fig. 9. $\hat{\Xi}_{j,Ti}$ (= avg ln (j/Ti)) for selected trace elements. Uncertainties are $\pm 2\sigma$. Metamorphic zones: C + B = chlorite + biotite; GNT = garnet; ST = staurolite; KY = kyanite. (A) $\hat{\Xi}_{Sr,Ti}$. Ruled bar illustrates range in observed ln (Sr/Ti) values (see text). (B) $\hat{\Xi}_{Ba,Ti}$. $\hat{\Xi}_{Ba,Ti}$ for the chlorite + biotite and staurolite zones are significantly different at the 98.3% confidence level (see table 2). Compare with figure 8F. (C) $\hat{\Xi}_{Zn,Ti}$.

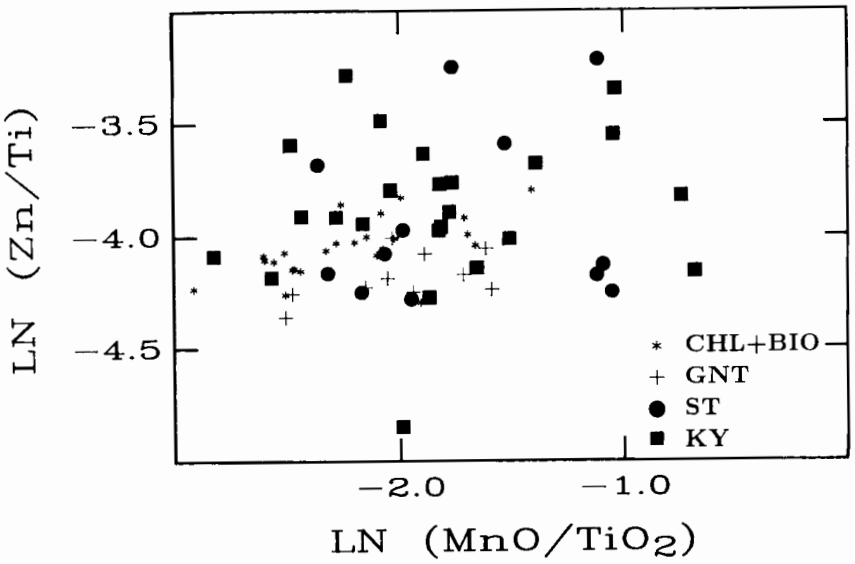

Fig. 10. ln (Zn/Ti) versus ln (MnO/TiO_2). Note the poor correlation between the two logratios for amphibolite facies rocks.

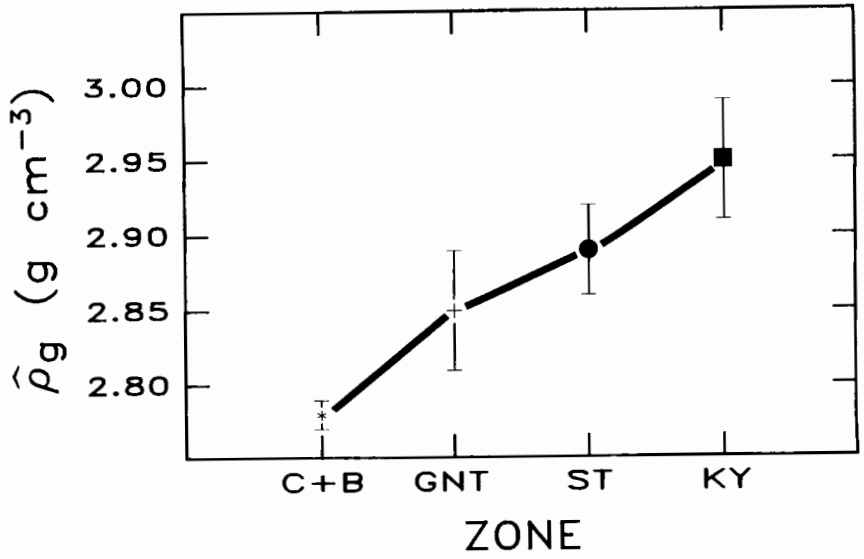

Fig. 11. Average grain densities ($\hat{\rho}_g$) for the various metamorphic zones. Note progressive increase in $\hat{\rho}_g$ with increasing metamorphic grade. Uncertainties are $\pm 2\sigma$. Metamorphic zones: C + B = chlorite + biotite; GNT = garnet; ST = staurolite; KY = kyanite.

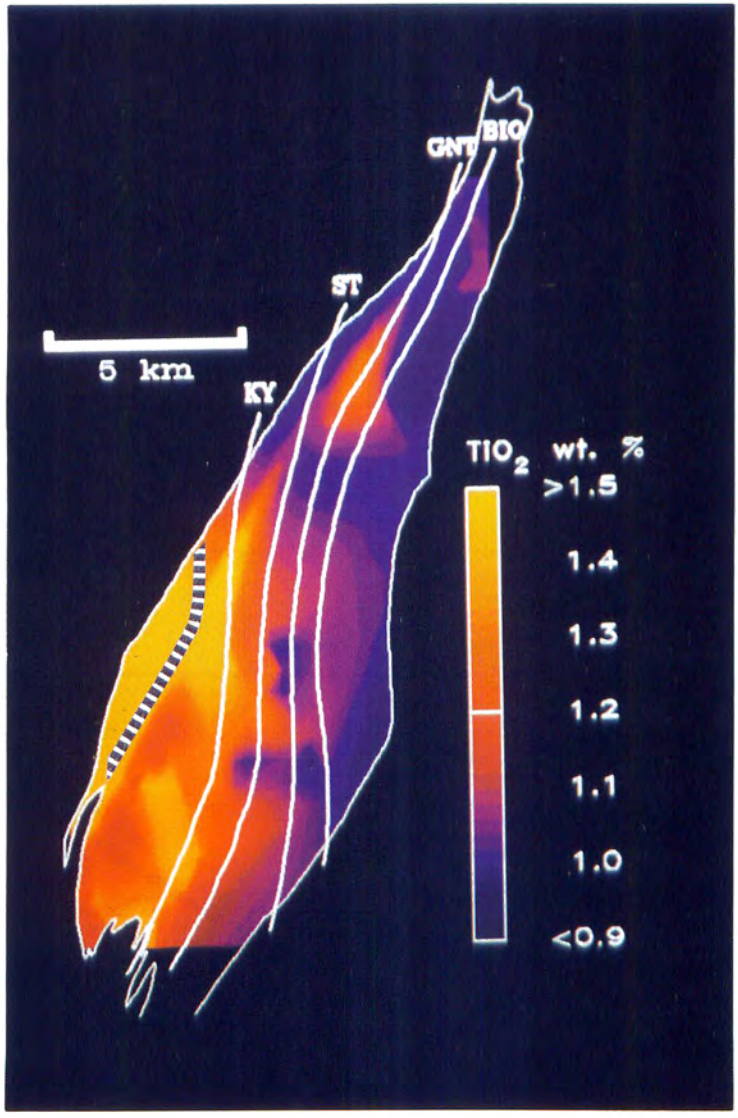

Fig. 12. Regional contour maps (A-H) of key physicochemical variables. Contours in the northwestern portion of the maps (west of the dashed line on A) should be regarded with caution because sampling density in this area is low owing to lack of exposure of fresh rock (fig. 3). (A) TiO_2 wt percent. Note the close spatial correspondence between the metamorphic isograds and the regional TiO_2 contours.

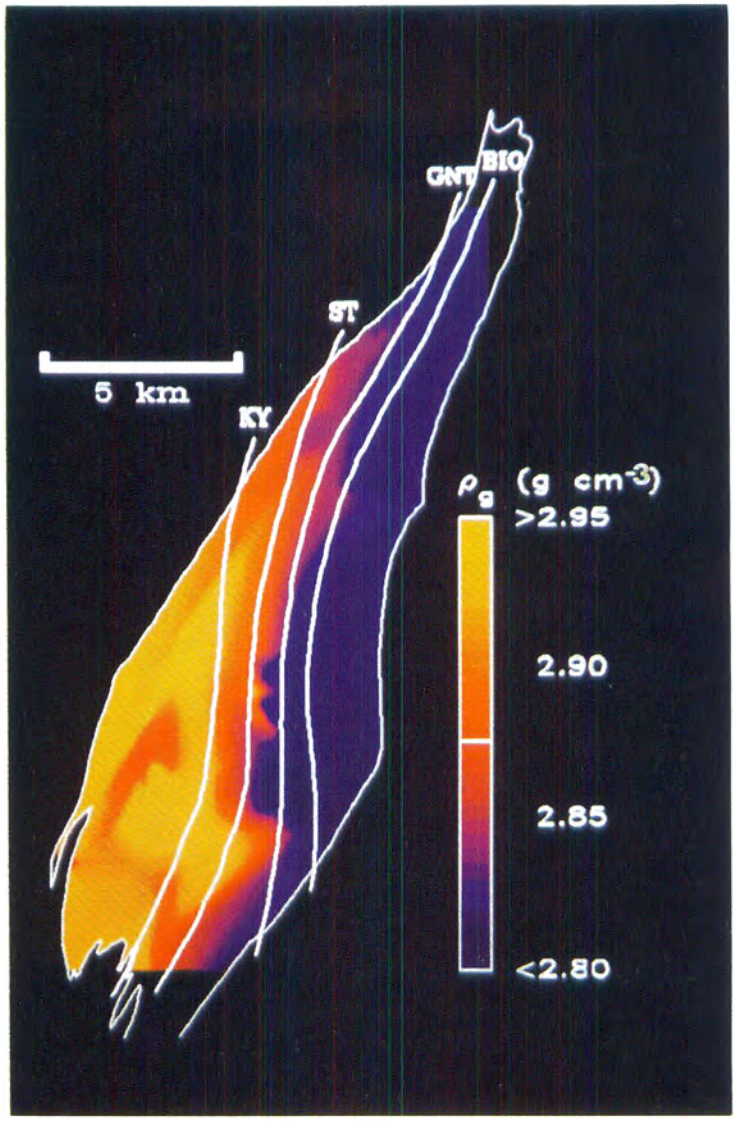

Fig. 12(B) ρ_g (g cm^{-3}).

TiO_2), ln (P_2O_5/TiO_2), and ln (Na_2O/TiO_2) decrease dramatically from east-to-west across the formation (fig. 12C, D, and E). Furthermore, the logratio contours are spatially correlated with the isograds, which suggests that a genetic relationship exists between bulk-rock compositional

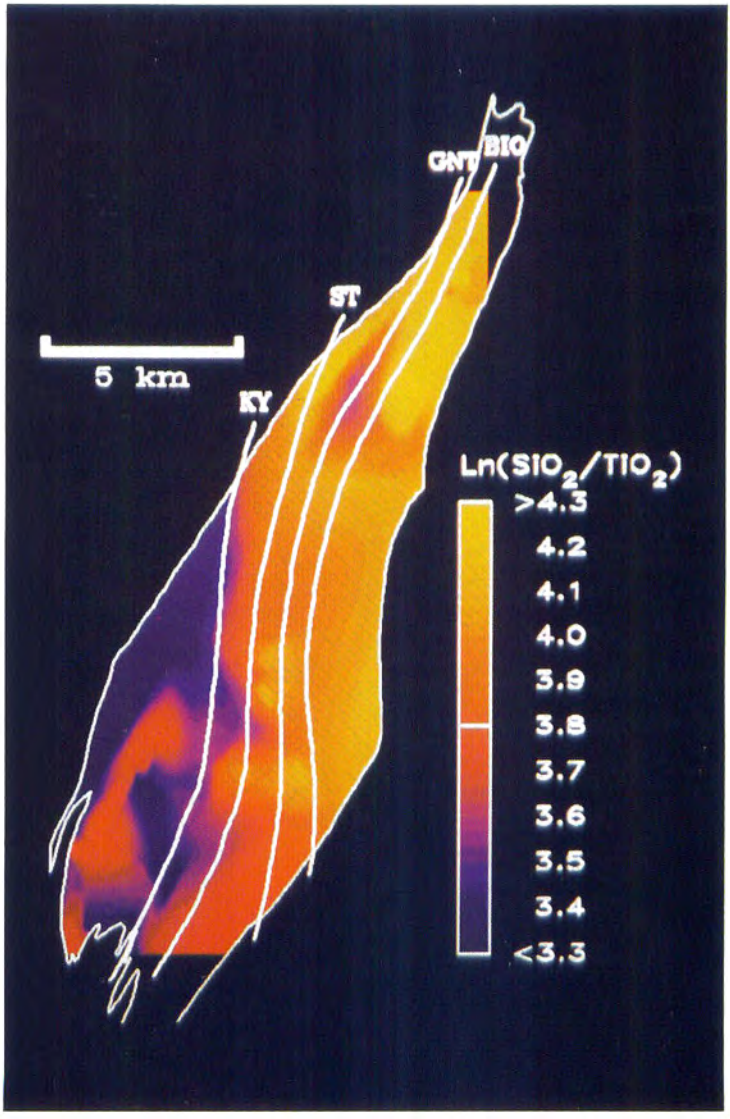

Fig. 12(C) ln (SiO_2/TiO_2).

changes and metamorphic processes. Hoschek (1967) and Thompson and others (1977) showed that the whole-rock Na/Al ratio is a critical factor in determining the mineralogy of pelites. As illustrated in figure 12F, ln (Na/Al) ratios (molar basis) attain extremely low values in the staurolite and kyanite zones.

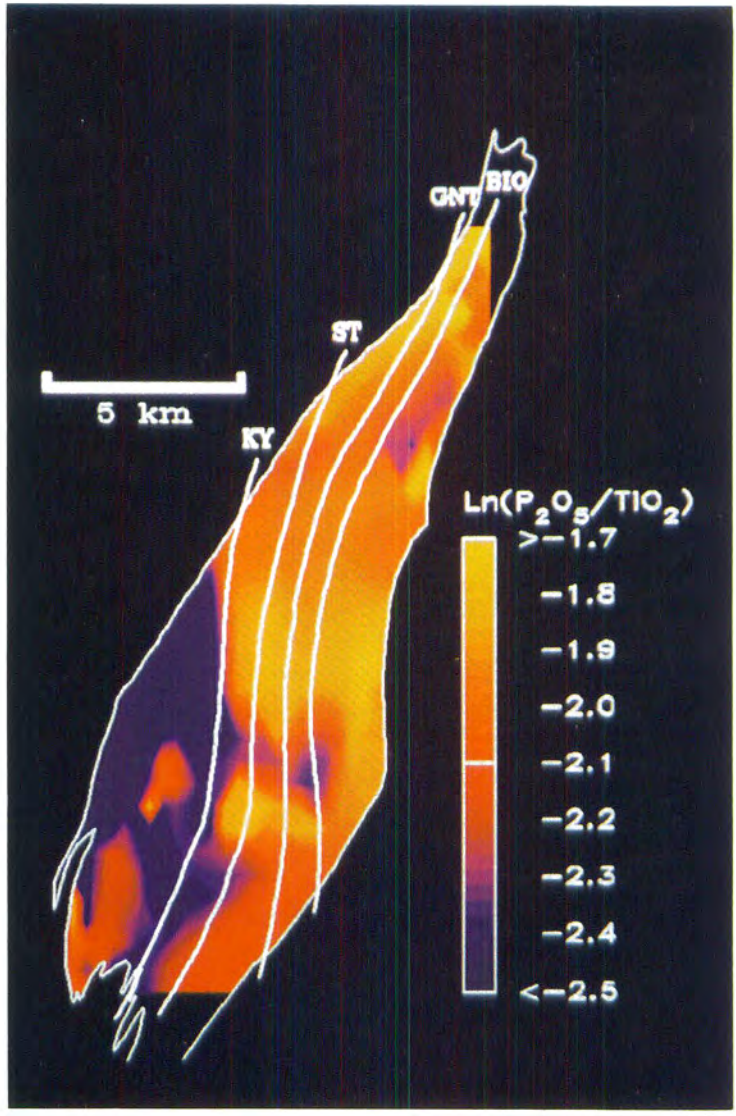

Fig. 12(D) ln (P_2O_5/TiO_2).

The regional variations in ln (MnO/TiO_2) and ln (Zn/Ti) are markedly different from the systematics of the other constituents discussed thus far (fig. 12G and H). Although the maximum values of the logratios are attained in the staurolite and kyanite zones (compare figs. 6E and 7D), there is no distinct relationship between the isograds and the

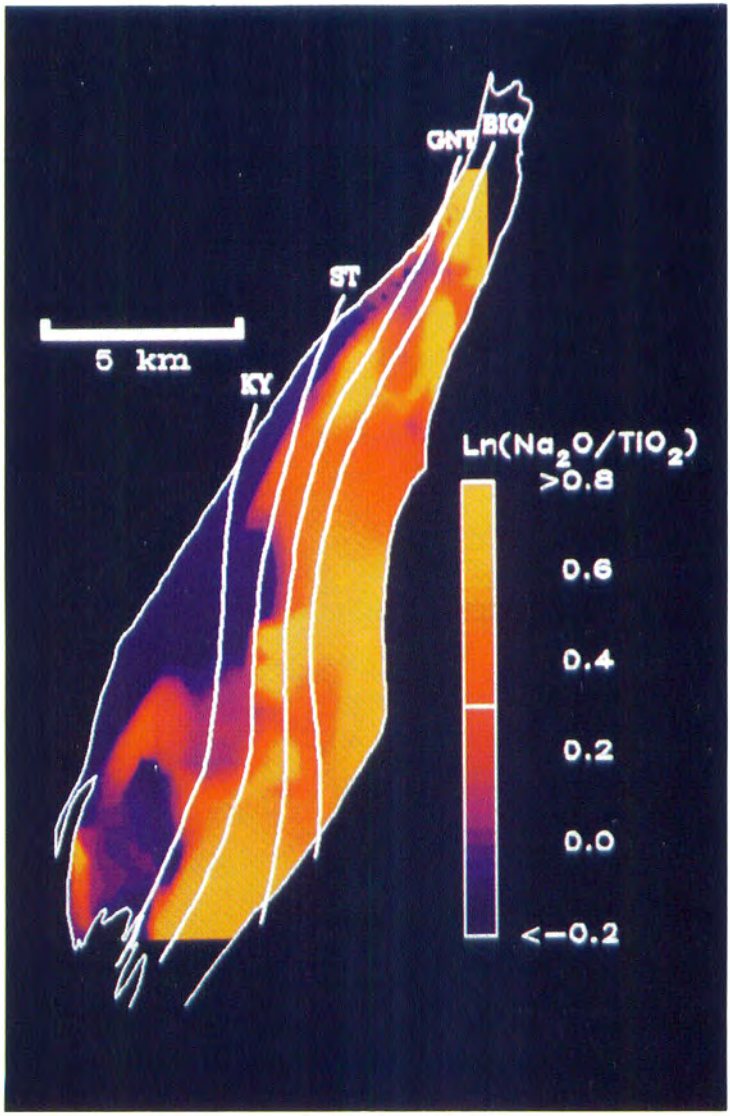

Fig. 12(E) ln (Na_2O/TiO_2).

regional ln (MnO/TiO_2) and ln (Zn/Ti) contours. The samples with the anomalously high whole-rock MnO/TiO_2 evident in figure 6E (corresponding to ln (MnO/TiO_2) > -1.3) are spatially restricted to the southernmost portions of the staurolite and kyanite zones. Although the

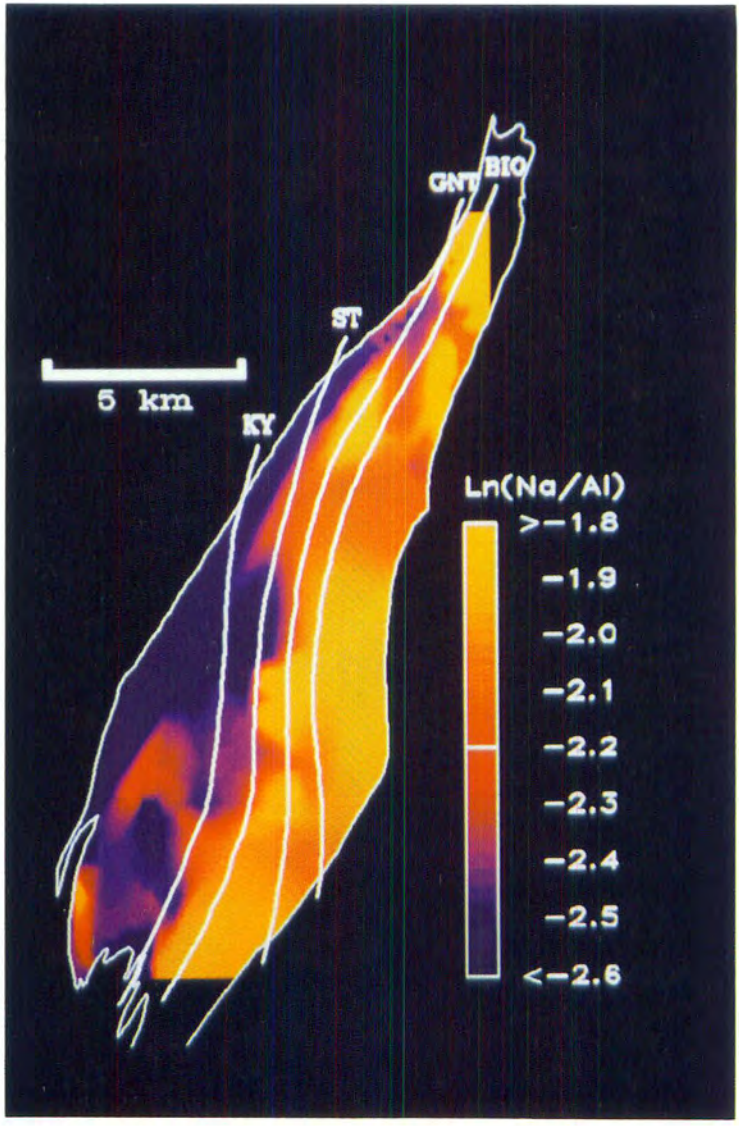

Fig. 12(F) ln (Na/Al) (molar ratio).

highest values of ln (Zn/Ti) also occur in the southern part of the amphibolite facies, the regional contours of ln (MnO/TiO_2) and ln (Zn/Ti) are noticeably different. This fact reflects the poor correlation between ln (MnO/TiO_2) and ln (Zn/Ti) discussed above (fig. 10).

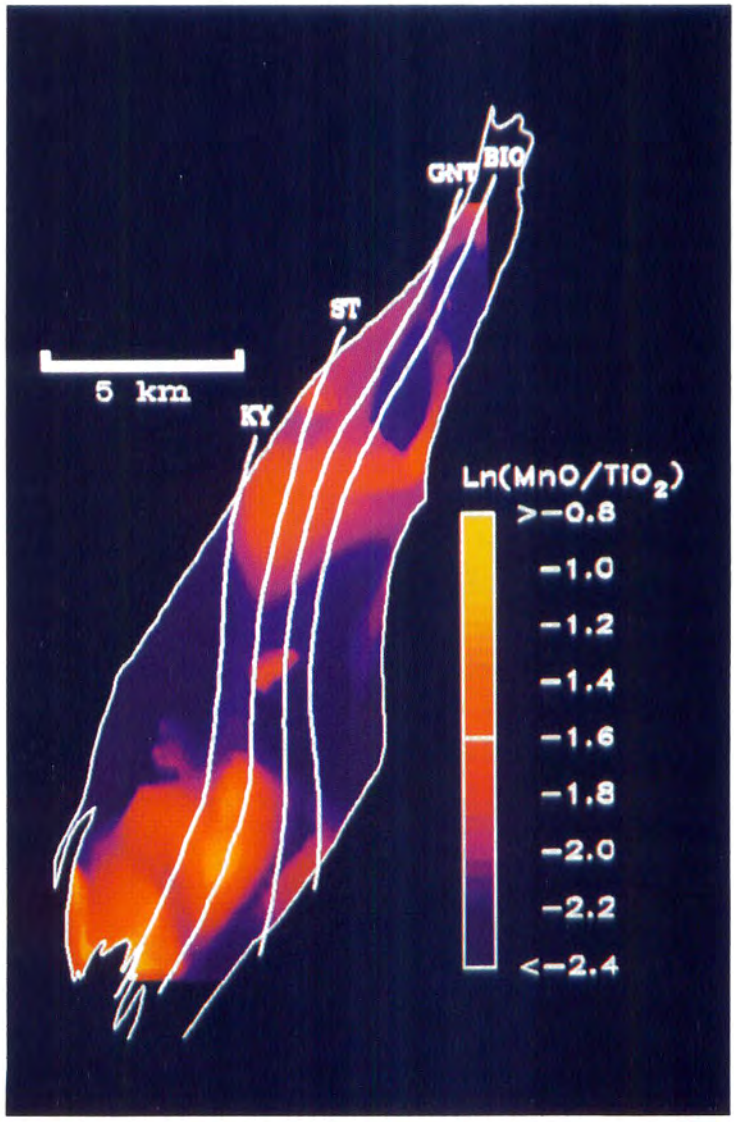

Fig. 12(G) ln (MnO/TiO_2). The highest ln (MnO/TiO_2) ratios are found in the southern portion of the field area.

ORIGIN OF THE PHYSICOCHEMICAL VARIATIONS

Statistical analysis and regional mapping of rock chemistry and density strongly suggest that significant variations in aluminous pelite compositions and physical properties exist across the Wepawaug Schist.

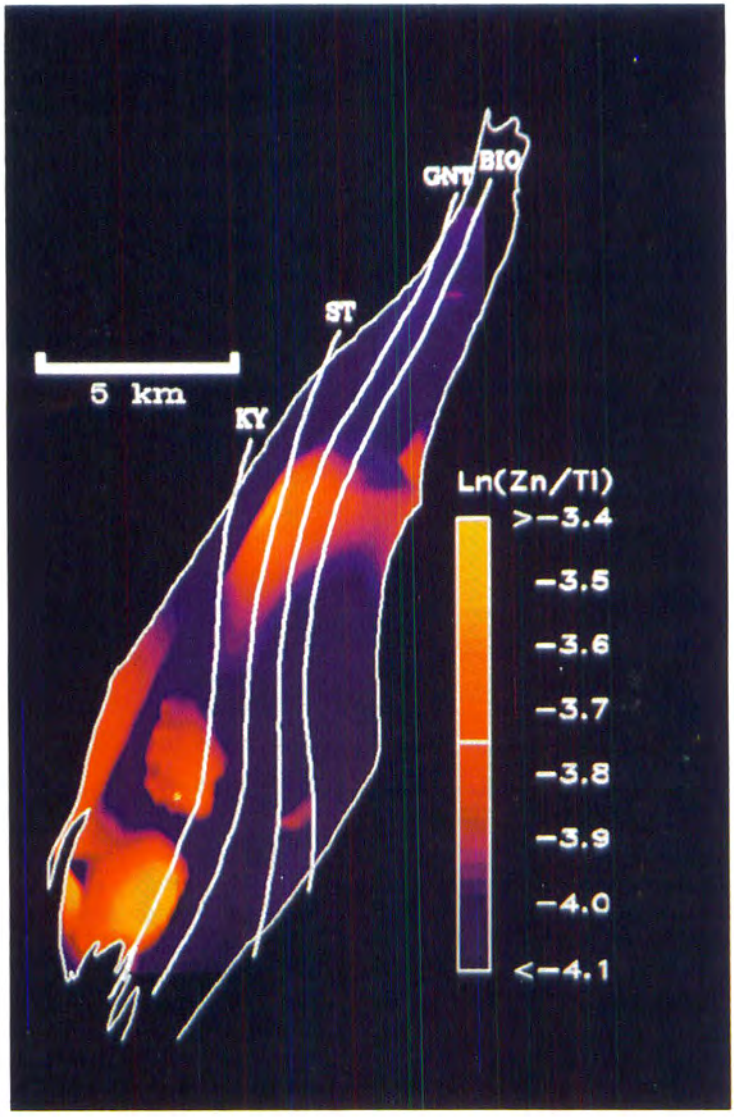

Fig. 12(H) ln (Zn/Ti).

The next task is to ascertain if the variations are the result of sedimentary processes or regional metamorphism.

Chemical comparisons with shale and slate.—If the observed chemical variations are a consequence of sedimentary processes, then the Wepawaug pelites should have compositions comparable to those of sedimen-

tary rocks. In table 1, the average low-grade Wepawaug pelite composition computed from the data given in app. D is shown relative to the average shale and slate composition computed from the data compiled by Ague (1991). From inspection, it can be seen that the two averages are very similar. The most obvious difference is that the Wepawaug rocks have less CaO than average shale and slate. The close correspondence between shale and slate and the low-grade Wepawaug pelite compositions strongly suggests that the low-grade Wepawaug rocks retain a sedimentary/diagenetic chemical signature that has not been severely modified by metamorphism (with the possible exception of Ca).

TABLE 1

Low-grade Wepawaug pelite compared to shale and slate

	Low-grade Wepawaug*	Shale and Slate†
SiO_2	60.34	60.34
TiO_2	0.99	0.76
Al_2O_3	18.20	17.05
Fe_2O_3	7.37	7.37
MgO	3.02	2.69
MnO	0.11	0.09
CaO	0.36	1.45
Na_2O	1.55	1.55
K_2O	3.52	3.64
H_2O	—	4.25
CO_2	—	1.05
LOI	4.42	—

Notes: All Fe as Fe_2O_3. LOI: Loss on ignition.
* Chlorite and biotite zone average computed using the method of Aitchison (1989).
† Average from Ague (1991).

The compositions of the higher-grade Wepawaug rocks, on the other hand, may deviate substantially from those of typical shale and slate. As shown in figure 13A and B, the medium- and high-grade Wepawaug schists may have extremely low SiO_2/TiO_2 and SiO_2/Al_2O_3—much lower than typical shales and slates. The most silica-poor Wepawaug sample has 32.7 wt percent Al_2O_3, 1.58 wt percent TiO_2, and only 38.1 wt percent SiO_2 (JAW-114A; kyanite zone). In contrast, the vast majority of shales and slates have Al_2O_3 and TiO_2 contents less than about 22 and 1.2 wt percent, respectively, and SiO_2 contents well in excess of 50 wt percent (compare Pettijohn, 1975; Ague, 1991; Wintsch and others, 1991). The greenschist and amphibolite facies rock compositions compiled by Ague (1991) also form a data array which extends to SiO_2/Al_2O_3 and SiO_2/TiO_2 values significantly lower than those of shales and slates (fig. 13C and D). A sizeable proportion of the higher-grade rocks studied here and by Ague (1991) apparently have *no* compositional analogues in the shale and slate group (fig. 13B, C, and D).

Residual clay-rich soils formed *in situ* due to severe weathering of underlying bedrock sometimes have SiO_2/TiO_2 or SiO_2/Al_2O_3 ratios

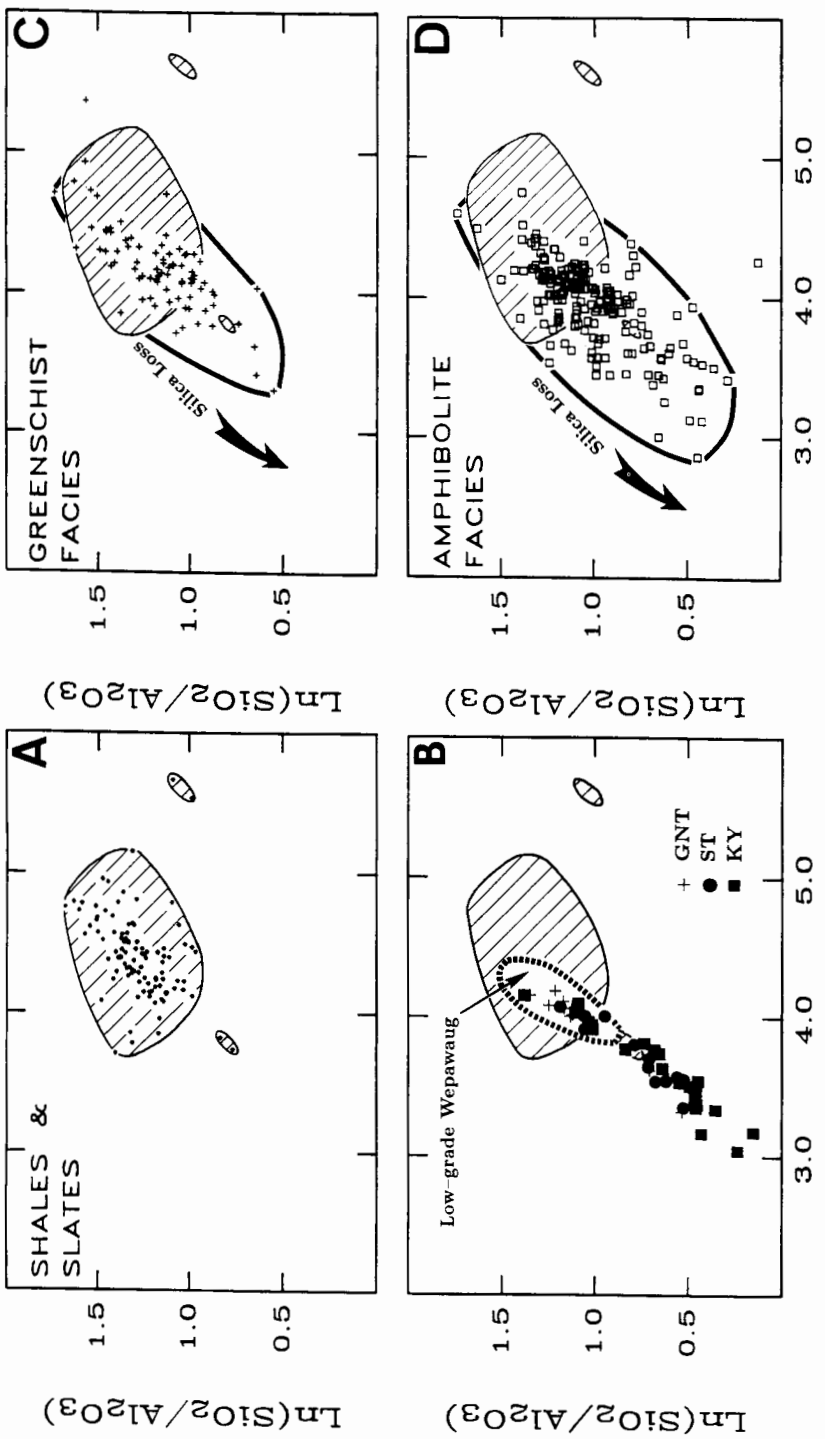

Fig. 13. ln (SiO_2/Al_2O_3) versus ln (SiO_2/TiO_2). (A) Previously published shale and slate compositions. Data compiled by Ague (1991), $N = 105$. (B) Wepawaug pelite ln (SiO_2/Al_2O_3) and ln (SiO_2/TiO_2) in relation to field of shale and slate compositions (ruled pattern). Note that the low-grade Wepawaug pelites (chlorite + biotite zone; data points omitted for clarity) have ln (SiO_2/Al_2O_3) and ln (SiO_2/TiO_2) comparable to shale and slate. However, the higher-grade rocks may have significantly lower ln (SiO_2/Al_2O_3) and ln (SiO_2/TiO_2). (C) Previously published greenschist facies (chlorite, biotite, and garnet zone) pelite analyses. Data compiled by Ague (1991), $N = 89$. (D) Previously published amphibolite facies (staurolite, kyanite, and sillimanite zone) pelite analyses. A significant proportion of the amphibolite facies rocks apparently have no chemical analogs among shales and slates. In addition to the data compiled by Ague (1991), this figure includes the data of Chinner (1960) and Hounslow and Moore (1967). $N = 183$.

comparable to the silica-poor compositions of many of the greenschist and amphibolite facies pelites. However, the prolonged leaching by meteoric fluids in the near-surface environment required to produce residual weathering clays results in bulk Na/Al, K/Al, and Ca/Al ratios far lower than those observed in metapelites (Pettijohn, 1975, p. 280). Furthermore, residual clay-rich soils form as relatively thin layers which mantle bedrock, in sharp contrast to the regionally extensive, voluminous accumulations of pelitic sediment deposited in sedimentary basins.

The simplest explanation of the Si–Ti–Al relations between shales and slates and the higher grade rocks is that silica can be removed from pelites by metamorphic processes which, in turn, results in increases in the concentrations of the more residual elements Ti and Al (Ague, 1991). The silica removal may produce SiO_2/Al_2O_3 and SiO_2/TiO_2 much lower than observed at the hand sample scale in typical shales and slates. The ubiquitous presence of quartz veins in the Wepawaug (Tracy and others, 1983; Ague, 1992; van Haren and others, 1992) and in orogenic belts worldwide provides clear evidence of silica mobility during regional metamorphism.

Protolith relations.—The residual model involving low-solubility species such as Ti and Zr (figs. 4 and 5) establishes the critical identifying links between the protolith and the altered rocks derived from it. As demonstrated above, Ti, Zr, Nb, Ni, Al, Fe, and Mg relations for the garnet, staurolite, and kyanite zones are consistent with a metasomatic residual enrichment model in which the low-grade chlorite and biotite zone pelites represent the protolith (fig. 5). Moreover, the compositional arrays formed by the garnet, staurolite, and kyanite zone samples emanate directly from the field of chlorite + biotite zone compositions in figure 5, A to F. This evidence strongly supports the hypothesis that the higher-grade samples had initial compositions corresponding to the chlorite + biotite zone rocks. The chlorite + biotite zone rocks have compositions typical for shale and slate (table 1). Because the concentrations of the residual species increase with increasing grade (compare fig. 4), the prograde metamorphism was almost certainly accompanied by significant mass loss—consistent with the evidence for major silica loss summarized in figure 13.

Regional systematics.—Most of the regional variations in key physicochemical variables are spatially coupled to the pattern of metamorphic isograds (fig. 12). A critical test of the hypothesis that the variations are due to metamorphism is to determine if the isograds cut across the original sedimentary layering in the sequence. Average attitudes of relict bedding were measured at a number of localities where pelite-massive psammite contacts (fig. 2) or pelite-marble contacts could be confidently identified (fig. 14). The results indicate that throughout the central and southern portions of the Wepawaug, the regional isograds *cut across* the strike of the relict layering at a significant angle (fig. 14). These relations imply that lithologic units exposed in the low-grade zones have lateral equivalents extending across the isograds into the high-grade zones. In

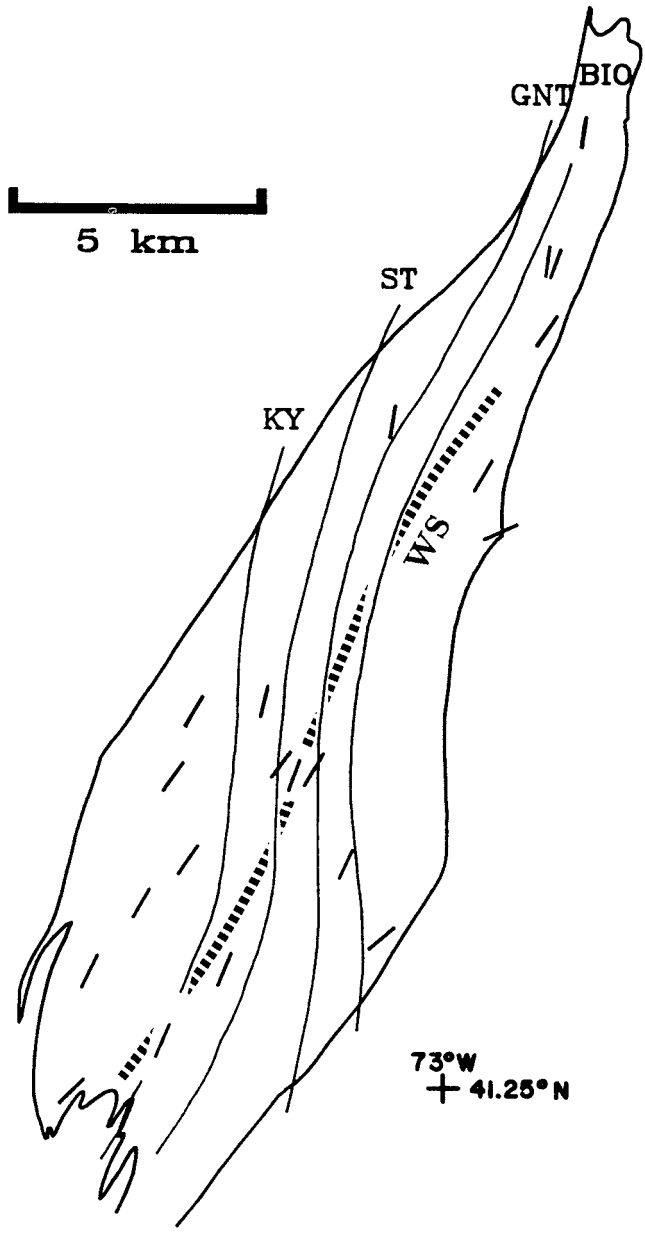

Fig. 14. Average strike of relict bedding (indicated by short lines). Note that in the central and southern portions of the Wepawaug, the isograds cut across relict bedding at a significant angle. WS: axis of the Wepawaug syncline (Fritts, 1965a; Dieterich, ms).

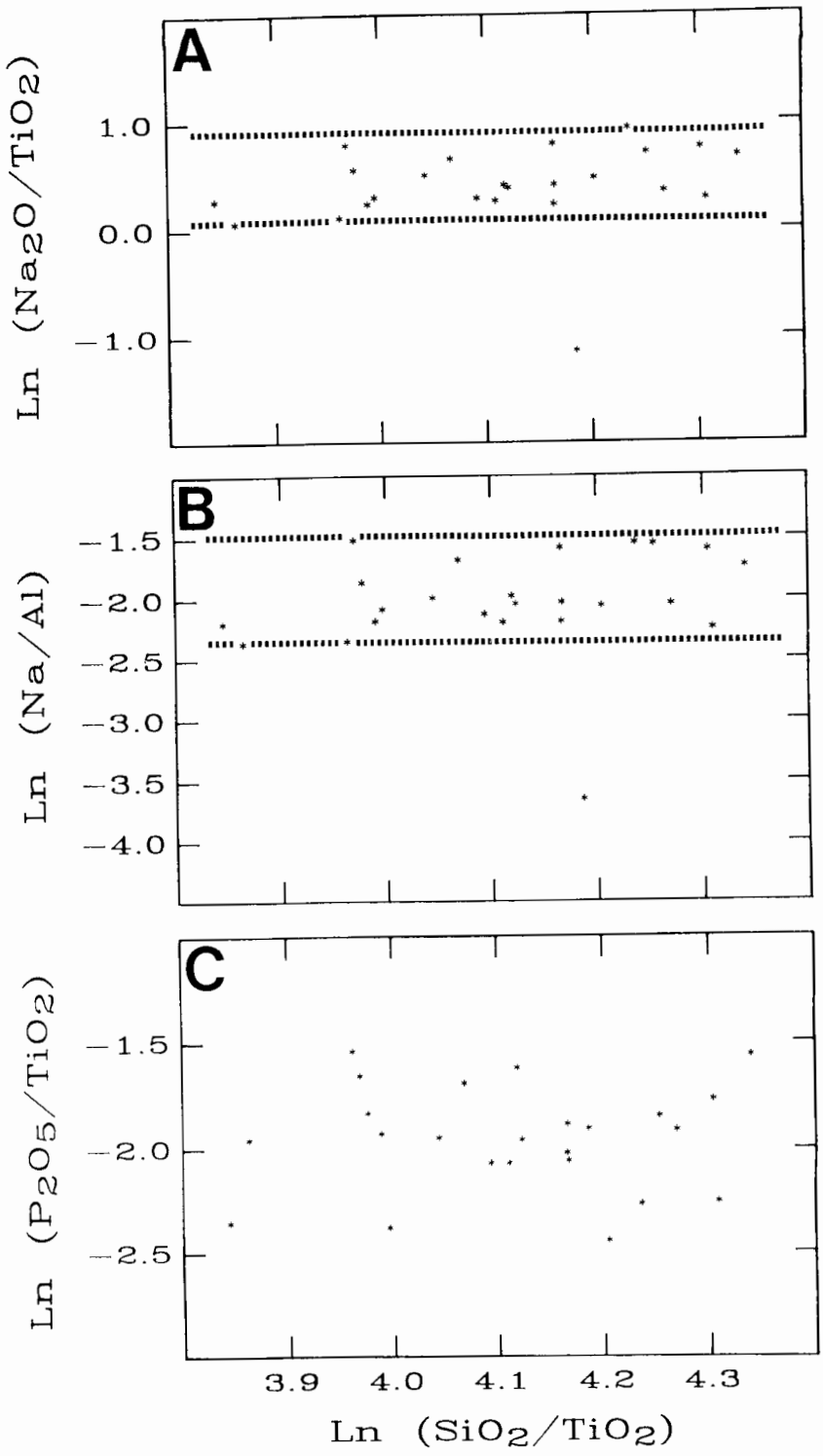

Fig. 15. Major and minor element chemical variations in the chlorite + biotite zone rocks. (A) ln (Na_2O/TiO_2) versus ln (SiO_2/TiO_2). (B) ln (Na/Al) versus ln (SiO_2/TiO_2). (C) ln (P_2O_5/TiO_2) versus ln (SiO_2/TiO_2).

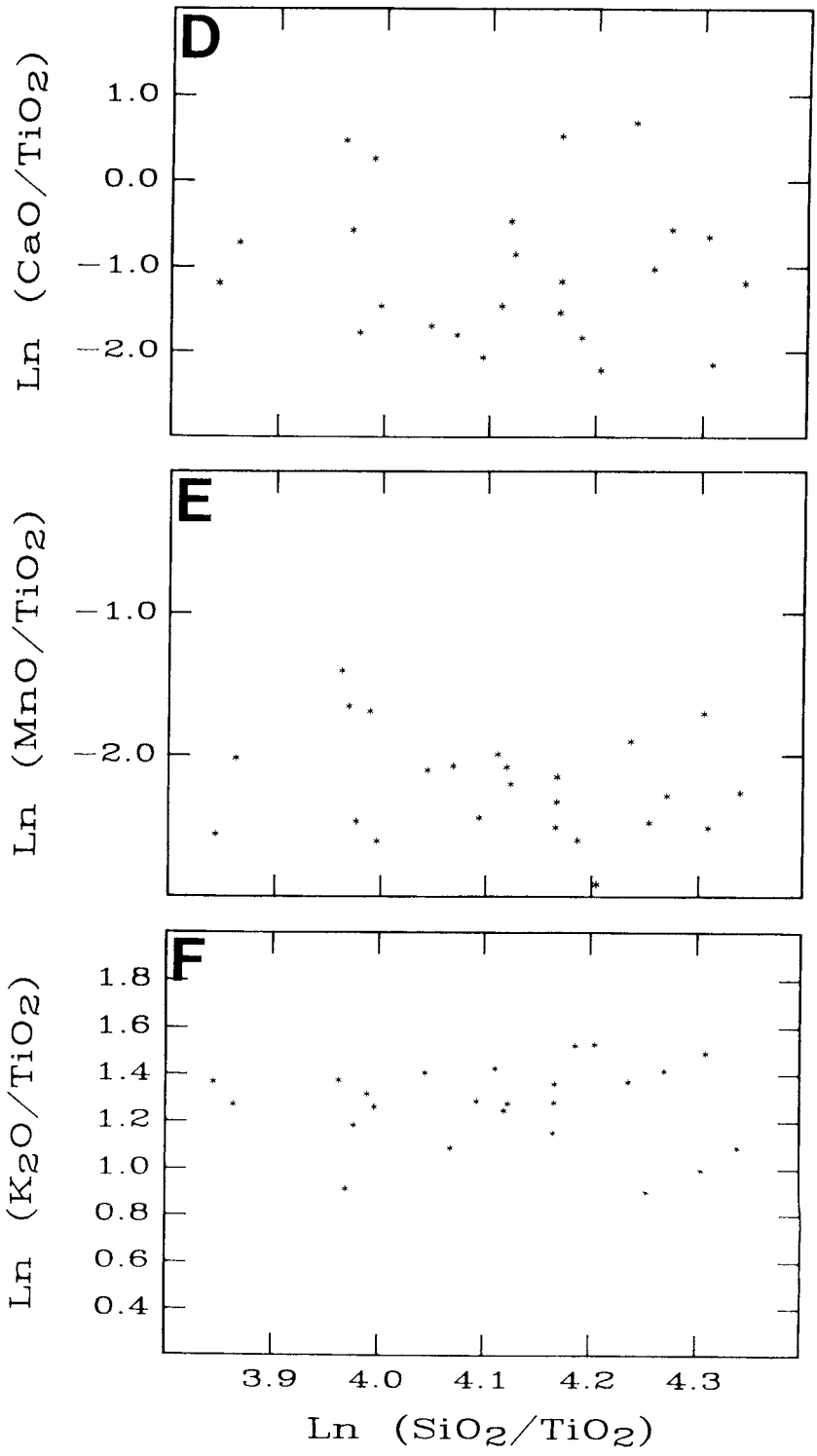

Fig. 15(D) ln (CaO/TiO_2) versus ln (SiO_2/TiO_2). (E) ln (MnO/TiO_2) versus ln (SiO_2/TiO_2). (F) ln (K_2O/TiO_2) versus ln (SiO_2/TiO_2).

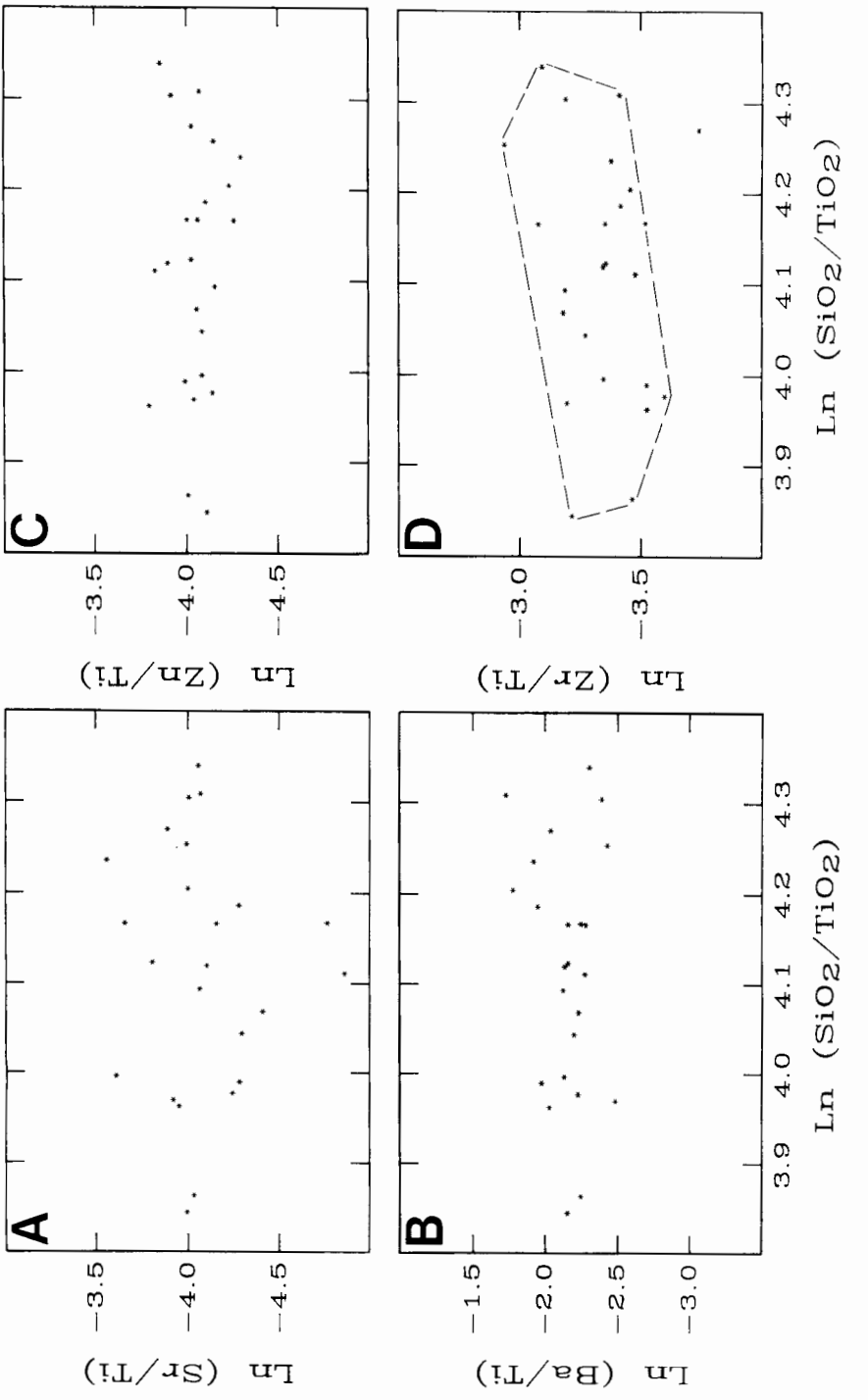

Fig. 16. Selected trace element chemical variations in the chlorite + biotite zone rocks. (A) ln (Sr/Ti) versus ln (SiO_2/TiO_2). (B) ln (Ba/Ti) versus ln (SiO_2/TiO_2). (C) ln (Zn/Ti) versus ln (SiO_2/TiO_2). (D) ln (Zr/Ti) versus ln (SiO_2/TiO_2).

addition, the isograds and the inferred axis of the major fold structure in the region (the Wepawaug syncline; Fritts, 1965a; Dietrich, ms) are not parallel (figs. 1 and 14). It is concluded that the observed east-to-west gradients in rock chemistry and density almost certainly reflect metamorphic processes. Regional chemical variations within the chlorite and biotite zones (fig. 12) are probably due mainly to original protolith heterogeneity.

Chemical trends in the inferred protolith.—Another way to assess the origins of the compositional changes in the Wepawaug is to examine the chemical trends in the chlorite + biotite zone rocks. Because these rocks have an average composition very similar to that of average shale and slate world-wide (table 1), it is reasonable to make the first-order assumption that their chemical variability is the result of low-temperature sedimentary or diagenetic processes. If the inferred sedimentary/diagenetic compositional trends differ from those observed in the higher-grade rocks, then it is logical to conclude that the higher-grade rocks were altered by metamorphic processes.

SiO_2/TiO_2 is a convenient reference variable for two reasons. First, it decreases dramatically with metamorphic grade (fig. 8A). Second, the chlorite + biotite zone rocks cover a fairly broad spectrum of SiO_2/TiO_2 values. For example, SiO_2 content ranges from about 52 to 67 wt percent (app. D). Thus, the slope of compositional trends as a function of primary (sedimentary/diagenetic) silica content should be easily observable. Consider the ln (Na_2O/TiO_2) versus ln (SiO_2/TiO_2) relations of figure 15A. From figure 8A and C it follows that if the observed decreases in Na_2O/TiO_2 in the high-grade rocks were the result of sedimentary processes, then ln (Na_2O/TiO_2) and ln (SiO_2/TiO_2) should be positively correlated in the chlorite + biotite zone group. However, this is not the case—ln (Na_2O/TiO_2) is virtually invariant as a function of ln (SiO_2/TiO_2). The same is true for ln (Na/Al) versus ln (SiO_2/TiO_2) (fig. 15B). Chlorite + biotite zone geochemical trends for the other elements that display evidence of mobility at higher grades (P, Ca, Mn, K, Sr, Ba, Zn) are shown in figures 15 and 16. In all cases, systematic trends in ln (j/TiO_2) (j = a given mobile element) as a function of ln (SiO_2/TiO_2) are not evident.

In terms of the reference species i identified previously, most have ln (i/TiO_2) values that are invariant as a function of ln (SiO_2/TiO_2). Zirconium, however, is a notable exception. ln (Zr/Ti) appears to *increase* with increasing ln (SiO_2/TiO_2) (fig. 16D). This behavior is in contrast to the relations summarized above (fig. 5A), where it was shown that Zr and Ti concentrations *both* increase according to the residual model with increasing grade (and decreasing average SiO_2/TiO_2).

The above relations indicate that the bulk of the compositional variations in the chlorite + biotite zone rocks are simply the result of variations in silica content. The variations are probably directly related to the detrital quartz content of the original sediments. In addition, the most siliceous pelitic sediments were apparently enriched in Zr. The

trends of chemical variation defined by the higher-grade pelites involve a broad spectrum of elements besides Si and are therefore inconsistent with the chemical signature of sedimentary/diagenetic processes preserved in the low-grade pelites.

Summary.—The following four lines of evidence support the hypothesis that the observed variations in rock composition are the result of metamorphism. First, upper greenschist and amphibolite facies pelites may have SiO_2/TiO_2 and SiO_2/Al_2O_3 values far lower than observed in the vast majority of shales and slates. Second, Ti, Zr, Nb, Ni, Al, Fe, and Mg relations for the garnet, staurolite, and kyanite zones are consistent with a metasomatic residual enrichment model in which the low-grade chlorite and biotite zone pelites represent the protolith. Third, regional scale gradients in key physicochemical variables are spatially correlated with the pattern of Barrovian isograds, not the pre-existing sedimentary layering in the sequence. Finally, the chemical trends that resulted from sedimentary or diagenetic processes, as inferred from the low-grade chlorite and biotite zone rocks, are inconsistent with the observed changes in rock composition as a function of metamorphic grade.

ESTIMATION OF MASS AND VOLUME CHANGES

Quantitative estimation of mass and volume changes requires knowledge of the protolith composition and the geochemical reference frame. Based on the full body of evidence presented above, we will make the reasonable assumptions that protolith composition is represented by the chlorite + biotite zone rocks, and that low-solubility species such as Ti and Zr form a geochemical reference frame. Ti is used as the reference because: (1) its relative immobility has been documented experimentally (Ayers and Watson, 1993), and (2) compared to the other residual species, it has the lowest relative compositional variability in the low-grade chlorite + biotite zone rocks.

Mass changes.—Mass changes resulting from metasomatism were estimated using the statistical mass balance formulation presented above. The calculation results strongly suggest that significant decreases in aluminous pelite mass accompanied progressive metamorphism (table 2). Total mass loss estimates increase systematically from the garnet to the kyanite zones, such that kyanite zone pelites are inferred to have lost, on average, ~23 percent of their mass, relative to the low-grade protolith. This amount of mass loss is comparable to that calculated by Ague (1991) for the "average" pelite undergoing metamorphism to amphibolite facies conditions. Volatile loss can account for only several percent of the total mass change that occurred at high metamorphic grades. Mass transfer of rock-forming constituents other than volatiles was the primary cause of the major changes in mass.

The mass change estimates for individual mobile constituents are also given in table 2. The diverse spectrum of elements that were mobile during metamorphism is striking. The most obvious chemical change is the progressive loss of silica as a function of increasing metamorphic

TABLE 2

Average mass changes

	Garnet Zone	Staurolite Zone	Kyanite Zone
Rock Mass	*−10* ± 9%	*−19* ± 6%	*−23* ± 6%
Si	−15 +17% −14%	*−32* +11% −9%	*−38* +9% −8%
P	4 +36% −26%	−9 +27% −21%	*−34* +19% −15%
Na	−2 +30% −23%	*−33* +19% −15%	*−37* +15% −12%
Mn	23 +35% −27%	*64* +64% −46%	*46* +45% −34%
Zn	*−12* +8% −7%	14 +29% −23%	*19* +19% −16%
K	−3 +10% −9%	*16* +15% −13%	8 +12% −11%
Ba	−4 +12% −11%	*21* +23% −19%	−5 +14% −13%
Ca*	—	−13 +45% −30%	−26 +31% −22%
Sr*	—	−22 +27% −20%	*−25* +19% −15%

Notes: Percentage mass changes computed relative to chlorite + biotite zone protolith using a Ti reference frame, unless otherwise noted. Underlined italic type indicates that the mass changes are statistically significant at the 95 percent (or greater) confidence level; plain type indicates that the mass changes are not statistically significant. Significance tests were done using Student's *t*-tests (Press and others, 1992, p. 615-619). Na results do not include JAW-41, because this sample has an anomalously low Na/Ti ratio. Uncertainties are $\pm 2\sigma$.
* Mass changes computed relative to garnet zone.

intensity. Considerable losses of P and Na also occurred at high metamorphic grades. On average, Mn and Zn were added to amphibolite facies pelites, and K and Ba were added to staurolite zone schists. Mass loss of Ca and Sr may have occurred in the amphibolite facies pelites, but the analysis is complicated by protolith heterogeneity.

The results of the quantitative mass balance analysis lead to the surprising conclusion that the bulk of the total rock mass change was due to loss of silica, not volatiles, from the schists. The correspondence between estimates of total rock mass change and silica loss is illustrated in figure 17. It could be argued that the Wepawaug pelites are somehow unusual in that they have suffered mass changes far greater than "normal" for rocks undergoing progressive Barrovian zone metamorphism. This is not the case, however, as illustrated in figure 13. The Wepawaug pelites have ln (SiO_2/TiO_2) and ln (SiO_2/Al_2O_3) values perfectly analogous to those of metamorphosed pelites from around the world. I conclude that the loss of silica that accompanied the metamorphism of the Wepawaug pelites was due to processes that operated in other Barrovian zone terranes worldwide.

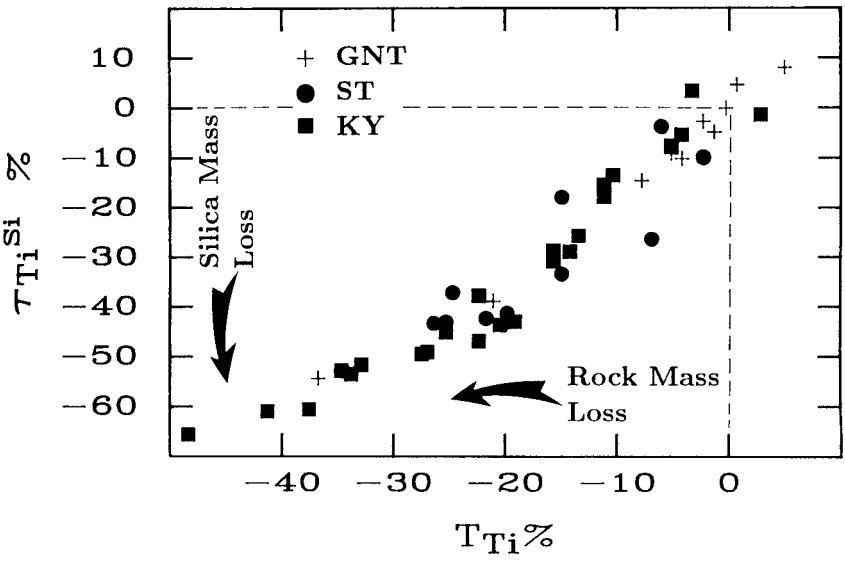

Fig. 17. Silica mass loss (τ_{Ti}^{Si}) versus total rock mass loss (T_{Ti}). The calculations indicate that some pelites have lost as much as half of their mass and 60 to 70 percent of their silica, relative to the average chlorite + biotite zone rock (the inferred protolith). The average chlorite + biotite zone rock would plot at $\tau_{Ti}^{Si} = 0$ and $T_{Ti} = 0$.

It should be noted that statistical uncertainties, particularly those due to protolith heterogeneity, can sometimes be so large that metasomatic mass changes are obscured. Given the degree of protolith variability and the number of samples analyzed in the present study, the minimum detectable relative mass changes for mobile elements are about ±10 percent. Thus, the possibility exists that some element mobility has gone undetected.

Mg/Fe ratios.—Because the bulk rock Mg/Fe ratio is an important control on pelite mineralogy (Thompson, 1957; Chinner, 1960; Hoschek, 1967; Thompson and others, 1977), a detailed investigation of Mg-Fe relations is warranted. As shown in figure 18, ln (Mg/Fe^T) (molar basis; Fe^T = total Fe) appears to be ~constant as a function of ln (SiO_2/TiO_2) or metamorphic grade. However, the sample with the lowest SiO_2/TiO_2 (indicative of severe silica depletion) also has the lowest Mg/Fe^T. This relationship may indicate that Mg/Fe^T can be modified in cases of extreme rock alteration.

A note on trace elements and closure.—It is worth making a small digression to point out a potentially serious pitfall in studies of trace element mobility during metamorphism. From figure 5A it is evident that major element mass transfer can affect significantly the concentrations of trace elements. For example, although the concentration of the trace

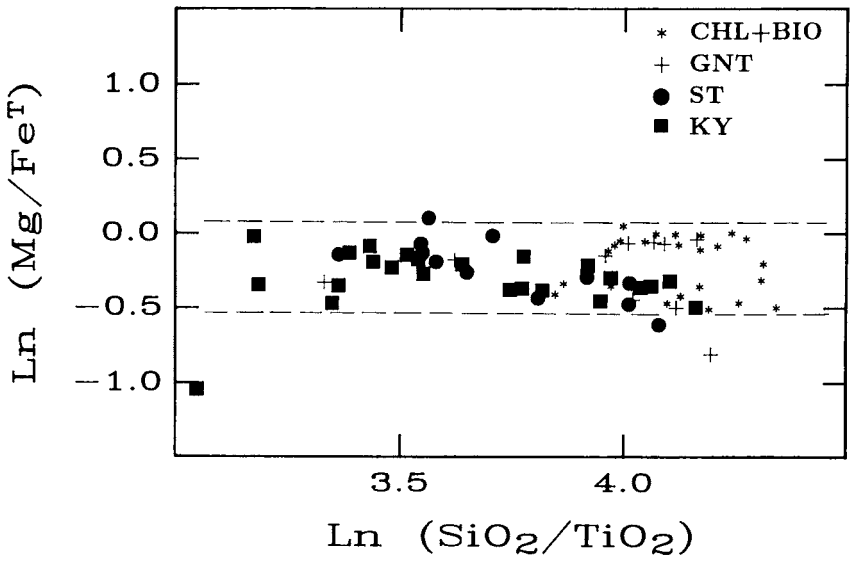

Fig. 18. ln (Mg/Fe^T) (molar basis; Fe^T = total iron) versus ln (SiO_2/TiO_2). The range in ln (SiO_2/TiO_2) for the chlorite + biotite zone rocks is shown with the dashed lines.

element Zr increases by as much as 100 percent from chlorite zone to kyanite zone rocks, no detectable changes in Zr *mass* occurred during metamorphism. The concentration changes are simply a result of the residual enrichment process. This example highlights the fact that the concentrations of trace elements are subject to closure just as are those of the major elements. Thus, in any study of trace element mass transfer, major element metasomatism must also be assessed.

Volume changes.—The quantitative relationship between changes in rock chemistry, ρ_g, and volume in the Wepawaug pelites is illustrated in figure 19. The loss of rock-forming constituents (table 2) and the well-defined increases in ρ_g (fig. 11) are inferred to have produced significant decreases in aluminous pelite volume. Application of the constitutive mass balance equation for volume strain (eq 3) yields the remarkable result that some schists have lost as much as half their volume owing to metamorphism (fig. 19). Estimates of average volume strain for the garnet, staurolite, and kyanite zones are -12 ± 10, -22 ± 6, and, -28 ± 6, percent respectively ($\pm 2\sigma$). At the scale of investigation, the metamorphism of the Wepawaug pelites was not isochemical, and it also was not isovolumetric.

Within-zone variations in metasomatic intensity.—One of the most provocative results of the mass balance analysis is that rocks within any given metamorphic zone have apparently undergone markedly different degrees of mass and volume change. For example, the suite of kyanite zone

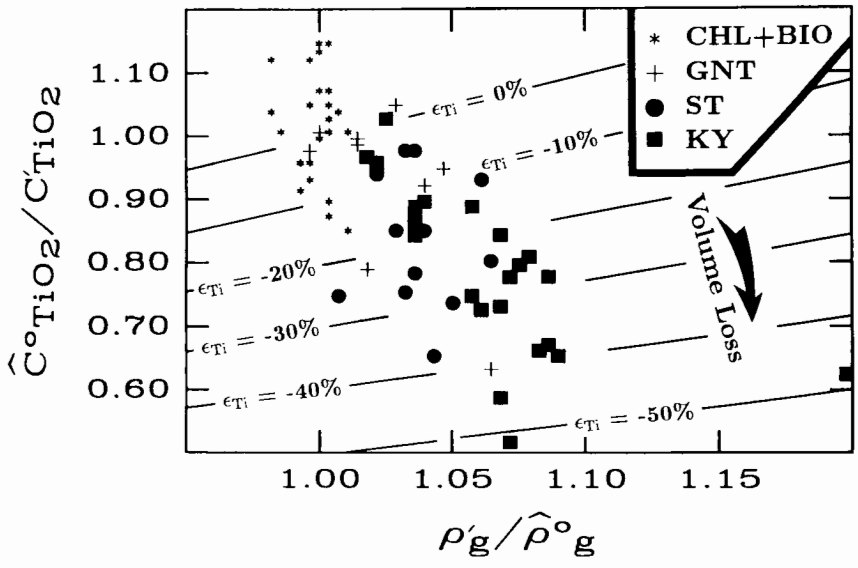

Fig. 19. $\hat{C}^o_{TiO_2}/C'_{TiO_2}$ versus $\rho'_g/\hat{\rho}^o_g$. Volume strain contours (ϵ_{Ti}) are also shown. Some aluminous pelites have lost as much as half their volume, relative to the average chlorite + biotite zone rock, as a result of metasomatic processes. The minimum length scales of volume change are on the order of typical hand sample dimensions. $\hat{C}^o_{TiO_2}$ (0.986 wt percent) and $\hat{\rho}^o$ (2.78 g cm^{-3}) are the mean TiO_2 content (computed using the AML) and grain density (arithmetic mean) of the chlorite + biotite zone rocks.

samples indicate mass changes ranging from around 0 to −50 percent (fig. 17). Therefore, metasomatic processes must have operated at different intensities in different parts of the formation, even within a single zone.

To investigate this phenomenon further, ln (Na/Al)—ln (SiO_2/TiO_2) relations of multiple samples from two large (100 m scale) railroad grades in the kyanite zone are shown in figure 20. We focus on Na and Si because these are the two major elements most strongly affected by mass transfer processes (table 2). In each sample suite, there is a notably wide variation in rock chemistry, ranging from compositions essentially equivalent to the chlorite + biotite zone rocks to low Na/Al and low SiO_2/TiO_2 compositions indicative of significant metasomatism. The Na loss is particularly important, because the bulk rock Na/Al ratio plays a crucial role in determining pelite mineralogy—low Na/Al favors the growth of aluminous index minerals such as staurolite and kyanite (Hoschek, 1967; Thompson, Lyttle, and Thompson, 1977). The main conclusion to be drawn from the data is that the intensity of metasomatism was variable even within individual outcrops. The fluid-driven processes responsible for this variation will be investigated in detail in forthcoming papers (including Ague, this journal, November, 1994).

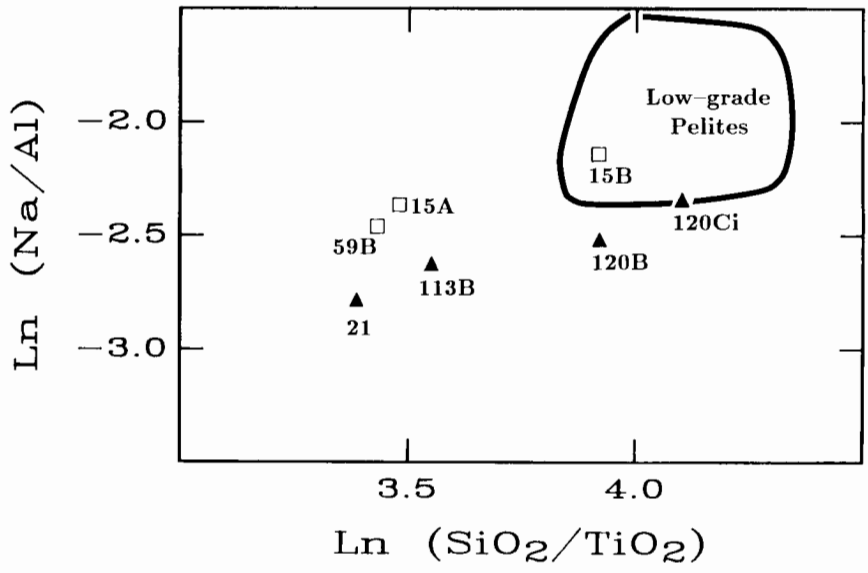

Fig. 20. ln (Na/Al) (molar basis) versus ln (SiO_2/TiO_2) for specimens from two large kyanite zone outcrops. JAW-15A, -15B, and -59B are from one of the outcrops, whereas JAW-21, -113B, -120B, and -120Ci are from the other (fig. 3). Note the positive correlation between ln (Na/Al) and ln (SiO_2/TiO_2). In the rocks with the highest Na/Al (-15B and -120Ci), staurolite and kyanite are rare (-15B) or absent (-120Ci). Field of low-grade (chlorite + biotite zone) logratios shown for comparison. See text for additional discussion.

CONCLUSIONS

Statistical analysis and regional mapping of rock chemistry and density relations strongly suggest that the composition and density of aluminous pelite varies significantly across the Wepawaug Schist. The nature and degree of the physicochemical variations indicate they are the result of metamorphic, not sedimentary or diagenetic, processes.

The results of quantitative mass balance analysis accounting for closure and the multivariate nature of compositional data (Aitchison, 1986) suggest that the rocks underwent significant chemical and volume changes as a result of metamorphism. The average degree of physicochemical change increases in a general way with metamorphic grade. The minimum scales of mass and volume change were on the order of typical hand sample dimensions. The compositional systematics of low solubility elements such as Ti and Zr are consistent with the hypothesis that the presently exposed chlorite + biotite zone rocks are representative of the "protolith" for the garnet, staurolite, and kyanite zone schists. The most striking compositional change is that, on average, silica was progressively lost from aluminous pelites with increasing metamorphic grade. Significant Na was lost from amphibolite facies pelites. Furthermore, on average, staurolite zone pelites gained K and Ba, kyanite zone

pelites lost P, and amphibolite facies pelites gained Mn and Zn. Some Ca and Sr may also have been lost from amphibolite facies rocks. The calculation results strongly suggest that aluminous pelites lost significant mass as a result of the metamorphism. Average total mass loss estimates increase from ~10 percent in the garnet zone to ~23 percent in the kyanite zone. The bulk of the lost mass was silica, not volatiles. Rock density on a porosity-free basis increases systematically with metamorphic grade. The density increases and overall rock mass loss are interpreted to have produced significant decreases in aluminous pelite volume. Average volume loss estimates range from ~12 percent for the garnet zone to ~28 percent for the kyanite zone. The computations were done under the reasonable assumption that porosity changes did not contribute significantly to the volume changes. Metasomatic mass and volume changes were variable within individual outcrops.

It is concluded that aluminous pelites may undergo substantial chemical alteration and volume strain during Barrovian metamorphism. Forthcoming papers in this series will focus on clarifying the relationships between regional scale fluid flow, local and regional scale element transport, and the mineralogical evolution of pelitic terranes.

ACKNOWLEDGMENTS

I would like to thank D. M. Rye, M. T. Brandon, A. C. Lasaga, and B. F. Skinner for many thoughtful discussions which have contributed substantially to this study and G. M. Dipple, C. V. Guidotti, and S. S. Sorensen for their critical and constructive reviews. W. C. Phelps provided valuable assistance with sample preparation. Support from National Science Foundation grant EAR-918006 and Yale University is gratefully acknowledged.

APPENDIX A

Review of the mass balance equations

The basic mass balance equation for a reference species i is simply:

$$V^o\rho^oC_i^o = V'\rho'C_i', \tag{A-1}$$

where V^o and V' are the initial (protolith) and final (altered state) rock volumes, ρ^o and ρ' are the initial and final rock densities, and C_i^o and C_i' are the initial and final concentrations (for example wt percents) of i. Because the focus here is on mass and volume changes of solid rock material, the composition, density, and volume of pore fluids are ignored. The volume strain ϵ is given by:

$$\epsilon = \frac{V' - V^o}{V^o}. \tag{A-2}$$

By combining eqs (A-1) and (A-2) we obtain (Brimhall and Dietrich, 1987; Brimhall and others, 1988):

$$\epsilon_i = \left[\left(\frac{C_i^o}{C_i'}\right)\left(\frac{\rho^o}{\rho'}\right) - 1\right], \tag{A-3}$$

where ϵ_i denotes that strain is being computed on the basis of a reference species i. It follows that residual enrichment or dilution of i is given by:

$$C_i' = \frac{\rho^oC_i^o}{(\epsilon_i + 1)\rho'}. \tag{A-4}$$

Eq (A-3) can be expanded by taking into account the relationship between the bulk density of the rock, ρ, the density of the mineral grains, ρ_g, and porosity, n:

$$\textit{porosity} = n = 1 - \frac{\rho}{\rho_g}. \tag{A-5}$$

Substitution for the density terms in eq (A-3) yields (Brimhall and Dietrich, 1987):

$$\epsilon_i = \left[\left(\frac{C_i^o}{C_i'}\right)\left(\frac{\rho_g^o}{\rho_g'}\right)\left(\frac{(1 - n^o)}{(1 - n')}\right) - 1\right]. \tag{A-6}$$

The concentration ratio term describes changes in volume due to addition or subtraction of mass from the rock. In pelites, dehydration reactions leading to the loss of volatile species can result in bulk volume loss. Furthermore, mass transfer of rock-forming elements, such as Si, can produce significant volume strain at high metamorphic grades (Ague, 1991). The second term describes volume changes that result from changes in grain density (rock density on a porosity-free basis). In aluminous pelites, the growth of high density phases such as garnet, staurolite, and kyanite at high metamorphic grades can give rise to small overall bulk density increases and corresponding decreases in rock volume. More importantly, major removal of low-density rock-forming constituents, such as quartz, by mass transfer processes can leave the residual rock enriched in high density aluminous phases. Here, proper interpretation of volume strain requires that changes in both chemical composition and rock density be known. The third term in eq (A-6) describes changes in rock volume owing to porosity gain or porosity loss. In our case, it is reasonable to assume that the porosities of the pelites under metamorphic conditions were small ($\sim$ 1 percent or less), and that the porosities of the protolith and the higher-grade rocks were approximately equal. Under these assumptions, $(1 - n^o)/(1 - n')$ will be $\sim$ 1, and, therefore, porosity changes can be neglected when computing volume strain. Eq. (A-6) is the complete

expression for the total volume strain attending metasomatism which links quantitatively changes in rock chemical and physical properties. Although no direct information is provided about the nature of shape change, it is reasonable to expect that in metamorphic rocks, a significant amount of volume strain occurs parallel to penetrative cleavage fabrics (Wright and Platt, 1982).

The total change in mass resulting from metasomatism, denoted as T by Ague (1991), is defined as:

$$T \equiv \left[\frac{\textit{Final Mass} - \textit{Initial Mass}}{\textit{Initial Mass}}\right] = \frac{V'\rho'}{V^o\rho^o} - 1. \tag{A-7}$$

Given that:

$$V'\rho' = V^o\rho^o \frac{C_i^o}{C_i'} \tag{A-8}$$

eq (A-7) can be rearranged to yield:

$$T_i = \left[\frac{C_i^o}{C_i'} - 1\right]. \tag{A-9}$$

The total change in mass based on the reference species i, T_i, is the result of the individual mass fluxes of all mobile species j. Following Brimhall and others (1988), a transport function τ^j, relevant for each mobile species, is defined as follows:

$$\tau^j \equiv \left[\frac{\textit{Final Mass } j - \textit{Initial Mass } j}{\textit{Initial Mass } j}\right] = \frac{V'\rho'C_j'}{V^o\rho^oC_j^o} - 1. \tag{A-10}$$

Because

$$\frac{V'}{V^o} = \epsilon_i + 1, \tag{A-11}$$

it follows that:

$$\tau_i^j = \frac{\rho'}{\rho^o}\frac{C_j'}{C_j^o}(\epsilon_i + 1) - 1. \tag{A-12}$$

Eq (A-12) provides a quantitative relationship between mass change, and rock physical, chemical, and volumetric properties. However, it may be simplified further by substituting for the ϵ_i term (Ague, 1991):

$$\tau_i^j = \left[\left(\frac{C_i^o}{C_i'}\right)\left(\frac{C_j'}{C_j^o}\right) - 1\right]. \tag{A-13}$$

Therefore, changes in the mass of mobile species can be computed without knowledge of rock density terms, but the volumetric strain (eq A-6) cannot. Negative values of T_i and τ_i^j indicate mass loss, whereas positive values correspond to mass gain. For example, a τ_i^j value of +1 (+100 percent) means that the mass of element j has doubled in going from an initial to a final state.

APPENDIX B

Prograde silicate mineralogy

	Zone	Chl	<2mm Gnt*	Bio	Alm Gnt	St	Ky
JAW-1	CHL	X	—	—	—	—	—
JAW-2	CHL	X	—	—	—	—	—
JAW-3	CHL	X	—	—	—	—	—
JAW-4	CHL	X	—	—	—	—	—
JAW-5	CHL	X	—	—	—	—	—
JAW-6	CHL	X	—	—	—	—	—
JAW-12	GNT	—	—	X	X	—	—
JAW-15A	KY	—	—	X	X	X	X
JAW-15B§	KY	—	—	X	X	X	X
JAW-19D	ST	—	—	X	X	X	—
JAW-21	KY	—	—	X	X	X	X
JAW-22A	KY	—	—	X	X	X	X
JAW-22B	KY	—	—	X	X	X	X
JAW-24	CHL	X	X	—	—	—	—
JAW-25	BIO	X	X	X	—	—	—
JAW-25-2	BIO	X	X	X	—	—	—
JAW-26A	ST	—	—	X	X	X	—
JAW-29	BIO	X	X	X	—	—	—
JAW-30	GNT	—	—	X	X	—	—
JAW-31	GNT	X	—	X	X	—	—
JAW-32A	ST	—	—	X	X	—	—
JAW-32B	ST	—	—	X	X	X	—
JAW-32C	ST	—	—	X	X	X	—
JAW-33	CHL	X	—	—	—	—	—
JAW-34A	CHL	X	—	—	—	—	—
JAW-35B	GNT	—	—	X	X	—	—
JAW-36	ST	—	—	X	X	—	—
JAW-37	ST	—	—	X	X	X	—
JAW-39A	GNT	X	—	X	X	—	—
JAW-40	CHL	X	—	—	—	—	—
JAW-41	CHL	X	—	—	—	—	—
JAW-42	CHL	X	—	—	—	—	—
JAW-43	CHL	X	—	—	—	—	—
JAW-44	CHL	X	—	—	—	—	—
JAW-44-2	CHL	X	—	—	—	—	—
JAW-45A	CHL	X	—	—	—	—	—
JAW-47	CHL	X	X	—	—	—	—
JAW-48	ST	—	—	X	X	X	—
JAW-49	BIO	X	X	X	—	—	—
JAW-50	KY	—	—	X	X	X	X
JAW-53	KY	—	—	X	X	X	—
JAW-57	KY	—	—	X	X	—	—
JAW-59B	KY	—	—	X	X	X	X

APPENDIX B
(continued)

	Zone	Chl	<2mm Gnt*	Bio	Alm Gnt	St	Ky
JAW-61	ST	—	—	X	X	—	—
JAW-63	KY	—	—	X	X	X	X
JAW-68	CHL	X	—	—	—	—	—
JAW-69	BIO	X	—	X	—	—	—
JAW-71A	KY	—	—	X	X	X	X
JAW-72	ST	—	—	X	X	X	—
JAW-75	GNT	—	—	X	X	—	—
JAW-78	KY	—	—	X	X	X	—
JAW-83	KY	—	—	X	X	X	X
JAW-88	KY	—	—	X	X	X	X
JAW-90A	KY	—	—	X	X	X	X
JAW-92	GNT	—	—	X	X	—	—
JAW-93	GNT	X	—	X	X	—	—
JAW-99A	GNT	X	—	X	X	—	—
JAW-100	ST	X	—	X	X	—	—
JAW-103A	KY	—	—	X	X	X	—
JAW-104	KY	—	—	X	X	X	X
JAW-105A	KY	—	—	X	X	X	X
JAW-110	KY	—	—	X	X	—	—
JAW-113B	KY	—	—	X	X	X	X
JAW-114A†	KY	—	—	X	X	X	X
JAW-120B	KY	—	—	X	X	X	X
JAW-120C§	KY	—	—	X	X	—	—
JAW-124	CHL	X	—	—	—	—	—
JAW-126A	GNT	—	—	X	X	—	—
JAW-127A	ST	—	—	X	X	—	—
JAW-137B	KY	—	—	X	X	—	—

Notes: CHL = chlorite, BIO = biotite, GNT = garnet, ST = staurolite, KY = kyanite. All rocks contain quartz and muscovite, unless noted otherwise.

* Small spessartine-rich garnets which occur sporadically in the chlorite and biotite zones.

† This sample lacks prograde muscovite.

§ Contains only trace amounts (<0.1 volume percent) of staurolite and kyanite.

APPENDIX C

Sample locations and grain densities

	Zone	Latitude*	Longitude*	ρ_g (g cm^{-3})
JAW-1	CHL	41.34496	72.98642	2.77
JAW-2	CHL	41.34526	72.98665	2.80
JAW-3	CHL	41.35421	72.99062	2.81
JAW-4	CHL	41.35977	72.99243	2.79
JAW-5	CHL	41.36320	72.99265	2.79
JAW-6	CHL	41.37625	72.97782	2.78
JAW-12	GNT	41.39332	72.98638	2.82
JAW-15A	KY	41.24784	73.08859	3.02
JAW-15B	KY	41.24784	73.08859	2.94
JAW-19D	ST	41.25703	73.06730	2.92
JAW-21	KY	41.26932	73.08272	3.02
JAW-22A	KY	41.27101	73.08257	2.89
JAW-22B	KY	41.27101	73.08257	2.84
JAW-24	CHL	41.39541	72.97417	2.74
JAW-25	BIO	41.41277	72.96707	2.73
JAW-25-2	BIO	41.41277	72.96707	2.79
JAW-26A	ST	41.36208	73.02187	2.84
JAW-29	BIO	41.28229	73.02335	2.77
JAW-30	GNT	41.28138	73.02885	2.77
JAW-31	GNT	41.30351	73.03416	2.84
JAW-32A	ST	41.31104	73.04129	2.95
JAW-32B	ST	41.31104	73.04129	2.86
JAW-32C	ST	41.31104	73.04129	2.87
JAW-33	CHL	41.31259	73.00334	2.76
JAW-34A	CHL	41.31522	73.01623	2.77
JAW-35B	GNT	41.30564	73.03456	2.82
JAW-36	ST	41.29265	73.03834	2.88
JAW-37	ST	41.28328	73.04586	2.87
JAW-39A	GNT	41.29992	73.03537	2.78
JAW-40	CHL	41.39087	72.97361	2.78
JAW-41	CHL	41.39061	72.97359	2.79
JAW-42	CHL	41.38920	72.97380	2.76
JAW-43	CHL	41.38807	72.97400	2.79
JAW-44	CHL	41.38730	72.97414	2.73
JAW-44-2	CHL	41.38730	72.97414	2.81

APPENDIX C
(continued)

	Zone	Latitude*	Longitude*	ρ_g (g cm^{-3})
JAW-45A	CHL	41.38576	72.97458	2.78
JAW-47	CHL	41.39398	72.97389	2.78
JAW-48	ST	41.34736	73.02722	2.88
JAW-49	BIO	41.27762	73.01971	2.79
JAW-50	KY	41.31417	73.05777	2.97
JAW-53	KY	41.26916	73.09617	2.98
JAW-57	KY	41.28632	73.07076	2.88
JAW-59B	KY	41.24917	73.08732	2.95
JAW-61	ST	41.27000	73.05094	2.96
JAW-63	KY	41.28154	73.05216	2.94
JAW-68	CHL	41.27481	73.01536	2.79
JAW-69	BIO	41.28769	73.02283	2.76
JAW-71A	KY	41.24312	73.09220	2.97
JAW-72	ST	41.25869	73.06437	2.90
JAW-75	GNT	41.36696	73.01851	2.86
JAW-78	KY	41.28308	73.06904	2.88
JAW-83	KY	41.28313	73.06761	2.97
JAW-88	KY	41.28492	73.06704	2.98
JAW-90A	KY	41.28114	73.06999	3.03
JAW-92	GNT	41.30317	73.03555	2.91
JAW-93	GNT	41.29890	73.03584	2.89
JAW-99A	GNT	41.36626	73.00736	2.83
JAW-100	ST	41.24488	73.06666	2.89
JAW-103A	KY	41.26513	73.08997	3.01
JAW-104	KY	41.26500	73.09099	2.84
JAW-105A	KY	41.26427	73.09124	2.99
JAW-110	KY	41.28862	73.06788	2.88
JAW-113B	KY	41.26932	73.08272	3.00
JAW-114A	KY	41.24402	73.07619	3.33
JAW-120B	KY	41.26932	73.08272	2.88
JAW-120Ci	KY	41.26932	73.08272	2.85
JAW-124	CHL	41.35304	72.99098	2.77
JAW-126A	GNT	41.30317	73.03555	2.96
JAW-127A	ST	41.29265	73.03834	2.80
JAW-137B	KY	41.26513	73.08997	2.83

* Format: degrees.decimal degrees.

APPENDIX D

Bulk chemistry

Sample JAW-45A was analyzed four times over the period September 7, 1990 through February 3, 1993. The arithmetic mean $\pm\sigma$ sample standard deviation for each oxide or element is listed below to illustrate the long-term reproducibility of results. Major and minor oxide results are given in wt percent, whereas the trace element concentrations are in ppm. Bulk-compositional variations due to original protolith heterogeneity and metasomatism are far greater than the analytical uncertaintly levels.

SiO_2	59.05	±0.310	Rb	153	±2.7
TiO_2	0.92	±0.014	Sr	142	±4.8
Al_2O_3	16.83	±0.150	Ba	633	±16.1
Fe_2O_3*	7.46	±0.060	Zr	193	±9.0
MgO	3.36	±0.024	Zn	95	±7.0
MnO	0.09	±0.003	Ni	72	±0.5
CaO	1.53	±0.013	Nb	26	±3.4
Na_2O	1.15	±0.030			
K_2O	3.19	±0.040			
P_2O_5	0.14	±0.009			
LOI	5.58	±0.180			

For the following bulk chemistry tables, the average of the four JAW-45A analyses was computed using the method of Aitchison (1989).

General notes for bulk chemistry tables

All Fe is taken as Fe^{3+} (Fe_2O_3*). LOI refers to loss on ignition. A dash (—) indicates that the element was present at levels below the detection limit (10 ppm for trace elements). Total weight percents include the trace elements summed as oxides.

Chlorite and biotite zones; major and minor elements (wt %)

	SiO_2	TiO_2	Al_2O_3	Fe_2O_3*	MgO	MnO	CaO	Na_2O	K_2O	P_2O_5	LOI	Total
JAW-1	60.6	0.94	17.7	7.51	3.74	0.11	0.29	1.41	3.66	0.12	3.93	100.1
JAW-2	57.9	0.95	18.2	8.31	4.16	0.13	0.22	1.23	3.95	0.12	4.54	99.8
JAW-3	51.5	0.98	18.8	9.86	4.41	0.24	1.56	1.09	3.87	0.21	6.54	99.2
JAW-4	61.6	0.92	19.0	5.39	2.49	0.05	0.10	1.47	4.24	0.08	4.23	99.7
JAW-5	63.9	0.86	17.6	5.51	2.26	0.07	0.10	1.13	3.82	0.09	3.85	99.4
JAW-6	60.1	0.87	17.1	5.39	2.72	0.13	1.71	2.21	3.42	0.09	5.77	99.7
JAW-24	63.1	0.98	17.3	6.01	2.12	0.08	0.21	2.15	3.10	0.13	3.85	99.2
JAW-25	65.1	0.88	15.2	7.09	2.61	0.16	0.46	1.86	2.38	0.15	3.70	99.7
JAW-25-2	58.2	1.10	18.1	8.15	2.88	0.21	0.62	2.41	2.74	0.21	4.16	98.9
JAW-29	62.9	0.88	15.8	6.54	3.18	0.09	0.50	1.24	3.62	0.13	3.77	98.8
JAW-33	60.2	1.03	17.5	7.71	3.87	0.13	0.17	1.98	3.06	0.19	4.47	100.5
JAW-34A	56.5	1.06	19.5	8.69	4.04	0.09	0.18	1.84	3.46	0.17	4.93	100.6
JAW-40	61.1	0.99	18.4	7.09	2.34	0.11	0.42	1.45	3.55	0.14	4.23	100.0
JAW-41	61.8	0.94	19.0	6.84	2.07	0.07	0.15	0.30	4.31	0.14	4.08	99.9
JAW-42	61.7	1.03	18.9	6.67	2.10	0.09	0.13	1.37	3.73	0.13	3.93	99.9
JAW-43	53.8	1.13	21.0	9.01	3.24	0.15	0.55	1.20	4.03	0.16	5.23	99.7
JAW-44	66.8	0.95	15.0	6.05	1.91	0.08	0.34	1.92	2.34	0.15	3.62	99.3
JAW-44-2	54.2	1.16	22.5	8.02	2.68	0.09	0.35	1.52	4.55	0.11	4.70	100.1
JAW-45A	59.3	0.92	16.9	7.49	3.38	0.09	1.54	1.15	3.31	0.14	5.59	100.0
JAW-47	65.9	0.86	15.7	6.89	2.11	0.09	0.26	1.68	2.56	0.18	3.47	99.8
JAW-49	59.0	0.96	17.1	8.20	3.82	0.12	0.60	1.44	3.34	0.19	4.00	98.9
JAW-68	55.9	0.98	19.5	9.01	4.29	0.12	0.18	1.62	4.00	0.14	4.23	100.1
JAW-69	58.7	1.08	19.2	7.48	3.96	0.08	0.25	1.45	3.81	0.10	4.23	100.5
JAW-124	55.6	1.03	19.0	8.41	4.03	0.19	1.33	1.30	3.84	0.15	5.23	100.3

APPENDIX D
(continued)

Chlorite and biotite zones; trace elements (ppm)

	Rb	Sr	Ba	Zr	Zn	Ni	Nb
JAW-1	142	48	595	167	103	69	16
JAW-2	162	44	585	176	124	85	—
JAW-3	162	113	771	173	132	88	32
JAW-4	181	101	931	174	80	26	23
JAW-5	168	88	914	170	88	25	23
JAW-6	140	148	762	178	71	43	20
JAW-24	153	92	599	271	83	52	24
JAW-25	113	96	482	217	105	60	16
JAW-25-2	132	131	551	270	116	77	16
JAW-29	182	108	684	125	94	63	15
JAW-33	126	75	662	257	107	40	32
JAW-34A	156	91	685	174	101	61	24
JAW-40	168	132	684	207	106	70	33
JAW-41	208	78	801	185	93	43	14
JAW-42	168	106	736	255	97	49	22
JAW-43	203	120	715	212	123	103	32
JAW-44	113	105	501	302	90	41	16
JAW-44-2	211	128	805	279	114	57	31
JAW-45A	153	142	635	193	95	72	25
JAW-47	118	89	513	234	109	58	18
JAW-49	147	95	679	203	117	56	17
JAW-68	157	80	650	223	99	76	13
JAW-69	163	175	767	228	109	73	25
JAW-124	184	85	856	182	114	74	42

APPENDIX D
(continued)

Garnet zone; major and minor elements (wt %)

	SiO_2	TiO_2	Al_2O_3	Fe_2O_3*	MgO	MnO	CaO	Na_2O	K_2O	P_2O_5	LOI	Total
JAW-12	60.5	0.99	18.8	7.33	2.24	0.13	0.67	0.92	3.49	0.16	4.08	99.5
JAW-30	60.1	1.01	17.3	7.28	3.42	0.13	0.77	1.90	3.15	0.16	3.77	99.1
JAW-31	56.6	1.03	18.3	8.29	3.91	0.12	1.56	1.85	3.87	0.16	3.31	99.2
JAW-35B	58.2	1.00	18.2	7.52	3.57	0.20	1.80	2.60	3.32	0.16	2.23	99.0
JAW-39A	62.7	0.98	16.3	6.73	3.26	0.08	0.89	2.17	2.82	0.16	2.93	99.2
JAW-75	62.1	0.94	18.5	7.76	1.74	0.17	0.48	0.78	3.39	0.14	3.54	99.7
JAW-92	57.8	1.04	18.9	9.25	2.98	0.15	1.04	1.68	3.32	0.38	3.23	99.9
JAW-93	55.9	1.07	20.0	7.84	3.40	0.09	1.07	1.95	4.49	0.11	3.04	99.2
JAW-99A	46.7	1.25	23.0	10.10	4.26	0.19	1.13	2.23	4.91	0.16	4.31	98.5
JAW-126A	43.5	1.56	25.5	12.70	4.61	0.32	1.46	1.44	4.98	0.10	3.70	100.1

Garnet zone; trace elements (ppm)

	Rb	Sr	Ba	Zr	Zn	Ni	Nb
JAW-12	124	95	669	210	108	48	26
JAW-30	139	129	640	203	92	63	14
JAW-31	171	171	840	215	90	82	22
JAW-35B	187	210	588	184	104	70	18
JAW-39A	135	217	525	280	75	38	39
JAW-75	162	83	691	233	87	37	23
JAW-92	185	136	638	293	89	46	18
JAW-93	192	179	911	292	91	52	30
JAW-99A	255	193	785	359	127	92	29
JAW-126A	212	160	1080	544	135	85	53

APPENDIX D
(continued)

Staurolite zone; major and minor elements (wt %)

	SiO_2	TiO_2	Al_2O_3	Fe_2O_3*	MgO	MnO	CaO	Na_2O	K_2O	P_2O_5	LOI	Total
JAW-19D	46.4	1.34	23.6	10.50	4.93	0.44	0.76	1.31	5.19	0.13	4.47	99.3
JAW-26A	61.8	1.05	18.9	7.37	2.01	0.15	0.29	1.04	3.71	0.12	3.23	99.8
JAW-32A	47.7	1.06	21.7	13.40	4.37	0.10	0.64	0.41	6.21	0.20	3.62	99.6
JAW-32B	58.2	1.16	20.3	6.69	2.51	0.16	1.54	1.32	4.04	0.16	2.93	99.2
JAW-32C	50.3	1.31	24.6	7.27	2.82	0.15	1.29	1.19	5.55	0.20	3.93	98.8
JAW-36	44.4	1.26	26.3	8.15	4.55	0.16	1.32	1.58	6.44	0.12	4.39	99.0
JAW-37	55.7	1.01	19.4	9.34	3.37	0.33	1.71	1.07	4.03	0.38	2.77	99.3
JAW-48	55.6	1.01	21.6	7.96	2.49	0.22	0.97	1.41	3.90	0.14	3.85	99.3
JAW-61	44.1	1.23	25.2	11.80	4.91	0.43	1.81	1.97	5.17	0.12	3.31	100.3
JAW-72	43.5	1.51	25.7	12.50	5.46	0.26	0.45	1.23	4.70	0.12	4.70	100.4
JAW-100	47.2	1.16	23.2	9.95	4.93	0.39	1.75	2.23	5.17	0.13	2.70	99.0
JAW-127A	45.9	1.32	24.7	10.00	4.42	0.13	0.85	1.26	5.80	0.15	5.62	100.4

Staurolite zone; trace elements (ppm)

	Rb	Sr	Ba	Zr	Zn	Ni	Nb
JAW-19D	231	106	955	278	321	78	32
JAW-26A	172	118	617	259	87	33	29
JAW-32A	301	70	865	170	160	39	29
JAW-32B	172	161	876	319	131	35	25
JAW-32C	206	153	1120	355	112	33	43
JAW-36	216	178	1870	237	128	85	27
JAW-37	179	129	931	288	93	63	34
JAW-48	197	192	776	220	167	65	17
JAW-61	215	173	1390	217	105	106	30
JAW-72	207	101	919	311	350	94	40
JAW-100	188	173	844	246	112	100	11
JAW-127A	219	85	1520	237	123	72	55

APPENDIX D
(continued)

Kyanite zone; major and minor elements (wt %)

	SiO_2	TiO_2	Al_2O_3	Fe_2O_3*	MgO	MnO	CaO	Na_2O	K_2O	P_2O_5	LOI	Total
JAW-15A	41.2	1.27	26.1	12.10	4.85	0.64	1.28	1.49	5.52	0.10	4.62	99.4
JAW-15B	55.8	1.11	20.3	9.33	3.79	0.39	1.09	1.45	3.87	0.13	2.47	99.9
JAW-21	43.4	1.47	27.6	11.40	5.04	0.25	1.37	1.04	4.97	0.17	3.16	100.1
JAW-22A	58.2	1.10	20.7	7.35	2.75	0.18	1.08	1.56	4.01	0.13	2.70	99.9
JAW-22B	58.8	1.04	19.5	7.91	2.77	0.12	0.65	0.86	4.59	0.15	3.62	100.2
JAW-50	40.1	1.68	26.1	13.20	6.51	0.10	0.41	1.01	7.05	0.05	3.47	100.0
JAW-53	40.2	1.91	31.7	11.60	2.06	0.16	0.11	1.19	6.21	0.07	4.70	100.2
JAW-57	49.5	1.17	25.7	7.68	2.65	0.09	0.67	1.67	5.99	0.10	4.70	100.1
JAW-59B	42.0	1.36	26.4	12.00	5.55	0.34	1.19	1.37	5.12	0.17	3.85	99.6
JAW-63	44.3	1.32	27.1	10.50	4.58	0.20	1.37	1.35	5.96	0.11	3.47	100.5
JAW-71A	51.0	1.17	22.1	10.80	4.66	0.26	1.07	1.17	4.26	0.16	2.93	99.8
JAW-78	51.8	1.14	24.8	7.45	2.56	0.10	0.99	1.57	5.35	0.30	4.00	100.3
JAW-83	42.0	1.35	26.4	11.50	4.78	0.22	1.34	1.50	5.91	0.12	3.47	98.8
JAW-88	48.3	1.27	25.5	10.10	4.13	0.13	1.33	1.59	3.99	0.14	2.77	99.4
JAW-90A	43.5	1.51	27.5	11.30	4.01	0.29	1.57	1.29	5.26	0.12	3.31	99.9
JAW-103A	42.3	1.49	29.7	11.40	3.59	0.16	0.41	1.30	4.55	0.03	4.00	99.1
JAW-104	59.6	1.03	20.0	7.02	2.48	0.16	0.57	1.25	4.29	0.10	2.70	99.4
JAW-105A	42.7	1.24	24.7	12.90	5.48	0.44	1.54	2.41	4.32	0.19	2.62	98.7
JAW-110	50.0	1.15	25.3	8.27	2.88	0.15	1.08	1.47	5.50	0.16	4.10	100.3
JAW-113B	42.5	1.22	27.2	12.50	4.80	0.21	0.99	1.20	5.56	0.13	3.00	99.5
JAW-114A	38.1	1.58	32.7	15.00	5.35	0.75	1.41	0.27	3.70	0.09	1.47	100.6
JAW-120B	57.4	1.11	20.8	8.41	2.69	0.18	0.69	1.09	4.31	0.12	2.93	100.0
JAW-120Ci	57.9	0.96	19.5	9.14	3.34	0.12	0.66	1.14	4.37	0.14	2.62	100.1
JAW-137B	64.5	1.01	16.3	7.78	2.39	0.15	0.85	1.31	3.27	0.11	2.12	100.0

APPENDIX D
(continued)

Kyanite zone; trace elements (ppm)

	Rb	Sr	Ba	Zr	Zn	Ni	Nb
JAW-15A	210	118	1020	259	119	122	30
JAW-15B	163	128	602	218	191	76	33
JAW-21	274	101	692	264	180	129	32
JAW-22A	172	169	794	231	126	54	29
JAW-22B	179	113	846	226	121	53	32
JAW-50	329	97	1140	391	169	140	29
JAW-53	238	180	1020	630	315	60	43
JAW-57	238	133	1020	226	107	54	27
JAW-59B	239	136	651	305	206	124	29
JAW-63	217	140	1330	247	209	74	33
JAW-71A	201	105	739	228	127	108	32
JAW-78	207	163	1040	242	137	34	17
JAW-83	276	151	1120	235	187	88	22
JAW-88	203	142	687	239	152	124	12
JAW-90A	233	120	1230	400	144	87	44
JAW-103A	209	153	760	304	334	58	23
JAW-104	170	103	919	245	86	52	24
JAW-105A	273	149	633	213	261	114	39
JAW-110	220	161	923	196	155	—	31
JAW-113B	277	80	926	213	170	113	—
JAW-114A	196	—	454	337	207	132	36
JAW-120B	193	122	856	238	125	37	34
JAW-120Ci	233	119	771	190	176	78	28
JAW-137B	152	186	535	336	47	38	23

REFERENCES

Ague, J. J., 1991, Evidence for major mass transfer and volume strain during regional metamorphism of pelites: Geology, v. 19, p. 855–858.

———— 1992, Hydrochemical differentiation during metamorphism of pelites: Fracture flow-controlled major element mass transfer and the growth of Barrovian zone index minerals: Geological Society of America Abstracts with Programs, v. 24, p. A264.

———— 1994, Mass transfer during Barrovian metamorphism of pelites, south-central Connecticut. II: Channelized fluid flow and the growth of staurolite and kyanite: American Journal of Science, v. 294, p. 1061–1130.

Ague, J. J., and Brimhall, G. H., 1988, Regional variations in bulk chemistry, mineralogy, and the compositions of mafic and accessory minerals in the batholiths of California: Geological Society of America Bulletin, v. 100, p. 891–911.

Aitchison, J., 1986, The statistical analysis of compositional data: London, Chapman and Hall, 416 p.

———— 1989, Measures of location of compositional data sets: Mathematical Geology, v. 21, p. 787–790.

———— 1990, Relative variation diagrams for describing patterns of compositional variability: Mathematical Geology, v. 22, p. 487–511.

Ayers, J. C., and Watson, E. B., 1991, Solubility of apatite, monazite, zircon, and rutile in supercritical aqueous fluids with implications for subduction zone geochemistry: Philosophical Transactions of the Royal Society of London, A, v. 335, p. 365–375.

———— 1993, Rutile solubility and mobility in supercritical aqueous fluids: Contributions to Mineralogy and Petrology, v. 114, p. 321–330.

Barrow, G., 1893, On an intrusion of muscovite-biotite gneiss in the south-east highlands of Scotland and its accompanying metamorphism: Geological Society of London Quarterly Journal, v. 49, p. 330–358.

———— 1912, On the geology of the lower Dee-side and the southern Highland border: Proceedings of the Geologist's Association, v. 23, p. 268–284.

Beach, A., 1976, The interrelations of fluid transport, deformation, geochemistry and heat flow in early Proterozoic shear zones in the Lewisian complex: Philosophical Transactions of the Royal Society, v. A280, p. 569–604.

Bebout, G. E., and Barton, M. D., 1989, Fluid flow and metasomatism in a subduction zone hydrothermal system: Catalina schist terrane, California: Geology, v. 17, p. 976–980.

Bell, A. M., 1985, Strain paths during slaty cleavage formation—the role of volume loss: Journal of Structural Geology, v. 7, p. 563–568.

Beutner, E. C., and Charles, E. G., 1985, Large volume loss during cleavage formation, Hamburg sequence, Pennsylvania: Geology, v. 13, p. 803–805.

Bickle, M. J., and McKenzie, D., 1987, The transport of heat and matter by fluids during metamorphism: Contributions to Mineralogy and Petrology, v. 95, p. 384–392.

Brady, J. B., 1988, The role of volatiles in the thermal history of metamorphic terranes: Journal of Petrology, v. 29, p. 1187–1213.

Bridgwater, D., Rosing, M., Schiotte, L., and Austrhiem, H., 1989, The effect of fluid-controlled element mobility during metamorphism on whole rock isotope systems, some theoretical aspects and possible examples, *in* Bridgwater, D., editor, Fluid Movements—Element Transport and the Composition of the Deep Crust (NATO ASI series): Dordrecht, Kluwer Academic Publishers, p. 277–298.

Brimhall, G. H., Jr., 1979, Lithologic determination of mass transfer mechanisms of multiple-stage porphyry copper mineralization at Butte, Montana: Vein formation by hypogene leaching and enrichment of potassium silicate protore: Economic Geology, v. 74, p. 556–589.

Brimhall, G. H., and Dietrich, W. E., 1987, Constitutive mass balance relations between chemical composition, volume, density, porosity, and strain in metasomatic hydrochemical systems: Results on weathering and pedogenesis: Geochimica et Cosmochimica Acta, v. 51, p. 567–587.

Brimhall, G. H., Lewis, C. J., Ague, J. J., Dietrich, W. E., Hampel, J., Teague, T., and Rix, Peter, 1988, Metal enrichment in bauxites by deposition of chemically mature aeolian dust: Nature, v. 333, p. 819–824.

Butler, B. C. M., 1965, A chemical study of some rocks of the Moine Series of Scotland: Geological Society of London Quarterly Journal, v. 121, p. 163–208.

Chamberlain, C. P., and Rumble, D., 1988, Thermal anomalies in a regional metamorphic terrane: An isotopic study of the role of fluids: Journal of Petrology, v. 29, p. 1215–1232.

Chayes, F., 1960, On correlation between variables of constant sum: Journal of Geophysical Research, v. 65, p. 4185–4193.

Chinner, G. A., 1960, Pelitic gneisses with varying ferrous/ferric ratios from Glen Clova, Angus, Scotland: Journal of Petrology, v. 1, p. 178–217.

Dieterich, J. H., ms, 1968, Sequence and mechanics of folding in the area of New Haven, Naugatuck, and Westport, Connecticut: Ph.D. thesis, Yale University, New Haven, 153 p.
Dipple, G. M., and Ferry, J. M., 1992, Metasomatism and fluid flow in ductile fault zones: Contributions to Mineralogy and Petrology, v. 112, p. 149–164.
Dipple, G. M., Wintsch, R. P., and Andrews, M. S., 1990, Identification of the scales of differential element mobility in a ductile fault zone: Journal of Metamorphic Geology, v. 8, p. 645–661.
Efron, B., 1982, The Jackknife, the Bootstrap, and other Resampling Plans: Philadelphia, Society for Industrial and Applied Mathematics, 92 p.
Emmons, W. H., 1918, The principles of economic geology: New York, McGraw-Hill, 153 p.
Erslev, E., and Mann, C., 1984, Pressure solution shortening in the Martinsburg Slate, New Jersey: Proceedings of the Pennsylvania Academy of Science, v. 58, p. 84–88.
Ferry, J. M., 1982, A comparative geochemical study of pelitic schists and metamorphosed carbonate rocks from south-central Maine, USA: Contributions to Mineralogy and Petrology, v. 80, p. 59–72.
———— 1983, On the control of temperature, fluid composition, and reaction progress during metamorphism: American Journal of Science, v. 282-A, p. 201–232.
———— 1988, Infiltration-driven metamorphism in northern New England, USA: Journal of Petrology, v. 29, p. 1121–1159.
———— 1992, Regional Metamorphism of the Waits River Formation, eastern Vermont, Delineation of a new type of giant metamorphic hydrothermal system: Journal of Petrology, v. 33, p. 45–94.
Ferry, J. M., and Dipple, G. M., 1991, Fluid flow, mineral reactions, and metasomatism: Geology, v. 19, p. 211–214.
Fritts, C. E., 1962a, Bedrock geology of the Mount Carmel and Southington quadrangles, Connecticut: U.S. Geological Survey Open-file Report 644, 213 p.
———— 1962b, Age and sequence of metasedimentary and metavolcanic formations northwest of New Haven, Connecticut: U.S. Geological Survey Professional Paper 450-D, p. 32–36.
———— 1963, Bedrock geology of the Mount Carmel quadrangle, Connecticut: U.S. Geological Survey Quadrangle Map GQ-199.
———— 1965a, Bedrock geologic map of the Ansonia quadrangle, Fairfield and New Haven Counties, Connecticut: U.S. Geological Survey Quadrangle Map GQ-426.
———— 1965b, Bedrock geologic map of the Milford quadrangle, Fairfield and New Haven Counties, Connecticut: U.S. Geological Survey Quadrangle Map GQ-427.
Gaddum, J. H., 1945, Lognormal Distributions: Nature, v. 156, p. 463–466.
Garlick, G. D., and Epstein, S., 1966, Oxygen isotope ratios in coexisting minerals of regionally metamorphosed rocks: Geochimica et Cosmochimica Acta, v. 31, p. 181–214.
Grant, J. A., 1986, The isocon diagram—A simple solution to Gresens' equation for metasomatic alteration: Economic Geology, v. 81, p. 1976–1982.
Gresens, R. L., 1967, Composition-volume relations of metasomatism: Chemical Geology, v. 2, p. 47–65.
Haack, U., Heinrichs, H., Boness, M., and Schneider, A., 1984, Loss of metals from pelites during regional metamorphism: Contributions to Mineralogy and Petrology, v. 85, p. 116–132.
Harte, B., and Hudson, N. F. C., 1979, Pelite facies series and temperatures and pressures of metamorphism in eastern Scotland, *in* Harris, A. L., Holland, C. H., and Leake, B. E., editors, The Caledonides of the British Isles-Reviewed: Geological Society of London Special Publication 8, p. 323–327.
Henderson, J. R., Wright, T. O., and Henderson, M. N., 1988, A history of cleavage and folding: An example from the Goldenville Formation, Nova Scotia: Geological Society of America Bulletin, v. 97, p. 1354–1366.
Hewitt, D. A., 1973, The metamorphism of micaceous limestones from south-central Connecticut: American Journal of Science, v. 273-A, p. 444–469.
Hoisch, T. D., 1991, The thermal effects of pervasive and channelized fluid flow in the deep crust: Journal of Geology, v. 99, p. 69–80.
Hoschek, G., 1967, Untersuchungen zum stabilitätsbereich von chloritoid und staurolith: Contributions to Mineralogy and Petrology, v. 14, p. 123–162.
Hounslow, A. W., and Moore, J. M., Jr., 1967, Chemical petrology of Grenville schists near Fernleigh, Ontario: Journal of Petrology, v. 8, p. 1–28.

Kerrich, R., Allison, I., Barnett, R. L., Moss, S., and Starkey, J., 1980, Microstructural and chemical transformations accompanying deformation of granite in a shear zone at Mieville, Switzerland; with implications for stress corrosion cracking and superplastic flow: Contributions to Mineralogy and Petrology, v. 73, p. 221–242.

Korzhinsky, D. S., 1950, Differential mobility of components and metasomatic zoning in metamorphism: International Geological Congress, 18th, Great Britain, Report, part II, p. 50–65.

Lanzirotti, A. and Hanson, G. N., 1992, Multiple generations of monazite growth in the Wepawaug Schist, southern Connecticut: Geological Society of America Abstracts with Programs, v. 24, no. 7, p. A219.

Leger, A. and Ferry, J. M., 1993, Fluid infiltration and regional metamorphism of the Waits River Formation, northeast Vermont, USA: Journal of Metamorphic Geology, v. 11, p. 3–29.

Lowell, J. D., and Guilbert, J. M., 1970, Lateral and vertical alteration-mineralization zoning in porphyry ore deposits: Economic Geology, v. 65, p. 373–408.

MacLean, W. H., and Kranidiotis, P., 1987, Immobile elements as monitors of mass transfer in hydrothermal alteration: Phelps Dodge massive sulfide deposit, Matagami, Quebec: Economic Geology, v. 82, p. 951–962.

McLellan, E. L., 1985, Metamorphic reactions in the kyanite and sillimanite zones of the Barrovian type area: Journal of Petrology, v. 26, p. 789–818.

Meyer, C., Shea, E. P., Goddard, C. C., Jr., and staff, 1968, Ore deposits at Butte, Montana, *in* Ridge, J. D., editor, Ore Deposits of the United States, 1933–1967, Graton-Sales volume: New York, American Institute of Mining, Metallurgical, and Petroleum Engineers, v. 2, p. 1650–1672.

Moss, B. E., Haskin, L. A., Dymek, R. F., and Shaw, D. M., 1992, A reexamination of the Littleton Formation in New Hampshire: Implications for element mobility during regional metamorphism: Geological Society of America Abstracts with Programs, v. 24, p. A304.

Nicholls, J., 1988, The statistics of Pearce element diagrams and the Chayes closure problem: Contributions to Mineralogy and Petrology, v. 99, p. 11–24.

O'Hara, K., and Blackburn, W. H., 1989, Volume-loss model for trace-element enrichments in mylonites: Geology, v. 17, p. 524–527.

Orville, P. M., 1969, A model for metamorphic differentiation origin of thin-layered amphibolites: American Journal of Science, v. 267, p. 64–86.

Palin, J. M., ms, 1992, Petrologic and stable isotopic studies of the Wepawaug Schist, Connecticut: Ph.D. thesis, Yale University, New Haven, 170 p.

Palin, J. M., and Rye, D. M., 1992, Direct comparison of mineralogic and stable isotopic records of metamorphic fluid flow: Geological Society of America Abstracts with Programs, v. 24, no. 7, p. A172.

Palin, J. M., and Seidemann, D. E., 1990, Intergranular control of argon and oxygen isotope transport in metamorphic rocks: Implications for cooling-rate studies [abstract]: M. Goldschmidt Conference, 2d, Baltimore, Maryland, Program and Abstracts, p. 71. (The Geochemical Society).

Pettijohn, F. J., 1975, Sedimentary rocks (3d edition): New York, Harper and Row, 628 p.

Philippot, P., and Selverstone, J., 1991, Trace-element-rich brines in eclogitic veins: Implications for fluid composition and transport during subduction: Contributions to Mineralogy and Petrology, v. 106, p. 417–430.

Phillips, G. N., 1988, Widespread fluid infiltration during metamorphism of the Witwatersrand goldfields: Generation of chloritoid and pyrophyllite: Journal of Metamorphic Geology, v. 6, p. 311–332.

Poldervaart, A., 1953, Petrological calculations in metasomatic processes: American Journal of Science, v. 251, p. 481–504.

Press, W. H., Teukolsky, S. A., Vetterling, W. T., and Flannery, B. P., 1992, Numerical Recipes in C (2d edition): New York, Cambridge University Press, 994 p.

Ramberg, H., 1952, The origin of metamorphic and metasomatic rocks: Chicago, University of Chicago Press, 317 p.

Ridge, J. D., 1949, Replacement and the equating of volume and weight: Journal of Geology, v. 57, p. 522–550.

———— 1961, Gain and loss of material in a series of replacements: Geological Society of America Special Papers, 68, p. 252–253.

Rodgers, John, 1985, Bedrock Geological Map of Connecticut: Connecticut Geological and Natural History Survey, Department of Environmental Protection, scale 1:125,000.

Ronov, A. B., Migdisov, A. A., and Lobach-Zhuchenko, S. B., 1977, Regional metamorphism and sediment composition evolution: Geochemistry International, v. 14, p. 90–112.

Rumble, D., Ferry, J. M., Hoering, T. C., and Boucot, A. J., 1982, Fluid flow during metamorphism at the Beaver Brook fossil locality: American Journal of Science: v. 282, p. 886–919.

Rye, D. M., and Rye, R. O., 1974, Homestake gold mine, South Dakota: I. Stable isotope studies: Economic Geology, v. 69, p. 293–317.

Rye, R. O., Schuiling, R. D., Rye, D. M., and Jansen, J. B. H., 1976, Carbon, hydrogen and oxygen isotope studies of the regional metamorphic complex at Naxos, Greece: Geochimica et Cosmochimica Acta, v. 40, p. 1031–1049.

Schandl, E. S., Davis, D. W., Krogh, T. E., 1990, Are the alteration halos of massive sulfide deposits syngenetic? Evidence from U-Pb dating of hydrothermal rutile at the Kidd volcanic center, Abitibi subprovince, Canada: Geology, v. 18, p. 505–508.

Shaw, D. M., 1956, Geochemistry of pelitic rocks. Part III: Major elements and general geochemistry: Geological Society of America Bulletin, v. 67, p. 919–934.

Sinha, A. K., Hewitt, D. A., and Rimstidt, J. D., 1986, Fluid interaction and element mobility in the development of ultramylonites: Geology, v. 14, p. 883–886.

Sorensen, S. S., 1988, Petrology of amphibolite-facies mafic and ultramafic rocks from the Catalina schist, southern California: Metasomatism and migmatization in a subduction zone metamorphic setting: Journal of Metamorphic Geology, v. 6, p. 405–435.

Spiegel, M. R., 1961, Theory and problems of statistics: New York, McGraw-Hill, 359 p.

Spry, A., 1969, Metamorphic Textures: New York, Pergamon Press, 350 p.

Symmes, G. H., and Ferry, J. M., 1991, Evidence from mineral assemblages for infiltration of pelitic schists by aqueous fluids during metamorphism: Contributions to Mineralogy and Petrology, v. 108, p. 419–438.

Taylor, H. P., Jr., 1974, The application of oxygen and hydrogen isotope studies to problems of hydrothermal alteration and ore deposition: Economic Geology, v. 69, p. 843–883.

Thompson, A. B., 1975, Calc-silicate diffusion zones between marble and pelitic schist: Journal of Petrology, v. 16, p. 314–346.

Thompson, A. B., Lyttle, P. T., and Thompson, J. B., Jr., 1977, Mineral reactions and A-Na-K and A-F-M facies types in the Gassetts Schist, Vermont: American Journal of Science, v. 277, p. 1152–1167.

Thompson, J. B., Jr., 1957, The graphical analysis of mineral assemblages in pelitic schists: American Mineralogist, v. 42, p. 842–858.

———— 1959, Local equilibrium in metasomatic processes, *in* Abelson, P. H., editor, Researches in Geochemistry: New York, John Wiley, p. 427–457.

Tracy, R. J., Rye, D. M., Hewitt, D. A., and Schiffries, C. M., 1983, Petrologic and stable-isotopic studies of fluid-rock interactions, south-central Connecticut: I. The role of infiltration in producing reaction assemblages in impure marbles: American Journal of Science, v. 283-A, p. 589–616.

Turner, F. J., and Verhoogen, J., 1960, Igneous and metamorphic petrology: New York, McGraw-Hill, 694 p.

van Haren, J. L. M., Rye, D. M., and Ague, J. J., 1992, Fluid flow history determined from a petrographic and oxygen isotope study of a metamorphic quartz vein: EOS (Transactions of the American Geophysical Union), v. 73, p. 147.

Vidale, R. J., 1974, Vein assemblages and metamorphism in Dutchess County, New York: Geological Society of America Bulletin, v. 85, p. 303–306.

Vidale, R. J., and Hewitt, D. A., 1973, "Mobile" components in the formation of calc-silicate bands: American Mineralogist, v. 58, p. 991–997.

Walther, J. V., and Orville, P. M., 1982, Volatile production and transport in regional metamorphism: Contributions to Mineralogy and Petrology, v. 79, p. 252–257.

Wickham, S. M., and Taylor, H. P., Jr., 1985, Stable isotopic evidence for large-scale seawater infiltration in a regional metamorphic terrane: The Trois Seigneurs Massif, Pyrenees, France: Contributions to Mineralogy and Petrology, v. 91, p. 122–137.

Wintsch, R. P., Kvale, C. M., and Kisch, H. J., 1991, Open-system, constant-volume development of slaty cleavage, and strain induced replacement reactions in the Martinsburg Formation, Lehigh Gap, Pennsylvania: Geological Society of America Bulletin, v. 103, p. 916–927.

Wood, B. J., and Walther, J. V., 1986, Fluid flow during metamorphism and its implications for fluid-rock ratios, *in* Walther, J. V., and Wood, B. J., editors, Fluid-rock interactions during metamorphism: New York, Springer-Verlag, p. 89–108.

Wood, D. A., Sibson, I. L., and Thompson, R. N., 1976, Elemental mobility during zeolite facies metamorphism of the Tertiary basalts of eastern Iceland: Contributions to Mineralogy and Petrology, v. 55, p. 241.

Woronow, A., and Love, K. M., 1990, Quantifying and testing differences among means of compositional data suites: Mathematical Geology, v. 22, p. 837–852.

Wright, T. O., and Platt, L. B., 1982, Pressure dissolution and cleavage in the Martinsburg Shale: American Journal of Science, v. 282, p. 122–135.

Yardley, B. W. D., 1977, Relationships between the chemical and modal compositions of metapelites from Connemara, Ireland: Lithos, v. 10, p. 235–242.

———— 1986, Fluid migration and veining in the Connemara schists, Ireland, *in* Walther, J. V., and Wood, B. J., editors, Fluid-rock interactions during metamorphism: New York, Springer-Verlag, p. 109–131.

Zeitler, P. K., Barreiro, B., Chamberlain, C. P., and Rumble, D., III, 1990, Ion-microprobe dating of zircon from quartz-graphite veins at the Bristol, New Hampshire, metamorphic hot spot: Geology, v. 18, p. 626–629.